SIGNAL PROCESSING AND FREQUENCY ANALYSIS OF CARPENTIER-EDWARDS BIOPROSTHETIC HEART VALVE SOUNDS

Rajan Bedi

A thesis submitted for the degree of Doctor of Philosophy.

The University of Edinburgh.

- November 1994 -

Abstract

The advent of the prosthetic heart valve has dramatically transformed the outcome of valvular heart disease. Valve replacement is frequently life-saving and following implantation most patients experience a marked improvement in their symptomatic state and quality of life. The most common bioprosthesis currently implanted in Scotland is the Carpentier-Edwards bioprosthetic heart valve. However, dramatic as its influence on the outcome of valvular heart disease has been, there is a major problem associated with this prosthesis: gradual tissue degeneration leads to valvular dysfunction. Generally this is due to torn leaflets or as a result of leaflet calcification leading to valvular regurgitation or stenosis. Ultimately, this deterioration limits the duration of the period of implantation.

As a result of the inevitable patient risk associated with the Carpentier-Edwards bioprosthesis, reliable, periodic, post-operative evaluation of the integrity of the implanted valve is essential. The research detailed in this thesis proposes a method whereby diagnostic information concerning the functionality of the valve is extracted from the acoustic output produced by the operation of the prosthesis. This is achieved by analysing the spectral characteristics of the principal heart sound components contained within this acoustic signal. The aim of this investigation is to identify normally functioning and dysfunctioning prostheses by examination of this diagnostic information and ultimately to predict impending valve failure. As a clinical physiological measurement technique for periodically monitoring patients with implanted Carpentier-Edwards bioprostheses, frequency analysis of valve sounds is particularly attractive as it is noninvasive, passive and atraumatic, especially when compared to traditional evaluation procedures.

A data-acquisition system was designed and developed which records and digitises the sounds produced by implanted bioprostheses using the Hewlett Packard 21050A phonocardiographic contact microphone. Heart sounds were recorded from sixteen patients with implanted mitral Carpentier-Edwards bioprostheses and from twenty-four patients with implanted aortic Carpentier-Edwards prostheses. The acquired sounds were preprocessed which involved filtering to accentuate the principal components and automatic extraction of the relevant sounds from each recording for subsequent frequency analysis. Various spectral estimation techniques were investigated with a view to assessing the performance and suitability of these methods when analysing the heart sound signal. Algorithms implemented were: classical Fourier transform-based methods and high-resolution parametric techniques based on autoregressive-moving average (ARMA) models, autoregressive (AR)/linear-prediction analysis and a damped sinusoidal Prony model. Results are presented which illustrate the performance of these signal processing techniques over the range of recorded sounds and demonstrate the diagnostic potential of frequency analysis. Examination of the sound spectrum revealed features of diagnostic significance such as the dominant frequency peaks, their relative intensities and metrics associated with the overall spectral profile of the sound spectrum. These features were able to discriminate between physiological and pathological functionality.

Results show that normally functioning, leaky and stiffening prostheses each exhibit unique spectral characteristics. Normally functioning aortic prostheses are characterised by four to five dominant frequency peaks, with the major concentration of spectral energy occurring in the region between 25Hz and 125Hz. Normally functioning mitral prostheses are characterised by two to three dominant peaks with the major concentration of spectral energy occurring in the region between d.c. and 100Hz. For leaky regurgitant bioprostheses and prostheses diagnosed as having stiffening calcified cusps, a shift was observed in spectral energy. For leaky mitral and aortic prostheses, the major distribution of spectral energy now occurs in the region between d.c. and 75Hz, whereas for stiffening aortic prostheses, the major concentration of spectral energy now occurs in the region between 50Hz and 200Hz. It was observed that the highest frequency which occurs at a level of -10dB below the maximum spectral response (0dB), may be used to discriminate between normally functioning, leaky and stiffening aortic prostheses, where mean frequencies for these conditions at the -10dB level were observed to be 113.6Hz, 53.7Hz and 238.1Hz respectively. A single discriminating parameter was not observed from the analysis of mitral sounds.

Acknowledgements

Many people deserve thanks for their guidance and support throughout this research. In particular, I wish to express my sincere gratitude to my supervisor, Dr. Edward McDonnell, without whose insight and encouragement this work would not have been possible.

There are numerous other members of the Signals and Systems group both past and present to whom I am endebted. Foremost among these are Mr. Paul Bentley and Mr. Herkole Sava, for their assistance in the recording of heart sounds and for their contribution to my understanding of this and many other subjects. I would also like to thank Professor Peter Grant for his support during my three years and John Thompson for his excellent photography.

Special thanks must go the Cardiovascular Research Unit at The University of Edinburgh, The Royal Infirmary of Edinburgh and the Astley Ainslie Hospital in Edinburgh for providing access to subjects with implanted Carpentier-Edwards bioprosthetic heart valves and recording venues. In particular, I wish to acknowledge Dr. Peter Bloomfield, Professor Keith Fox, Dr. I. Todd, Mrs A. Colthart and the staff at both hospitals for their kind cooperation.

I also wish to thank Dr. Richard Stephens from the University of Leicester for his helpful suggestions during my visit to Leicester in 1993.

Finally, I wish to thank my family for their unwavering support.

Contents

Abbreviations

AIC	Akaike Information Criterion
AR	Autoregressive
ARMA	Autoregressive-Moving Average
BMI	Body Mass Index
CRO	Cathode Ray Oscilloscope
CAT	Criterion Autoregressive Transfer
DFT	Discrete Fourier Transform
ECG	Electrocardiogram
EEG	Electroencephalogram
EMG	Electromyogram
FPE	Final Prediction Error
FIR	Finite Impulse Response
MDL	Minimum Description Length
MCV	Modified Covariance
MA	Moving Average
NRMSE	Normalised Root Mean Square Error
PCG	Phonocardiogram
PSD	Power Spectral Density
SNR	Signal-to-noise ratio
SVD	Singular Value Decomposition

Glossary of Medical Terms

Aorta	The large vessel arising from the left ventricle and distributing, by its branches, arterial blood to every part of the body.
Aortic valve	The semilunar heart valve situated at the junction of the left ventricle and the arterial network.
Artery	A vessel which carries blood away from the heart to all parts of the body.
Atrium	The upper chamber on either side of the heart which receives blood directly from the viens.
Auscultation	The act of listening to the sounds and murmurs produced by the operation of the heart using a stethoscope.
Bioprosthesis	A tissue (biological) artificial heart valve.
Bundle Branch Block	The delay or block of conduction within the heart causing one ventricle to be activated and contract before the other.
Calcification	The deposition of calcareous (limestone) matter within the tissues of the body.
Diastole	The rhythmic period of relaxation and dilatation of the chambers of the heart during which it fills with blood. The duration of diastole is the time interval between the beginning of a second heart sound and the beginning of the first heart sound of the following heartbeat.
Dysfunction	An impairment or abnormality in functioning.
Electrocardiogram	A visual record of the electrical activity within the heart.
Electroencephalogram	A visual record of the electrical activity within the brain.
Electromyogram	A visual record of the electrical activity of a muscle.
Embolus	A bit of foreign matter in the bloodstream, *e.g.* a clot, which is carried by the bloodstream until it lodges in a blood vessel and obstructs it.
Endocarditis	Inflammation of the heart cavities and its valves.

Hemodynamics	The study of the interrelationships between blood pressure, blood flow, vascular volumes, physical properties of the blood, heart rate and ventricular function.
Mitral Valve	The atrioventricular valve of the left side of the heart.
Phonocardiogram	A visual record of the sounds and murmurs heard during auscultation.
Prosthetic	Man-made limb or other body part.
Regurgitation	A backflow of blood through a heart valve that is defective.
Stenosis	Constriction or narrowing of the heart valve orifice.
Systole	The contraction phase of the cardiac cycle. The duration of systole is the time interval between the beginning of a first heart sound and the beginning of the second sound in the same beat.
Thromboembolic	An embolism due to a dislodged thrombus.
Thrombus	A clot of blood formed during life within the heart or blood vessels.
Ventricle	The lower two chambers of the heart that pump blood into the arteries.
Xenograft	A transplant from one species to another.

Chapter 1

Introduction

The Carpentier-Edwards artificial heart valve has dramatically transformed the treatment of diseased native heart valves. Following valve replacement, most patients experience a marked improvement in their symptomatic state and quality of life. However, dramatic as its influence on the outcome of valvular heart disease has been, there is a major problem associated with the operation of this prosthesis: gradual tissue degeneration leads to valvular dysfunction. Generally this is due to torn leaflets or calcification leading to valvular regurgitation or stenosis. Ultimately, this deterioration leads to valve failure.

The risk of severe heart problems as a result of changes in the properties of the Carpentier-Edwards bioprostheses warrants the follow-up of subjects with implanted valves. Therefore reliable, periodic, post-operative evaluation of the integrity of implanted prostheses is essential. Current monitoring procedures entail the combined use of some the following methods: auscultation, ultrasound echocardiography, angiography, cardiac catheterisation and cinefluoroscopy. However, the practice of some of these methods involves the use of expensive equipment and custom laboratories that are generally only available in medium or large-sized hospitals, and the need for personnel specially trained in the use of such techniques. Furthermore, some of these procedures are traumatic and not without risk, often necessitating invasive surgery. In addition, the reliability and subjectivity of auscultation has always been in question [1, 2].

Ideally, a low-cost, repeatable, noninvasive, atraumatic, passive technique is required, capable of providing physicians with reliable post-operative evaluation of the functionality of the Carpentier-Edwards bioprostheses. In collaboration with the Cardiovascular Research Unit of The University of Edinburgh and The Royal Infirmary of Edinburgh, the research detailed

in this thesis proposes an alternative physiological measurement technique based on signal processing and analysis methods, whereby diagnostic information concerning the functionality of the valve is extracted from the acoustic output produced by the operation of the prosthesis. The aim is to identify normally functioning and dysfunctioning prostheses by examination of this diagnostic information and ultimately to predict impending valve failure.

The following sections describe the principal motivation for the research reported in this thesis including a list of specific objectives, an introduction to the Carpentier-Edwards bioprosthetic heart valve and current post-operative evaluation procedures, and a discussion of the application of signal processing methods to biomedical signals. The chapter ends with a conspectus of the work contained in this thesis.

1.1 Motivation

The testing of industrial machinery and equipment is often performed nondestructively by analysing the emitted sounds [3]. This is accomplished by risk-assessment devices that measure the energy level and then evaluate the frequency spectrum of the emitted sounds, *i.e.* a sound 'signature' is analysed and malfunction is determined noninvasively by using spectral analysis. Based on this principle of nondestructive, noninvasive testing, the motivation for the research described in this thesis is to investigate whether analysing the sounds produced by the operation of the Carpentier-Edwards bioprostheses, using signal processing methods, reveals information of diagnostic significance concerning the functionality of the valve. The rationale for this hypothesis is that the sounds produced by the operation of the Carpentier-Edwards bioprostheses are a result of its geometric configuration, the density of the materials used in its construction and the interaction of the valve components with dynamic blood masses and surrounding tissues. It is proposed that changes in any of these factors should affect the frequency spectrum of the emitted sounds. Using spectral analysis and examination of the frequency spectrum of the sounds produced by the operation of the Carpentier-Edwards bioprostheses, the aim is to identify and distinguish between normally functioning and dysfunctioning prostheses and ultimately to predict impending valve failure. If a relationship can be found between the functionality of the prosthesis and the frequency spectrum of these sounds, this would demonstrate the diagnostic potential of frequency analysis as an alternative physiological measurement technique capable of assisting physicians in their post-operative assessment of the Carpentier-Edwards bioprosthetic heart valve. As a clinical technique for periodically monitoring patients with implanted bioprostheses, spectral analysis of valve sounds is particularly attractive as it is noninvasive,

atraumatic, passive, reliable and sensitive. The very low-cost, repeatability and portability of this technique are added benefits. From a signal processing perspective, the specific objectives of this thesis are:

1. To investigate the development of a data-acquisition system to record and digitise efficiently and with a high degree of fidelity the heart sounds produced by the operation of the Carpentier-Edwards bioprostheses . The data-acquisition system will interface to a phonocardiographic transducer to convert the sounds measured at the chest surface to an equivalent electrical signal. The design will also consider appropriate sampling frequencies, signal-conditioning circuitry and anti-aliasing filters.

2. To investigate the preprocessing of the acquired phonocardiogram (PCG) using time domain signal analysis methods with a view to accentuating the principal heart sounds over background noise and extracting the appropriate sound components for further analysis.

3. To investigate signal processing methods for the frequency analysis of heart sounds. The aim is to refine the application of spectral estimation techniques to heart sounds and to identify optimum methods for this thesis.

4. To investigate whether a relationship exists between the features derived from the frequency spectrum of heart sounds produced by the operation of the Carpentier-Edwards bioprosthesis and the functionality of this valve.

1.2 The Carpentier-Edwards Bioprosthetic Heart Valve

Since the first implant of a prosthetic heart valve to replace a defective native heart valve in 1960 [4], changes in the design and materials used by early mechanical prostheses have resulted in significant improvements in the durability and hemodynamic function of prostheses. However, despite these improvements, the risk of blood clotting remains an important problem [5]. In a search for a solution to the thromboembolic complications of mechanical prostheses, prosthetic heart valves constructed from biological tissue, *i.e.* bioprostheses, were developed, *e.g.* the Carpentier-Edwards porcine xenograft. However, despite recent improvements in tissue fixation and preservation techniques, tissue deterioration ultimately leading to valve failure is a major problem associated with the operation of the Carpentier-Edwards bioprostheses. The average lifespan of a porcine xenograft is typically thirteen years [6, 7].

1.3 Current Post-Operative Evaluation Procedures

There are currently five techniques used to assess the post-operative performance of implanted Carpentier-Edwards bioprostheses:

1. Auscultation: a diagnosis based on listening to heart sounds, murmurs and other vibratory phenomena originating in the heart using a stethoscope.

2. Ultrasound Echocardiography: a diagnosis based on a pictorial representation of the heart using an active pulse-echo (ultrasound) technique.

3. Cardiac Catheterisation: a diagnosis necessitating surgery where a flexible tube is inserted into the heart and passed through the dysfunctioning prostheses.

4. Angiography: a diagnosis based on determining the arrangement of blood vessels using either fluoroscopy or radiography, after the injection of a nontoxic radiopaque substance to aid visualisation of blood vessels.

5. Cinefluoroscopy: a diagnosis based on fluoroscopic imaging of the prostheses to photograph cusp movement, after the injection of a radiopaque contrast substance to aid visualisation of blood vessels.

Many pathological conditions of the cardiovascular system are responsible for murmurs and aberrations in heart sounds well before they manifest themselves as other symptoms, *e.g.* changes in the electrocardiogram (ECG) signal. For this reason, auscultation is the primary diagnosis performed by physicians to evaluate the condition of the heart [8,9]. However, from a study of the physical characteristics of heart sounds and the human range of audibility [10–14], it is seen that the human ear is poorly suited for cardiac auscultation. Human aural perception decreases exponentially as frequency decreases and is sensitive only to frequencies in the range from 50Hz to 2kHz. This response severely limits the ability of physicians, as further important diagnostic information may be present outside this spectrum of frequencies, or present at the low-frequencies where aural insensitivity is highest. Moreover, auscultation is subjective and prone to interpreter variations, *e.g.* qualitative descriptors, such as 'muffled component', of a sound, 'musical murmur', 'rumble' or 'whiff' difficult to quantify or measure [15,16]. Based on this lack of objectivity, any prognosis based solely on auscultation is questionable and is, in fact, seldom practised.

Echocardiography provides a method for the examination of bioprosthetic heart valves and has been useful in individual patients for detecting the thickening of leaflets and the formation

of vegetations [17, 18]. However, visualisation of cusp motion and thrombus by the ultrasound beam is made difficult by interference (echoes) from the stents supporting the valve and its sewing ring. Doppler methods of analysis offer the potential to assess the functionality of prostheses, *e.g.* accurate analysis of valve movement and blood flow, however, the sensitivity of this technique remains to be evaluated. Furthermore, this procedure is relatively expensive and is generally only available in medium and large-sized hospitals, requiring the need for personnel specially trained in the use of this technique. In addition, bacterial endocarditis, a bacterial infection of heart valves, may be missed by echocardiography [18–21].

Cardiac catheterisation and angiography are both invasive techniques which necessitate surgery. These procedures are traumatic for subjects, with the added risks of patient morbidity or even mortality. Furthermore, cardiac catheterisation is performed in a custom laboratory, which restricts the evaluation to prescreened patients only. Similarly, cinefluoroscopy requires an experienced fluoroscopist for an accurate evaluation of the prostheses, as it entails careful positioning of the patient to ensure that the angle of projection of the X-ray tube allows optimal visualisation of the prosthesis. The sewing ring is faintly visible and the valve leaflets are readily seen only when viewed directly on end [20, 22].

This thesis proposes an alternative post-operative evaluation technique based on phonocardiography, *i.e.* the graphic registration of auscultatory observations. Heart sounds are first recorded from the output of a phonocardiographic transducer, which converts the sounds measured at the chest surface to an equivalent electrical signal. Then, using signal analysis methods, information of diagnostic significance is extracted from the sounds produced by the operation of the Carpentier-Edwards bioprostheses. Signal processing of heart sounds is an accurate and quantitative procedure based on numerical computation, and reveals information such as the timing instants of sounds and their components, the structure of sounds, their frequency content and their location in the cardiac cycle. Using frequency analysis methods, the research will examine whether a relationship exists between the functionality of the prosthesis and the spectral parameters derived from the frequency spectrum of the heart sounds.

1.4 Biomedical Signal Processing

The analysis of physiological signals presents many unique challenges. Unlike the application of signal processing techniques to other disciplines, the characteristics of biomedical signals are often not well specified, as well as being subject to considerable nonstationarity. Compounded with this is the requirement that the measurement of biomedical signals be performed

noninvasively, *i.e.* without piercing the skin, thus, the transducer if often remote from the point of origin of the signal. This separation exposes biomedical signals to contamination by other active physiological processes which are simultaneously occurring in the vicinity. Furthermore, electrode, amplifier and instrumentation noise, variations in transducer placement from one recording to the next, the effects of respiration, and variations in every aspect of biomedical signals across populations and within individuals further contribute to the overall uncertainty.

1.5 Conspectus of the Thesis

The research detailed in this thesis investigates the application of signal processing methods to physiological signals, in particular, the heart sounds produced by the operation of the Carpentier-Edwards bioprosthetic heart valve.

Chapter 2 introduces the area of 'Heart Sound Processing' by first describing the function of the human heart, followed by a discussion detailing the origin of heart sounds and the physiological events which constitute a single heartbeat and hence the cardiac cycle. Examples are given of typical phonocardiograms recorded from normally functioning and dysfunctioning Carpentier-Edwards bioprostheses. The chapter concludes by reviewing publications reporting the analysis and processing of the sounds produced by the operation of prosthetic heart valves.

Chapter 3 describes the development of a data acquisition system to digitise and record the heart sounds produced by the operation of the Carpentier-Edwards bioprosthesis. Each stage of the design process is introduced, from signal transduction, following a review of suitable cardiac microphones; and the hardware, software and ergonomic decisions which dictated the choice of applicable equipment. A breakdown is also provided of the population of subjects with implanted Carpentier-Edwards bioprostheses selected for this thesis including details of the recording procedure.

Chapter 4 is concerned with techniques to preprocess the acquired PCG signal in the time domain with a view to accentuating the principal heart sounds over the background noise. This is followed by the extraction of the principal sound components of the heart sounds for further analysis. The chapter investigates the filtering of the PCG and describes the development of an automated heart sound extraction technique based on cross-correlation.

Methods for the frequency analysis of heart sounds are considered in chapter 5 with the aim of refining the use of spectral estimation techniques for this thesis. Algorithms considered for the frequency analysis were: the periodogram, the Bartlett power spectral density estimate, which reduces the variance of a conventional periodogram estimate through ensemble averaging;

ARMA-based, parametric linear modelling techniques, which attempt to synthesise the heart sound generation process; and Prony's method: a parametric modelling technique based on a damped sinusoidal model. Particular attention is paid to the physiological transient-oscillatory nature of the heart sound signal and the suitability of the spectral estimation techniques when analysing such a temporal signature.

The number of modelling coefficients used by the parametric spectral estimation techniques, *i.e.* the model order, is a very important variable when analysing bioprosthetic heart valve closing sounds. As the precise order of a principal component time series is not known *a priori*, variations in spectra can occur with different orders. Therefore determining an accurate order is essential. Chapter 5 also investigates methods which determine the optimal model order of time series. The model order selection criteria considered were: hypothesis-based methods, decision-based techniques, the FPE, the AIC, the MDL and the CAT; and methods which attempt to extract the optimum model order from the heart sound time series by first removing the numerical ill-conditioning inherent with the use of linear-algebra-based spectral estimation techniques.

The results from the frequency analysis of the heart sounds are presented and discussed as two chapters of this thesis. Chapter 6 focuses on the performance of the signal processing methods when evaluating the frequency spectrum of mitral and aortic components. The aim is to identify optimum signal analysis techniques for this thesis, capable of identifying features derived from the frequency spectrum of the heart sounds, which may be considered for use as heuristic parameters. Results are presented over the full range of recorded sounds. Chapter 7 concentrates on the relationship between the frequency spectrum of mitral and aortic components and the physiological and pathological functionality of the Carpentier-Edwards bioprostheses. Results are presented over the range of valve conditions.

Chapter 8 concludes by summarising the objectives, the methods and the findings drawn from the thesis. Finally, suggestions are proposed for possible extensions to the research.

Chapter 2

A Preface to Prosthetic Heart Valve Sound Processing

This chapter introduces the area of 'Heart Sound Processing' by first describing the function of the human heart, followed by a discussion detailing the origin of heart sounds and the physiological events which constitute a single heartbeat. The continuous rhythmic action of the heart produces the cardiac cycle, from which, electrical and acoustic measures may be obtained to provide an indication of patient well-being.

Since the first implant of a mechanical prosthesis to replace a defective native heart valve in 1960 [4], there have been a number of publications reporting on the analysis and processing of the sounds produced by the operation of these valves. The chapter concludes by reviewing this work, from the initial investigations which used analogue filter networks to the application of sophisticated signal processing methods of the present day.

2.1 The Human Heart

Every living organism however primitive, needs a circulatory system to fuel its parts and to remove waste. In the human body, this vital exchange is transacted by the fluid known as blood. The heart provides the motive power for this circulatory system.

The continuous rhythmic action of the heart is regulated by an 'electrical' timing system initiated by the pacemaker, *i.e.* a modified muscular tissue which generates the impulses that

trigger first the atria and then the ventricles to contract. A graphic record of this electrical activity with time is known as the ECG.

The heart is, in effect, a pump powering a double circuit. In the space of a single heartbeat, fresh oxygenated blood arrives from the lungs and enters the left side of the heart for dispersal to organs and tissues through the arterial network, while 'stale' or deoxygenated blood returns through veins to the right side of the heart where it is pumped to the lungs to be reoxygenated. The anatomy of the human heart is illustrated in Figure 2.1. It consists of two upper chambers known as the atria and two lower chambers referred to as the ventricles. The flow of blood between these chambers and away from the heart is controlled by four valves: the mitral, the tricuspid, the aortic and the pulmonary as shown in Figure 2.1. The mitral and tricuspid valves are interposed between the atria and ventricles and are collectively referred to as the atrioventricular valves. The smaller aortic and pulmonary valves are situated at the juncture of the ventricles and the arterial network and are commonly known as the semilunar valves. These cardiac valves are composed of tough but flexible cusps or leaflets of fibrous tissue, comprising two to three cusps symmetrically arranged around the circumference of an orifice and secured at their base by a fibrous ring. The valves permit a unidirectional flow of blood through, and away, from the heart.

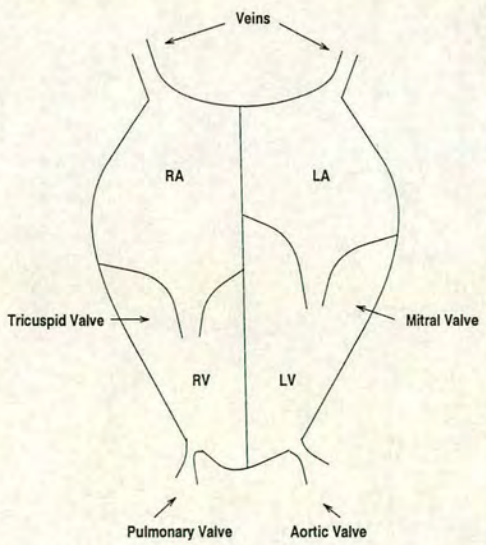

Figure 2.1: *Simplified anatomy of the human heart. RA = right atrium, RV = right ventricle, LA = left atrium and RV = right ventricle.*

2.2 The Origin of Heart Sounds

The exact means by which heart sounds are produced has been a contentious issue. Two opposing theories have been proposed to account for the generation of the sounds: the valvular

theory [8, 12] and the cardiohaemic system theory [13, 23]. The valvular theory asserts that as a result of the pressure differentials across the valves (which originate and reverse during the two contraction phases of the cardiac cycle), the sounds heard by auscultation arise directly from the closing of the leaflets. The cardiohaemic system theory, on the hand, ascribes to the theory that the sudden halting of blood by the closing of the leaflets sets the whole cardiohaemic system into vibration, *e.g.* the valve leaflets, the cardiac walls and adjacent structures, and the blood contained within the chambers of the heart.

The cardiohaemic system theory arose mainly as a result of work carried out on dogs in the United States by Luisada *et al.* [13, 23]. The basic structure of the heart is common to all mammals and dogs exhibit the same sound components and characteristics as humans. Luisada assumed that heart sounds were nonvalvular in origin and that the apposition of the valve leaflets should coincide exactly with the reversal of pressure (assumed as valve closure) in the atrium and ventricle. By simultaneously recording PCGs at the chest surface and intracardiac pressures using catheter tip micromanometers, Luisada observed a delay of 30ms between the crossover of the pressure gradient across the valves and the first vibrations registered in the PCG. As a result of this experimental evidence, Luisada concluded by discounting the valvular theory in the genesis of heart sounds. He proposed that the sounds were a result of the vibration of the cardiohaemic system as a whole.

As a result of work pioneered by Leatham *et al.* [8, 12], the valvular origin of heart sounds was the dominant theory in the U.K. Leatham, who had always been a proponent of the valvular theory, pointed out the weakness in the cardiohaemic theory lay in the expectation that the reversal of a pressure gradient across a valve should coincide directly with valve closure. His objection was that blood flowing through an open valve has momentum and the reversed pressure gradient takes a finite time to halt blood flow before the valve can close. Gradient crossover thus precedes valve closure by a variable interval influenced by the flow rate and the impedance characteristics of the downstream current [24]. To substantiate his argument, Leatham [25] later provided evidence using echophonocardiography. This showed that the onset of a heart sound as registered by a PCG was coincident with the moment of apposition of the valve leaflets.

Laniado *et al.* [26, 27] further validated the valvular origin of heart sounds by suturing electromagnetic flow probes in the annulus of mitral valves and in the ascending aorta just above the aortic valve. By observing valve movement using cinefluoroscopy to photograph cusp action, they demonstrated that blood continues to flow for 30 to 40ms after the crossover of pressure and that the vibrations registered in the PCG appear simultaneously after the cessation

of flow.

In recent years, data collected using newer methods, *e.g.* ultrasound echocardiography, has led to a reappraisal of the existing theories. The areas of investigation have been concentrated on the timing relationship between the amplitude of heart sounds and factors such as the separation of the valve leaflets before closing or their speed at closing [28]. In addition, abnormal splitting of the sounds has been considered [29] disturbances in the electrical conduction system, *e.g.* left and right bundle branch block, or mechanical defects, *e.g.* valvular stenosis. Craige *et al.* [30] demonstrated by simultaneously using echocardiography and phonocardiography that the first component of the first heart sound is synchronous with apposition of the mitral valve leaflets, and similarly, the second component is synchronous with the closing of the tricuspid valve. Since then, the valvular theory has been in the ascendant.

2.3 The Cardiac Cycle

The functioning of the human heart produces two principal sounds: the first heart sound (S1) and the second sound (S2). During ventricular evacuation, *i.e.* the circulation of oxygenated blood from the left ventricle to organs and tissues, the mitral and tricuspid valves are shut. Blood having had all the oxygen absorbed from it returns to the right atrium through veins, and reoxygenated blood from the lungs enters the heart and flows into the left atrium. The closed mitral and tricuspid valves prevent the blood accumulating in the atria gaining access to the ventricles. Once ventricular contraction (evacuation phase) has ended, the pressure differential reverses across the atrioventricular valves, forcing them to open and allowing the blood in the atria to flow rapidly into the ventricles. At this point the ventricles begin to contract, which causes the blood to attempt to flow back into the lower pressure atrial chambers. This reverse flow of blood is caught and arrested by the snapping shut of the atrioventricular valves which causes the first heart sound (S1). The rising ventricular pressure ensures that the leaflets of the mitral and tricuspid valves remain tightly sealed. The closure of the atrioventricular valves marks the beginning of systole (cardiac action phase), or conversely, the end of diastole (cardiac relaxation phase). The ventricular walls continue to contract and the pressure in the enclosed blood rises. Whenever the pressure becomes too great for the semilunar valves to withstand, the aortic and pulmonary valves open and the pressurised blood is rapidly ejected into the arteries. While the ventricles are being evacuated, the pressure in the remaining blood decreases with respect to that in the arteries. This pressure gradient causes the arterial blood to attempt to flow back into the ventricles. However, this reflux catches the cusps of the semilunar valves and

causes them to seal the orifice thereby abruptly stopping the flow and producing the second heart sound (S2). The closure of the semilunar valves marks the end of systole or conversely, the beginning of diastole. This complete sequence of events repeats and is referred to as the cardiac cycle.

The superior size of the left side of the heart leads to the fact that the sounds produced by the shutting of the mitral and aortic valves are often the loudest. In addition, ventricular contraction commences in the left ventricle, with left-sided sounds preceding right-sided components, *i.e.*. the mitral component precedes the tricuspid sound in S1 and the aortic component leads the pulmonary sound in S2. The separation between the aortic and pulmonary components in S2 can be influenced by respiration: increases with inspiration. This aids the extraction of the aortic component from the pulmonary sound for further analysis. S1 occurs at the onset of ventricular contraction and corresponds temporally to the QRS complex in the ECG signal, while S2 occurs during ventricular relaxation and corresponds approximately in time to the T-wave in the ECG. Simultaneously recording both signal allows identification of the principal heart sounds within the PCG. Figure 2.2 illustrates[1] a typical ECG and PCG signal set recorded from a subject with a normally functioning Carpentier-Edwards bioprostheses.

The intervals between S1 and S2 and S2 and S1 of the corresponding cycle (systole and diastole respectively) are normally silent. However, murmurs may occur in these intervals, *i.e.* sounds which arise when blood velocity becomes high in the presence of an irregularity through which the blood flows. Backflow (regurgitant) murmurs are produced by leaky valves while forward ('innocent') murmurs are associated with the ejection or flow of blood. Typical examples of the sounds and murmurs produced by the operation of normally functioning and dysfunctioning Carpentier-Edwards bioprostheses are illustrated in Figures 2.3 to 2.7. These sounds were recorded by the data-acquisition system described in chapter three.

2.4 Analysis of Prosthetic Heart Valve Sounds

Approximately a decade after the first implant of a prosthetic heart valve, Hylen *et al.* [31] were the first to apply signal analysis techniques to the sounds produced by the operation of prostheses. In their evaluation of mechanical prosthetic heart valves, an analogue instrument based on the sound spectrograph developed by Bell Laboratories was used to detect abnormally functioning Starr-Edwards ball valves. Hylen *et al.* report that in 24 of 25 control subjects

[1]The amplitude of all the sounds plotted in this thesis has been normalised to a value in the range (± 1), which represents the amplitude relative to the full input range of the twelve-bit analogue-to-digital convertor used by the data-acquisition system described in chapter three, *i.e.* $2^{12} = 4096$: +1 = 4096, 0 = 2048, -1 = 0.

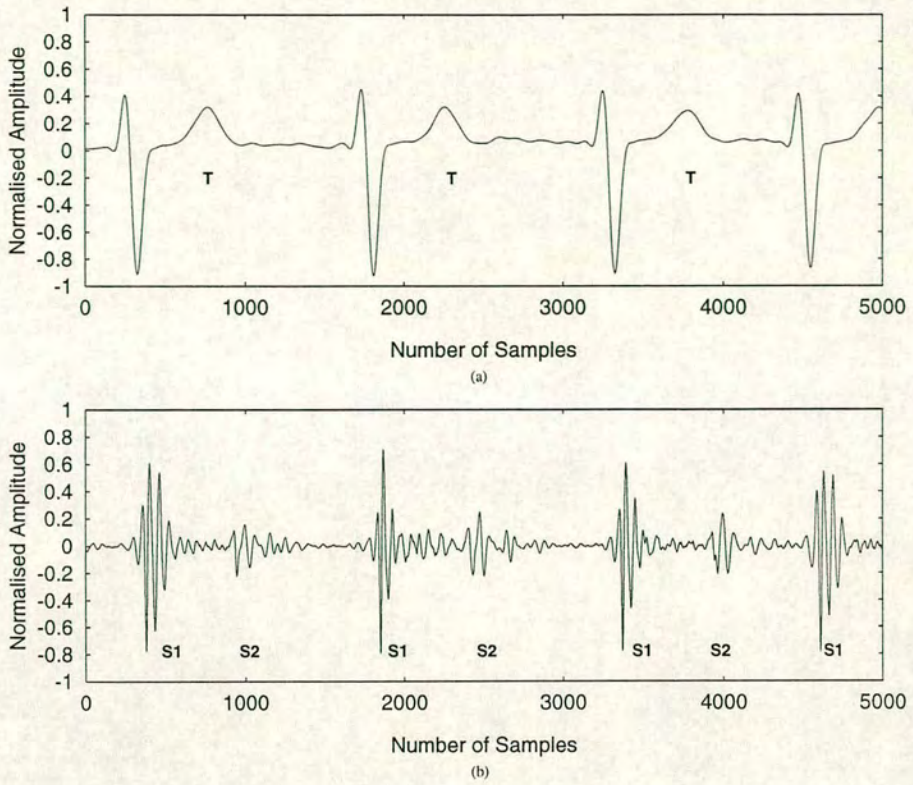

Figure 2.2: *Typical example of an ECG and PCG signal set recorded from a subject with a normally functioning Carpentier-Edwards bioprostheses. (a) ECG, where 'T' denotes the T-wave. (b) PCG (source: tm5).*

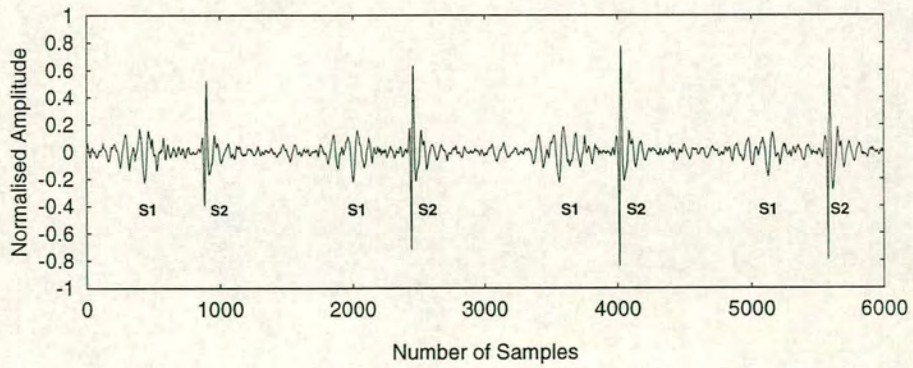

Figure 2.3: *Example of a PCG recorded from a subject with a normally functioning aortic prosthesis (source: jg3).*

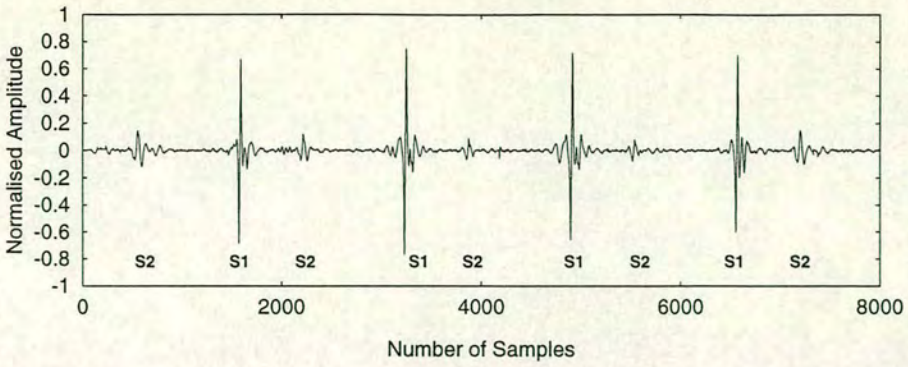

Figure 2.4: *Example of a PCG recorded from a subject with a normally functioning mitral prosthesis (source: dg4).*

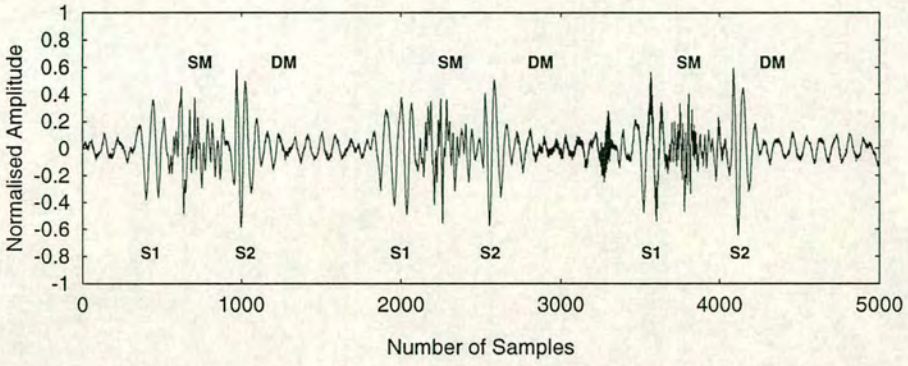

Figure 2.5: *Example of a PCG recorded from a subject with a leaky aortic prosthesis. Both systolic (SM) and diastolic murmurs (DM) are present (source: dt3).*

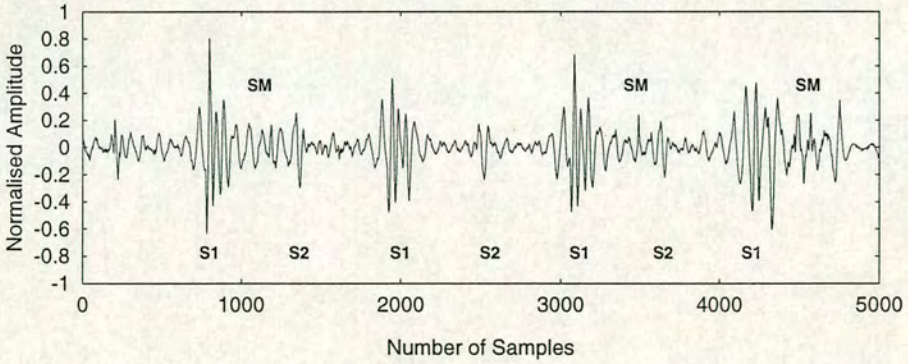

Figure 2.6: *Example of a PCG recorded from a subject with a leaky mitral prosthesis (source: is6).*

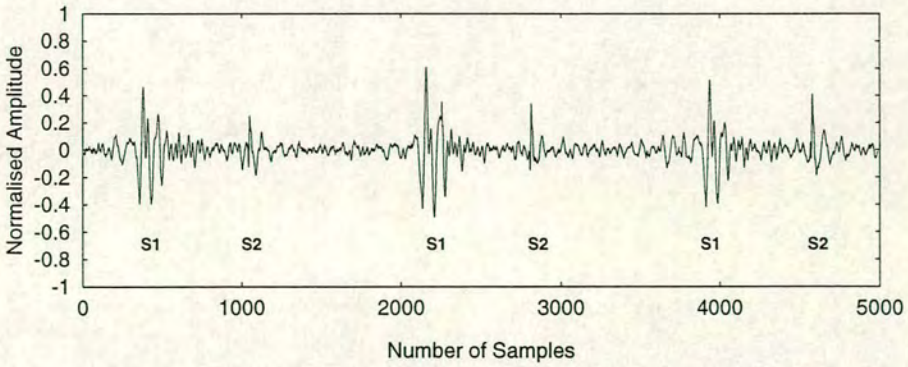

Figure 2.7: *Example of a PCG recorded from a subject with a stiffening aortic prosthesis (source: mh4).*

with implanted normally functioning aortic prostheses, the maximum frequency of the opening sound produced by operation of these valves was greater than 1.3kHz. In 11 of 12 patients with ball variance[2] of the aortic prosthesis documented at reoperation, the maximum frequency was observed to be less than 1.3kHz. Using an octave-band analyser, Gordon *et al.* [32] published similar results in 1974 from subjects having dysfunctioning mechanical ball and disc valves.

From 1977-1980, Kagawa *et al.* [33,34] developed a realtime sound spectral analyser based on a ceramic mechanical filter and a heterodyne technique to detect dysfunctioning implanted mechanical heart valves. Kagawa *et al.* observed that the opening and closing sounds produced by the operation of normally functioning Starr-Edwards ball and Björk-Shiley disc prostheses are characterised by mean dominant frequencies (normalised maximum amplitude of 0dB) at 2.25kHz and 2.15kHz and 1.41kHz and 2.07kHz respectively. For thrombosed prostheses, the adhesion of thrombus on the valve buffered these high-frequency components, with the dominant frequencies observed to decrease by more than 600Hz. For some of these subjects, no abnormal findings were obtained using echocardiography or catheterisation. More recent results obtained using this instrument [35] demonstrate that the heterodyne spectral analyser is useful but not sensitive enough to detect all cases of thrombosed mechanical prostheses.

In 1981 and then again in 1984, Stein *et al.* [36–38] were the first to analyse the sounds produced by the operation of bioprostheses: the Hancock porcine xenograft. Using the fast Fourier transform (FFT), Stein *et al.* report that the closing sounds (S1 and S2) produced by the operation of eighteen normally functioning mitral and seventeen normally functioning aortic Hancock bioprostheses are characterised by mean dominant frequencies of 51Hz and 63Hz respectively. Degenerated calcified mitral and aortic valves are characterised by mean dominant frequencies at 95Hz and 109Hz respectively.

In 1983, Foale *et al.* [39] carried out a study on thirty-seven subjects with implanted aortic porcine bioprostheses. Results show that the sounds produced by the operation of sixteen Hancock, ten modified Hancock (excision of the supportive band) and nine Carpentier- Edwards normally functioning valves implanted from two weeks to sixty-one months are characterised by a mean dominant frequency of 89Hz and a second peak of lower amplitude having a mean frequency at 154Hz. Patients with dysfunctioning bioprostheses having degenerated leaflets are characterised by a mean dominant frequency of 139Hz and a second peak of lower amplitude at 195Hz.

Another study in 1983 conducted by Joo *at al.* [40] reports that a pattern recognition al-

[2]Ball variance is defined as any physical or chemical alteration to the poppet in the prosthesis.

gorithm is useful in the diagnosis of aortic Hancock porcine bioprostheses. A feature vector comprising the two most dominant frequencies was derived from the acoustic characteristics produced by twenty prostheses: thirteen normally functioning and seven degenerated valves. This vector was used to design a Gaussian classifier to distinguish between normally functioning and degenerated bioprostheses. The performance of the classifier was evaluated using another test set of 20 implanted Hancock bioprostheses: fourteen normally functioning and six dysfunctioning valves. Seventeen of these twenty prostheses were correctly classified.

From 1986 to 1989 Durand *et al.* [41–46] characterised the temporal and spectral signature of the closing sounds produced by the operation of normally functioning bovine Ionescu-Shiley bioprostheses. By investigating the effects of truncation and signal-to-noise ratio on the closing sounds, as well as the modelling of sounds using an exponentially decaying sinusoid model, results demonstrate that accurate estimation of spectral features, *e.g.* dominant peaks and metrics associated with the frequency bandwidth, cannot be achieved using a single spectral estimation technique. It was observed the the FFT is the best technique to extract the most dominant frequency peak, while ARMA-based parametric methods are more accurate for evaluating the second most dominant peak and indices associated with the bandwidth and area of the spectrum.

Durand *et al.* [47] also used a Bayesian classifier to evaluate the diagnostic potential of spectral features derived from the sounds produced by fifty-seven normally functioning and forty-nine degenerated Hancock porcine bioprostheses. Results show that by separately considering mitral and aortic prostheses, the mean correct classification rate using the 'holdout' method is 77% for normally functioning and dysfunctioning mitral prostheses. The percentage of false positives is 15% and that of false negatives 30%. Likewise, for aortic valves, the mean correct classification rate is 71%, with the percentage of false positives 32% and that of false negatives 26%. Durand *et al.* [48] also compared the performance of the Bayesian classifier to that of the nearest-neighbour classifier using the 'leave-one-out' method. Results show that the best performance of both classifiers was above 94%, with sensitivity and specificity above 90%.

2.5 Summary and Conclusion

This chapter introduces the area of 'Heart Sound Processing' by first describing the functionality of the human heart, followed by a discussion detailing the origin of heart sounds and murmurs, and the dynamic events which constitute the cardiac cycle. Typical examples are illustrated of

sounds recorded from normally functioning and dysfunctioning mitral and aortic Carpentier-Edwards bioprostheses.

Since the first implant of a mechanical prosthesis to replace a defective native heart valve, there have been a number of publications reporting on the analysis and processing of the sounds produced by the operation of prosthetic heart valves. The chapter concludes by presenting a review of such work.

Chapter 3

Data Acquisition and Heart Sound Recording

In this thesis, the data to be processed is real, *i.e.* must actually be acquired as opposed to being generated numerically. This chapter investigates the development of a data-acquisition system to digitise and record the sounds produced by the operation of the Carpentier-Edwards bioprostheses. The design commences with a review of appropriate cardiac transducers, to convert sounds measured noninvasively at the chest surface to an equivalent electrical signal; followed by a survey of suitable analogue-to-digital conversion circuitry and computers to digitise and store the acquired sound samples respectively. Particular attention is directed towards the hardware, software and ergonomic design of the data-acquisition system to ensure efficient and high-quality reproduction. In addition, the design is included of some signal conditioning circuitry: a PCG preamplifier and an anti-aliasing filter.

The following sections also provide a breakdown of the population of subjects with implanted mitral or aortic Carpentier-Edwards bioprostheses selected for this thesis, and a description of the procedure for recording signals from patients.

3.1 Phonocardiographic Transducer

An acoustic-electro transducer is required to convert the heart sounds measured at the chest surface (displacement) into a proportionate electrical signal. Two major types of phonocardiographic transducers are commercially available: air coupled and direct coupled devices.

Air microphones are characterised by a cavity which is placed at the appropriate heart sound recording site on the chest surface. The air in the closed cavity acts as a transmission medium between the chest surface and a membrane coupled to a mechanical-electrical transducing device. Direct-coupled transducers, on the other hand, such as contact microphones, have an area which is directly applied to the chest surface making contact with a transducing element [49]. For both types of cardiac microphone, the transduction principle can be based on piezo-electric, magnetic or capacitive devices [13].

Recording the acoustic output produced by the operation of the Carpentier-Edwards bioprostheses presents several unique problems. Foremost, is the requirement that the detection be obtained noninvasively. Purely from a measurement perspective, the ideal would be to place the transducer within the chambers of the heart. However, adopting such an approach is clearly undesirable, particularly as this thesis is investigating the potential of an alternative noninvasive physiological measurement technique. The requirement of noninvasive measurement introduces a second problem: that the microphone is remote from the point of origin of the sounds. This separation exposes heart sounds to contamination by other active physiological processes, with the signal measured at the chest surface conditioned by the these processes and by the characteristics of the thorax as the sounds travel to the chest surface.

The ideal phonocardiographic transducer should produce an electrical output that is a faithful undistorted representation of the sound energy present at the input. In terms of dynamic range, the microphone should be capable of converting with equal fidelity sounds at both extremes of the frequency spectrum. In addition, the transducer should be insensitive to any extraneous ambient noise. After a review of cardiac microphone designs and a survey of appropriate transducers that were commercially available in 1991 [50–59], a contact microphone was selected to convert the sounds produced by the operation of the Carpentier-Edwards bioprostheses into an electrical signal. Air-coupled transducers were rejected because of their sensitivity to ambient noise. Also, previous work by Schwartz *et al.* [58] demonstrates that less than 1% of the incident sound energy is transmitted across the chest-air surface as a result of the impedance mismatch between the chest and air. Two models of contact microphone were available in 1991: the HP-21050A contact sensor marketed by Hewlett-Packard and the EMT25C phonocardiographic transducer marketed by Siemens-Elema. Due to its superior specification, in particular, a flat-frequency response from 0.02Hz to 2kHz, the HP-21050A contact sensor was selected for this thesis. This transducer was used in some of the previous research reported in chapter two [40,42–47]. Based on the structural properties of the porcine tissue used in the design of the Carpentier-Edwards bioprostheses [60–63], and the frequencies in chapter two reported by previous analyses of the

sounds produced by the operation of bovine bioprostheses, the Hancock porcine xenograft and native heart valves [36–48, 64], *i.e.* valves with similar construction to that of the Carpentier-Edwards bioprostheses, a flat-frequency response from 0.02Hz to 2kHz is appropriate for this thesis. The head of the HP-21050A contact sensor weighes 100g with a sensitivity of 10μV/dyne. Furthermore, it rejects extraneous ambient noise. The transduction principle of the HP-21050A contact sensor is based on the piezo-electric effect, where cardiac sounds at the chest surface excite a piezo-electric material which in turn generates a proportionate output alternating voltage across a crystal.

3.2 Design and Development of Data Acquisition System

A data-acquisition system based on a portable computer and an analogue-to-digital converter was developed to digitise and record the sounds produced by the operation of the Carpentier-Edwards bioprostheses. Heart Sounds are first measured noninvasively using the HP-21050A contact sensor, the output from which is conditioned (a PCG preamplifier and an anti-aliasing filter) to provide an analogue signal of a voltage range suitable for input to the data-acquisition system. To ensure high-quality reproduction, a number of significant hardware and software design considerations dictated the development of this system:

1. The need for the complete system to be portable to facilitate the transportation of equipment between recording venues.

2. The need for the system to operate from both a standard mains supply as well as a battery. During the recording of sounds, a battery ensures that no further electrical isolation is required between the subject and the equipment.

3. The analogue-to-digital converter should provide the necessary range of sampling frequencies to accurately digitise (reproduce) the recorded heart sounds and provide at least two bipolar analogue inputs. Two signals are to be recorded: the PCG and the ECG[1] Furthermore, the analogue-to-digital converter expansion card must physically fit within a portable computer, function when the computer is powered by either a mains supply or by battery.

[1] Lead 2 of the ECG signal was recorded from all subjects using the Siemens-Elema Mingocard 3 ECG Recorder. This unit was available for use at each of the recording venues and provides an analogue output of lead 2 of the ECG which was connected directly to the second analogue input of the data-acquisition system.

4. The power requirements of the analogue-to-digital converter are minimal to conserve as much battery power as possible for the actual recording of sounds. Immediately after sampling, the power demands of the hard-disc motor when storing the acquired samples further limits the overall time available for the recording of sounds.

5. The need for the system to provide a full graphical display of the signals being acquired before and during the recording of sounds. A display aids verification of signal strength, *i.e.* good signal-to-noise ratio (SNR), as well as avoiding the need to attach an additional display unit such as a cathode-ray oscilloscope (CRO) to the data-acquisition system [65–67]. Figure 3.1 illustrates a typical example of the graphical display provided by the acquisition software during the recording stage. The top trace (channel 1) shows an ECG, while the bottom trace (channel 2) a PCG. The software allows the timebase and amplitude variables of both channels to be preset prior to recording.

   Originally, a digital CRO was considered for use as the display device. However, utilising the display provided by the computer makes the complete system more portable. In addition, it was decided that by having only one major item of external hardware attached to a subject, that this would present an overall less 'intimidating' and less traumatic environment for the subject during the recording process.

After a review of appropriate computers and analogue-to-digital converter expansion cards available in 1991 [68–75], the Elonex LT-320X laptop personal computer and the twelve-bit ADC-42 input/output expansion card marketed by Blue Chip Technology were selected for this thesis. The specifications of both these items of hardware fulfil the design criteria. In total, the data acquisition system comprises three items of hardware: a portable computer fitted with an analogue-to-digital converter, the HP-21050A contact microphone and a small box containing some conditioning circuitry (a PCG preamplifier and an anti-aliasing filter). Figure 3.2 illustrates the major components of the data acquisition system and Figure 3.3 shows a photograph of the developed system. During the development of the data-acquisition system, particular attention was paid to the environment in which the system was to be used. During the actual recording of sounds, it is desirable to minimise operator-computer interaction. After having located the optimum position in which to place the transducer (best SNR), the remainder of the recording process is automatically controlled by the computer. At the start of the recording procedure, a tone is emitted by the computer. This is followed by a second tone fifteen seconds later to indicate the end of sampling. A final-third tone is emitted after the acquired samples have been stored on disc. Writing the samples to disc after recording, ensures

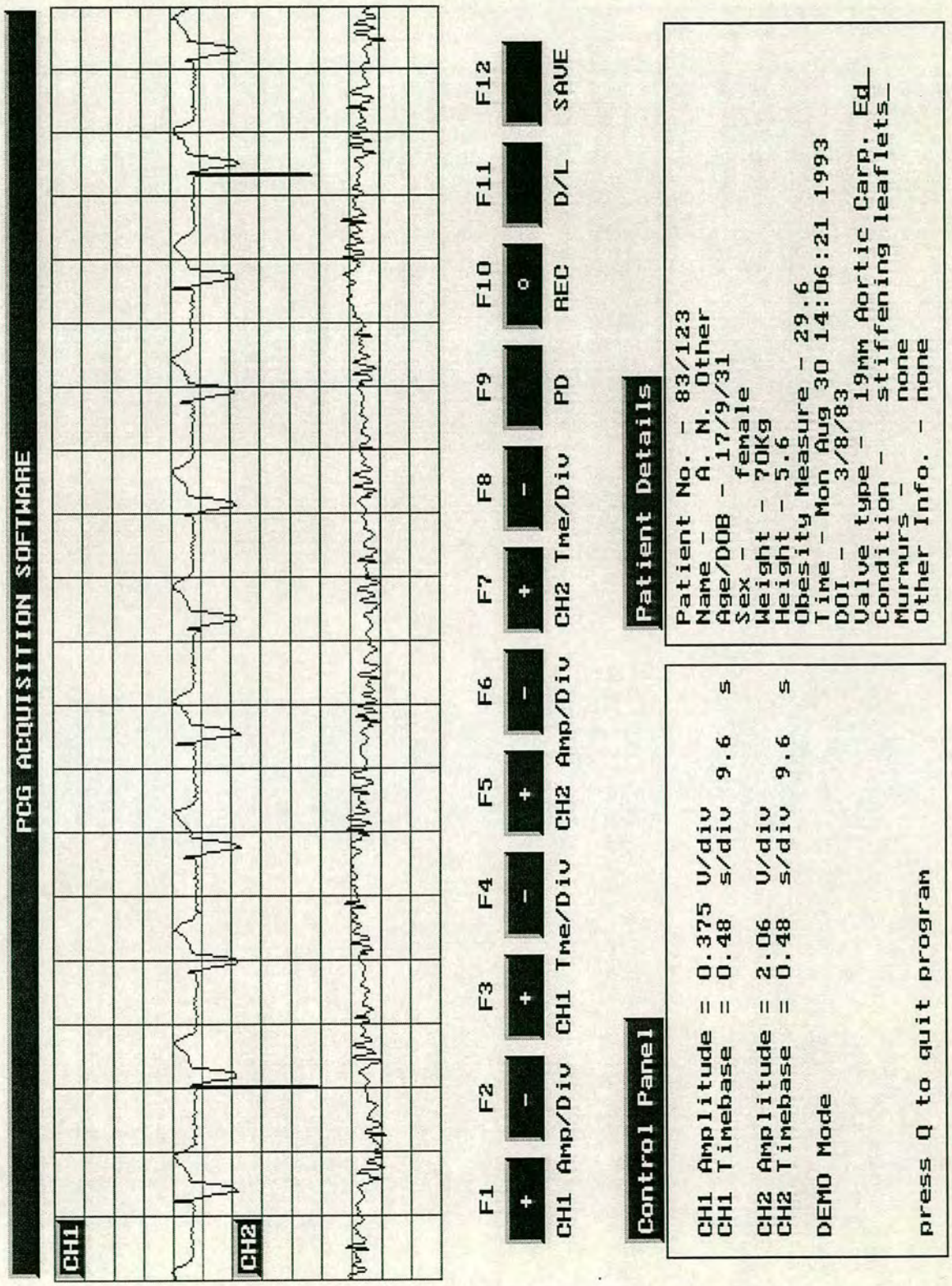

Figure 3.1: *Typical example of the graphical display provided by the acquisition software during the recording of sounds.*

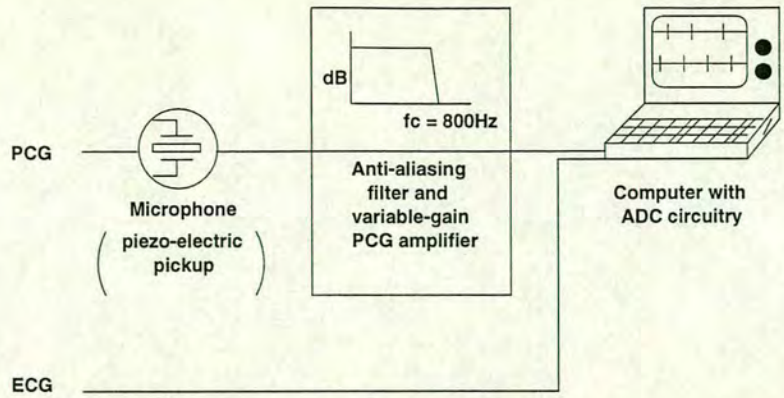

Figure 3.2: *Major components of the data-acquisition system.*

that only a single initiation of the hard-disc motor is required, in order to preserve battery power. On average, a battery lasted seventy minutes, equivalent to recording five fifteen-second records from four different subjects. A maximum sampling duration of fifteen seconds was imposed by the memory management control as a result of the segmented architecture of the Intel 80386 microprocessor used by the Elonex LT-320X computer [76].

3.3 Phonocardiographic Signal Conditioning

A PCG preamplifier was designed to amplify the output from the HP-21050A contact sensor ($\pm$ mV range) to a level suitable for input to the data-acquisition system ($\pm$ 5V). The design was based on a high-performance, low-noise, low-power operational amplifier, the TL064 marketed by Texas Instruments; ideal for battery-powered portable instrumentation. The phonocardiographic output from the preamplifier was then bandlimited using an anti-aliasing filter. The design of the anti-aliasing filter was based on a sixth-order, low-pass Bessel filter. A Bessel filter possesses optimum phase linearity (constant time delay with frequency) thus preserving the relative phasing of signal events. Based on the structural properties of the tissue used in the design of the Carpentier-Edwards bioprostheses [60–63], and the frequencies in chapter two reported by previous analyses of the sounds produced by the operation of bovine bioprostheses, the Hancock porcine xenograft and native heart valves [36–48, 64], *i.e.* the major concentration of spectral energy occurs in the region between 50Hz and 250Hz, the cut-off frequency of the low-pass anti-aliasing filter was selected to be 800Hz. Thus, the complete data-acquisition system has a flat bandwidth from 0.02Hz to 800Hz, ensuring optimum reproduction of all necessary sounds for this thesis. Both the PCG and the ECG were subsequently sampled at a rate of 2kHz.

Figure 3.3: *Photograph of the data-acquisition system. From left to right: the phonocardiographic transducer, the box containing the conditioning circuitry and the computer.*

3.4 Patient Population

The population of subjects with implanted Carpentier-Edwards bioprostheses selected for this thesis were chosen over an eleven-month period from patients admitted to The Royal Infirmary of Edinburgh for post-operative follow-up visits. This included subjects with suspected abnormality in valve function and routine visits by patients in the recovery period following valve replacement. Recordings were also obtained from subjects with dysfunctioning bioprostheses one day prior to prosthesis replacement. In addition, subjects were contacted who had undergone Carpentier-Edwards bioprosthetic heart valve implantation at The Royal Infirmary of Edinburgh between 1990 and 1992 and asked to attend a recording session at the Astley Ainslie Hospital in Edinburgh. This involved first writing to the patients' physicians to confirm the subject's present state of health, and then directly to the subject. In total, forty recordings were obtained, sixteen from subjects with the Carpentier-Edwards bioprostheses implanted in the mitral position and twenty-four from implanted aortic valves. The condition of each prosthesis was diagnosed by a cardiologist with all patients undergoing a physical examination which included: assessing the symptomatic state of the subject at the time of recording, auscultation, electrocardiography, chest x-rays and ultrasound echocardiography.

3.4.1 Population of Subjects with Mitral Prostheses

In total, sixteen recordings were obtained from subjects with implanted mitral bioprostheses. This group of patients was divided into two groups. Group One consists of twelve subjects with no symptoms of valve degeneration or dysfunction, regurgitant murmurs, systolic/diastolic beats or other auscultatory signs of valve deterioration, with all aspects of clinical and cardiac examination indicating normal prosthesis function. These subjects served as the control set as there was no evidence of bioprosthetic heart valve malfunction. Group Two consists of four patients diagnosed as having leaky valves. A detailed description of the population group with implanted mitral prostheses is given in Table 3.1. For each subject, the following information is included: a measure of obesity known as the body mass index (BMI), where BMI = $\frac{\text{weight}}{(\text{height})^2}$ (kg/m^2) [77], the size of each prosthesis in millimeters, where the size denotes the internal orifice diameter of the sewing, and the time of recording (TOR) in months after valve implantation.

3.4.2 Population of Subjects with Aortic Prostheses

In total, twenty-four recordings were obtained from subjects with implanted aortic bioprostheses. This group of patients was divided into three groups. Group One consists of thirteen subjects with no symptoms of valve degeneration or dysfunction, regurgitant murmurs, systolic/diastolic beats or other auscultatory signs of valve deterioration, with all aspects of clinical and cardiac examination indicating normal prosthesis function. These subjects served as the control set as there was no evidence of bioprosthetic heart valve malfunction. Group Two consists of six patients diagnosed as having leaky valves, with several recordings obtained one day prior to prosthesis replacement. Group Three consists of five patients with abnormal prosthetic valve function diagnosed as due to stiffening calcified cusps. One subject in particular (patient twenty-four), had a valve which was diagnosed as both leaky and stiffening. A detailed description of the population group with implanted aortic prostheses is given in Table 3.2.

Patient No.	Age	Sex	BMI	Size	TOR
Group 1					
1	75	M	18.2	35	41
2	78	F	27.1	29	29
3	68	M	25.3	29	33
4	77	M	23.5	35	10
5	78	M	21.1	29	36
6	78	F	22.4	29	34
7	69	F	26.3	29	28
8	58	F	30.0	27	107
9	74	F	28.9	27	144
10	75	M	27.4	29	150
11	73	F	22.0	35	119
12	78	M	24.1	33	132
Group 2					
13	70	F	21.7	29	156
14	62	M	28.1	27	140
15	78	M	23.4	29	134
16	69	F	19.9	35	147

Table 3.1: *Population of subjects with implanted mitral prostheses.*

Patient No.	Age	Sex	BMI	Size	TOR
Group 1					
1	76	M	22.1	21	9
2	79	M	21.7	19	11
3	82	F	19.3	19	18
4	77	F	23.5	21	10
5	78	M	21.1	25	36
6	78	M	22.4	21	34
7	80	F	24.7	21	33
8	63	M	23.5	23	39
9	83	F	22.4	19	34
10	84	F	21.7	21	17
11	73	M	25.5	25	12
12	76	F	23.3	21	9
13	69	M	24.8	25	22
Group 2					
14	55	F	22.9	21	120
15	81	M	21.3	23	93
16	80	M	25.6	19	226
17	74	F	23.7	21	88
18	67	M	25.4	23	81
19	81	M	24.6	25	109
Group 3					
20	76	F	24.0	19	121
21	78	M	22.6	23	141
22	66	M	19.9	23	133
23	69	F	23.8	25	116
24	42	M	24.8	21	108

Table 3.2: *Population of subjects with implanted aortic prostheses.*

3.5 Recording Procedure

Recordings were performed with the subjects supine and with the patient's head elevated. In addition to greatly facilitating the recording of sounds, a greater appreciation of heart sounds is obtained with the subject in this position [1]. The contact microphone was placed on the patient's chest using a retaining rubber belt to ensure that the transducer remained in the ideal position during the recording. It was observed during initial recordings that not using a suction cup to provide an air-tight attachment of the microphone to the chest, resulted in more coherent recordings. For mitral prostheses, the microphone was positioned at the apex to emphasise the contribution of the mitral component to the PCG. Likewise, for aortic valves, the transducer was placed at the 2RIS (aortic area) as illustrated in Figure 3.4. Locally around these recording sites, the microphone was positioned at the point where maximum PCG signal strength was observed (best SNR). For subjects with aortic prostheses, recordings were obtained both during normal respiration and with the patient's breath held at full expiration. Recording at full

inspiration eliminates respiratory sounds and other artifacts. In addition, inspiratory separation of the aortic sound from the pulmonary component aids extraction of the aortic sound for further analysis [12]. For all subjects, lead 2 of the ECG signal was also recorded to provide a reference to cardiac events.

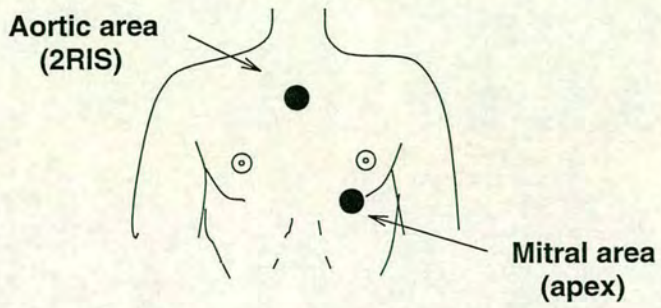

Figure 3.4: *Microphone positioning sites.*

3.6 Summary and Conclusion

This chapter investigates the design and development of a data-acquisition system to digitise and record the sounds produced by the operation of the Carpentier-Edwards bioprostheses. After a review of cardiac microphones, to convert the sounds measured at the chest surface to an equivalent electrical output; computers and analogue-to-digital conversion circuitry commercially available in 1991, a detailed description is included of the procurement of suitable equipment and hence the subsequent development of the data-acquisition system. The computer and the analogue-to-digital conversion circuitry chosen were: the Elonex LT-320X laptop personal computer and the ADC-42 input/output expansion card marketed by Blue Chip Technology. The phonocardiographic transducer selected for this thesis was the HP-21050A contact sensor marketed by Hewlett-Packard. The specification of this microphone includes a flat-frequency response from 0.02Hz to 2kHz, appropriate for the range of frequencies of the sounds produced by the operation of the Carpentier-Edwards bioprostheses; as well as being insensitive to extraneous ambient noise.

The chapter concludes by providing a breakdown of the population of subjects with implanted mitral or aortic Carpentier-Edwards bioprostheses selected for this thesis, and a description of the procedure for recording signals from patients.

Chapter 4

Time Domain Preprocessing of the Phonocardiogram

Preprocessing the PCG in the time domain prior to the frequency analysis of the principal heart sound components, can greatly facilitate the analysis and produce more accurate results overall. Effective signal processing results in the enhancement of the principal components and the reduction of noise.

The ultimate aim is the accentuation of the principal heart sounds to expedite the extraction of mitral or aortic components from each PCG record for subsequent spectral analysis. In this chapter, a technique is developed which automatically extracts these components from the PCG.

4.1 Enhancement of Principal Heart Sounds

The acquired PCG typically contains relatively high-frequency principal heart sounds superimposed on a low-frequency 'carrier'. The principal components are to be accentuated from this 'raw' composite signal[1] for further analysis. Fortunately, the spectral bandwidth of these sounds and the low-frequency artifact do not overlap, thereby, a linear-filtering operation may be applied to the PCG to remove the artifact. The time-varying low-frequency vibrations which

[1] Although the PCG record has been referred to as 'raw', at this stage in the analysis, this record will have been processed by the analogue, low-pass, anti-aliasing Bessel filter and subsequently digitised.

constitute this 'carrier' are due to instrumentation noise, respiration and the associated chest movements resulting from muscular contraction and relaxation.

Prefiltering[2] the PCG can be achieved using either dedicated, continuous-time hardware filters or equivalently, discrete-time filters implemented by evaluating a difference equation using software. The utility of a digital filter offers several inherent advantages over the analogue hardware filter. Firstly, a greater degree of precision can be obtained using a digital realisation, and secondly, to investigate the optimum filter cut-off frequency for bioprosthetic heart valve sounds, a greater range of digital filters can be built and tested with relative ease without having to encounter the practicalities of implementing their analogue hardware equivalents, *e.g.* negative inductance, the need for special components and input output impedance mismatch associated with cascaded analogue hardware designs [79–81].

A high-pass, nonrecursive, causal (impulse response = $h[n] = 0$ for $n < 0$) digital filter was used to remove the low-frequency artifact from the PCG. With nonrecursive filters, the present output, $y[n]$, depends only on present and previous inputs. The difference equation describing this digital filter is defined to be:

$$y[n] = \sum_{k=0}^{m} b[k]\, x[n-k] \tag{4.1}$$

where, $x[n]$, is the input PCG signal to be filtered, $b[k]$, are the filter multiplier coefficients (equivalent to the impulse response of the filter) and, m, is the number of coefficients. This filter implements the convolution sum directly where the lower and upper limits reflect the causality and the finite-duration characteristics of the filter. As the number of coefficients must be finite, a practical nonrecursive filter is known as a finite-impulse response (FIR) filter. Additionally, as there is no feedback between output and input, this filter is inherently stable [82,83]. FIR filters exhibit a linear-phase characteristic with no phase distortion, *i.e.* all frequency components which constitute a signal undergo the same delay thus preserving the relative phasing of signal events. Therefore the use of such a filter is ideal for processing heart sounds [84].

Based on the frequencies of the sounds produced by the operation of native heart valves [64], bovine and Hancock porcine bioprostheses reported in chapter two, and an investigation of suitable cut-off frequencies and an optimum number of coefficients (taps) by filtering many of the acquired PCG records, it was observed that the best SNRs were obtained, to a visual inspection, with a cut-off frequency of 20Hz and 320 coefficients (weights). The filter was

[2]Prior to filtering the PCG, the mean value was removed from each record. Signals with large d.c. levels or trends can corrupt the low-frequency end of the resulting spectral estimate [78].

designed using the 'window' method, which applied a Hamming window to truncate the impulse response of the filter [82, 85]. Figure 4.1 illustrates a typical example of the improvement achieved in the abstraction of the principal heart sounds from the low-frequency artifact using these parameters.

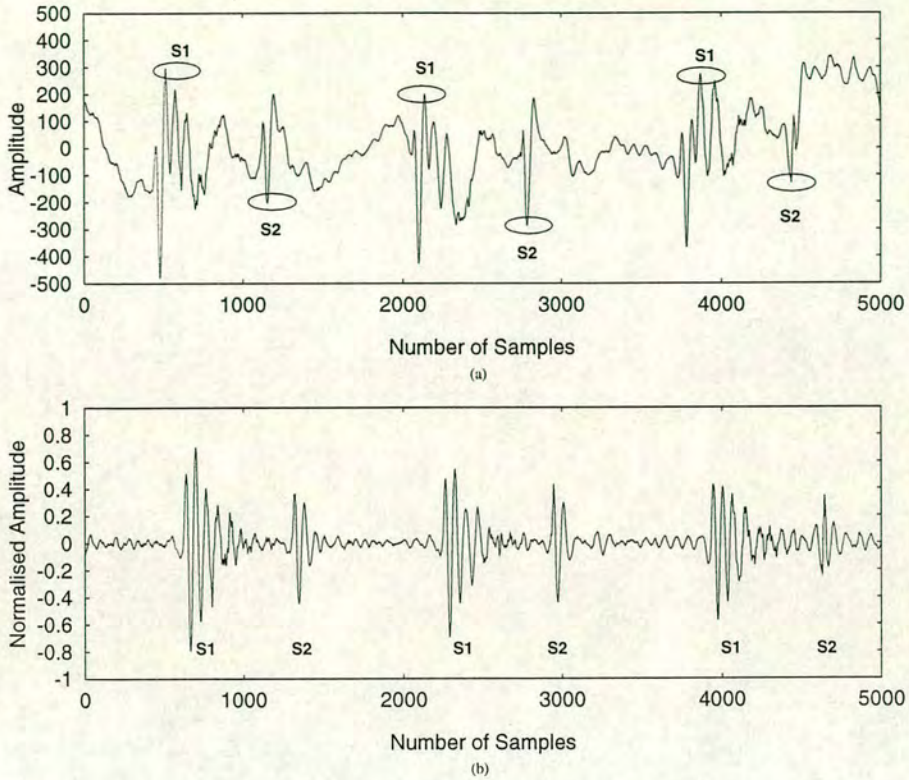

Figure 4.1: *Typical example of a PCG before and after high-pass filtering. (a) Before filtering. (b) After filtering (source: jp1).*

4.2 Extraction of Principal Heart Sound Components

The technique to be presented to extract mitral and aortic components from the PCG is based on initially manually identifying and selecting a representative sound from each PCG record under investigation, and matching this archetypal reference with similar successive occurrences, *i.e.* the other mitral or aortic components within each of the remaining cardiac cycles. The result of this comparison will be to identify the location of each of these other components within the PCG. A signal processing operation that provides a definitive quantitative measure of the degree to which two signal events are similar is **cross-correlation** [83]. The cross-correlation function is a time-averaged measure of shared signal properties, thus, making it particularly suitable for comparing random signal events such as heart sounds [86].

4.3 Cross-Correlation

The cross-correlation function, $\phi_{xy}[l]$, relating two finite-energy sequences $x[n]$ and $y[n]$ is defined to be:

$$\phi_{xy}[l] = \sum_{n=-\infty}^{\infty} x[n]\, y[n-l] \qquad \textit{for } l = 0,\ \pm 1,\ \pm 2,\ \ldots \tag{4.2}$$

where the index, l, is the time shift (lag) imposed upon sequence $y[n]$ relative to $x[n]$ and the subscripts xy on the cross-correlation function indicate the sequences being correlated. The order of these subscripts indicates the direction in which one sequence is shifted relative to the other. In (4.2) x precedes y, the sequence $x[n]$ remains unshifted while the sequence $y[n]$ is shifted l units in time: to the right for positive values of lag and to the left for negative values of lag.

In practice; however, both sequences $x[n]$ and $y[n]$, *i.e.* the PCG and the closing sound template, will be of finite duration and the cross-correlation function must be estimated from these finite records. In particular, when both $x[n]$ and $y[n]$ are causal sequences of finite duration N (N data samples indexed from $n = 0$ to $n = N-1$ and $[x] = [y] = 0$ for $n < 0$ and $n \geq N$), the range of the summation is altered in terms of these finite limits. The cross-correlation function estimate based on finite data records, $\hat{r}_{xy}[l]$, for positive values of lag is defined to be:

$$\hat{r}_{xy}[l] = \sum_{n=l}^{N-1} x[n]\, y[n-l] \qquad \textit{for } l = 0, 1, \ldots, N-1 \tag{4.3}$$

When attempting to automate the extraction of mitral or aortic components from a PCG, a further modification is required to (4.3). A fifteen-second PCG record (30,000 data samples) is to be correlated with a closing sound template typically having a duration in the range 20 to 80 ms (40 to 160 samples). If the PCG is $x[n]$, where $0 \leq n \leq N-1$, and the closing sound template is $y[n]$, where $0 \leq n \leq M-1$, the cross-correlation estimate defined in (4.3) is amended to account for the difference between the duration of the PCG and the closing sound template. As the template will always be of a shorter duration than the PCG, *i.e.* M < N, the cross-correlation of the PCG with the closing sound template for positive values of lag is defined to be:

$$\hat{r}_{xy}[l] = \sum_{n=l}^{M+l-1} x[n]\, y[n-l] \qquad \textit{for } l = 0, 1, \ldots, N-M \tag{4.4}$$

$$\hat{r}_{xy}[l] = \sum_{n=l}^{N-1} x[n]\, y[n-l] \qquad \textit{for } l = N-M+1, N-M+2, \ldots, N-1 \tag{4.5}$$

Implementation of (4.4) and (4.5) evaluate the cross-correlation estimate to the maximum

permissible positive lag based on the length of the PCG record and the closing sound template. When, $0 \leq l \leq N - M$, the template is shifted relative to the PCG and a constant number of product terms are involved in each summation. When, $N - M < l \leq N - 1$, the template is shifted relative to the end of the PCG record and the number of product terms involved in each summation decrements as the lag increments.

The amplitudes of the PCG and the template do not affect the shape of the cross-correlation estimate. Therefore as the scaling of these signal events is insignificant, the cross-correlation function is normalised to the range -1 to +1. This normalised cross-correlation estimate can be expressed as a percentage termed the **'Correlation coefficient'**, where a normalised cross-correlation coefficient of +1 equals 100%, *i.e.* a perfect temporal match between two signal events. The normalised cross-correlation estimate of the PCG with the closing sound template, $\hat{\rho}_{xy}[l]$, is defined to be:

$$\hat{\rho}_{xy}[l] = \frac{\hat{r}_{xy}[l]}{\sqrt{\hat{r}_{xx}[0]\,\hat{r}_{yy}[0]}} \tag{4.6}$$

where ,$\hat{r}_{xx}[0]$, and, $\hat{r}_{yy}[0]$, are the autocorrelation estimates at zero lag of the PCG and the closing sound template respectively. The autocorrelation function is a signal processing operation that provides a quantitative measure of the degree to which one part of a signal is similar to another part of the same signal. The autocorrelation estimate of a causal sequence $x[n]$ of finite duration N (N data samples indexed from $n = 0$ to $n = N - 1$ and $x[n] = 0$ for $n < 0$ and $n \geq N$) is defined to be:

$$\hat{r}_{xx}[l] = \sum_{n=l}^{N-1} x[n]x[n-l] \qquad for\ l = 0, 1, \ldots, N-1 \tag{4.7}$$

The autocorrelation estimate attains its maximum value at zero lag, *i.e.* a signal matches perfectly with itself at zero shift/lag, where it is equal to the mean-square value or average power [82].

4.4 Template Selection

Using cross-correlation, the extraction of either mitral or aortic components from a PCG requires the initial identification and selection of an archetypal reference to be used as the matching template. There are three options available for this selection: a single universal template for both mitral and aortic components for all subjects, a universal template for each principal component or the selection of a new template for each subject from the PCG under investigation.

The first and second options of using universal templates have the attraction that the initial user intervention required in selecting a representative sound is unnecessary. Such universal

templates would be chosen on the basis that they resembled idealised realisations with little or no background noise. However, from the examples of acquired sounds illustrated in section 2.3, there can be great variability in the temporal characteristics of heart sounds recorded from different subjects. Natural physiological differences exist throughout the patient population, *e.g.* differences in the acoustic transmission paths are related to a person's BMI. Variations in transducer placement from one recording to the next and the effects of respiration, *i.e.* splitting of A2 and P2, all further contribute to this variability. Consequently, the use of universal templates was rejected in favour of the third option, of initially manually selecting a representative reference from each PCG under investigation. This allows for the selection of a sound 'adaptive' to each patient recording, resulting in a more accurate analysis overall.

The selection of the closing sound template from the PCG was based on the following criterion: that the reference sound was representative of the remaining components within each of the other cardiac cycles of the PCG under investigation. The chosen component was extracted from the PCG delimited to include all significant data, *i.e.* the point at which the sound returned to the baseline. Figure 4.2 illustrates typical examples of mitral and aortic component templates extracted from first and second heart sounds respectively. The variability in the morphology of these components is clearly apparent, thus, substantiating the earlier decision of selecting a representative template from each PCG under investigation.

4.5 Mean Closing Sound

In addition to the automated extraction of mitral and aortic components from the PCG, an average component was computed from this ensemble. This mean sound is maximally correlated and time-aligned with the reference template, and is to be used by the model order selection criteria for quantitatively selecting an optimal order for the spectral estimation techniques to be discussed in chapter five. This technique of signal averaging is known as **coherent time averaging** [87–90], where coherence is established by aligning the maxima of the cross-correlation estimate between the reference template and the extracted sounds.

Provided that any PCG background noise is largely random (uncorrelated) from one beat to the next, the addition of successive repetitions of principal components results in a constructive enhanced signal with improved SNR, as the truly additive component time signal reinforces itself. The background noise, being random (uncorrelated) relative to the closing sound time signal, averages out to a constant level which reflects its mean value [86, 87, 91]. The effect of coherent time averaging is to maintain the amplitude of the mitral and aortic closing sounds

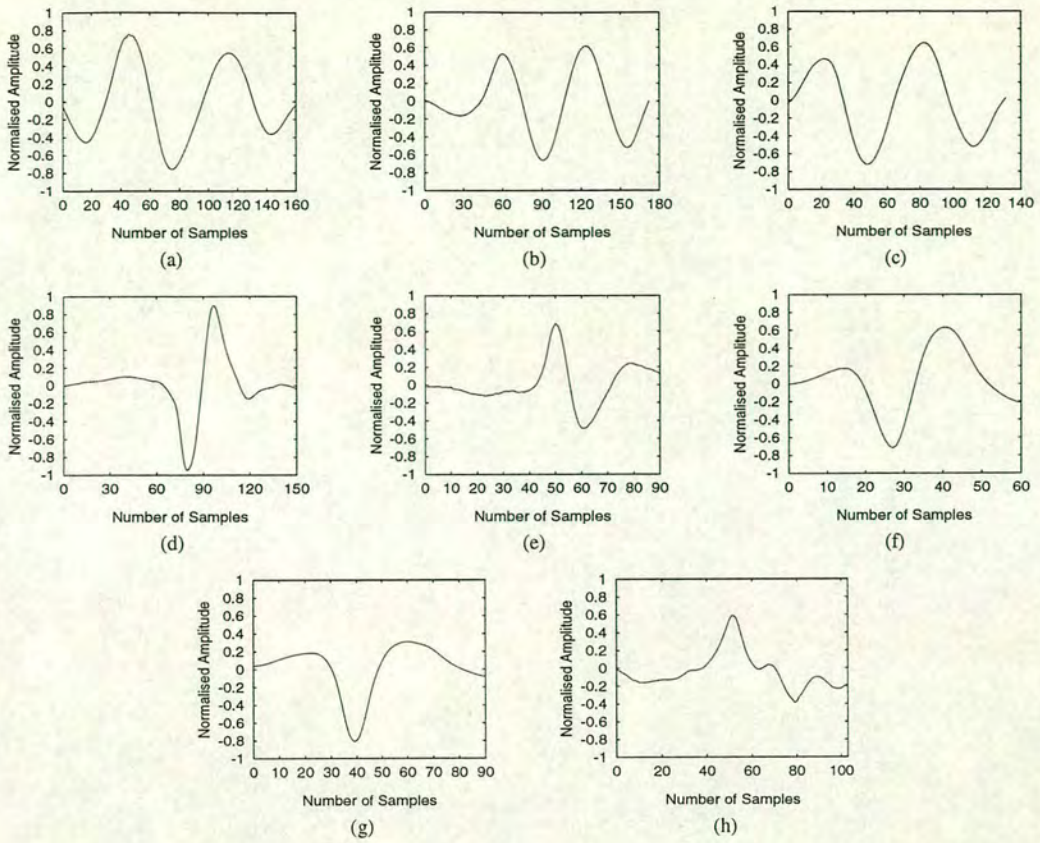

Figure 4.2: *Typical examples of mitral and aortic component templates extracted from first and second heart sounds respectively. (a-d) mitral component templates (sources: em1, jp3, jp1 and dg4 respectively), (e-h) aortic component templates (sources: an4, jg3, jg1 and jh6 respectively).*

and to reduce the variance of the noise by a factor N, where N is the number of sounds involved in the averaging [88]. In the ideal case, N averages will reduce noise by a factor of $\frac{1}{\sqrt{N}}$ with an improvement in the SNR of $\sqrt{N}$, *e.g.* a mean aortic component typically computed from eighteen aortic components extracted from a fifteen-second PCG record: the increase in SNR is $\sqrt{18}$ = 12.55 dB. In practice; however, properties of the background noise and the heart sound signal limit the efficacy of this averaging [82, 92]. For heart sounds, the sources of such background noise include: phonomyographic (PMG) muscle vibrations, amplifier and instrumentation noise. However, previous work [93] shows that the correlation between these noise sources and cardiac signals is negligible. Averaging over cardiac cycles also minimises contributions of undesirable transient sounds: T1 from M1 and P2 from A2. Figure 4.3 illustrates typical examples of mean mitral and aortic sounds computed from the mitral and aortic components automatically extracted from two fifteen-second PCG records. The extracted components are shown superimposed, highlighting the temporal alignment (maximum correlation) between each sound.

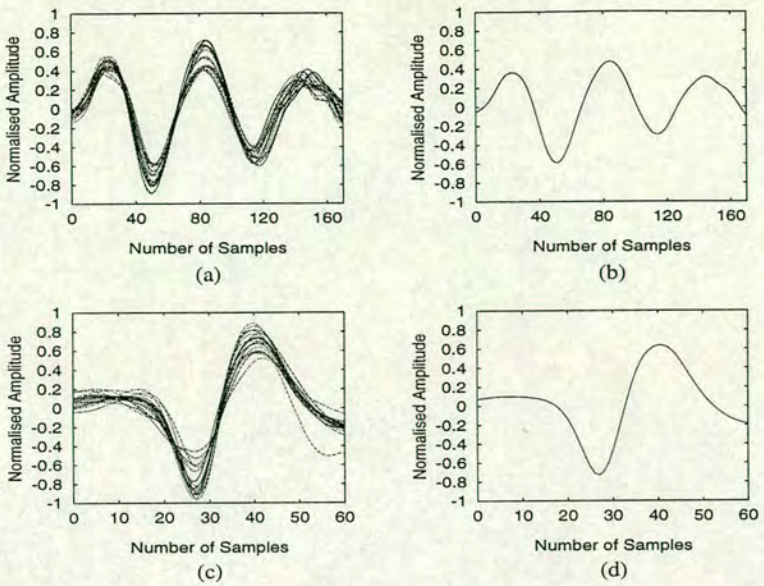

Figure 4.3: *Typical examples of mean mitral and aortic sounds. (a) Seventeen mitral components extracted from a fifteen-second PCG (source: jp1.snd1-17), (b) The computed mean mitral sound, (c) Seventeen aortic components extracted from a fifteen-second PCG (source: jg3.snd1-17), (d) The computed mean aortic sound.*

4.6 Cross-Correlation Output

As with all cardiovascular signals, locating an invariant, synchronising reference point is difficult because of biological variability. Normal cardiac function varies to some degree on a beat-to-beat basis, as cardiac excitation and contraction are controlled by a closed-loop process. This variability is manifest in the overall range in the amplitudes and structure of heart sounds. Furthermore, noise contamination from surrounding muscles (PMG vibrations), amplifier and instrumentation noise, variations in transducer placement from one recording to the next and the effects of respiration all further contribute to this variability. The net result can be an unpredictable variation in heart sound morphology from one beat to the next.

The use of a cross-correlation, template-based extraction approach results in maximally-correlated time-aligned sounds thereby overcoming the effect of any beat-to-beat delay that may have been introduced by biological variability. The result of the cross-correlation between the PCG and the reference template is to identify the location of the other mitral or aortic components within each of the remaining cardiac cycles of the PCG. Specifically, implementing this operation identifies the terminal points of these components, thus allowing for the automated extraction of components from the PCG.

4.6.1 Correlator Output Results: Method 1

When one of the principal heart sounds in each cardiac cycle has very large overall structure relative to the other, such that it can clearly be regarded to be the only dominant signal event in each cycle as illustrated in the examples shown in Figure 4.4, the result of the cross-correlation operation is to correctly identify the location of each of the remaining components within the PCG. Figures 4.5 and 4.6 illustrate the result of the cross-correlation operation for the PCG records identified in Figure 4.4(a and b) respectively.

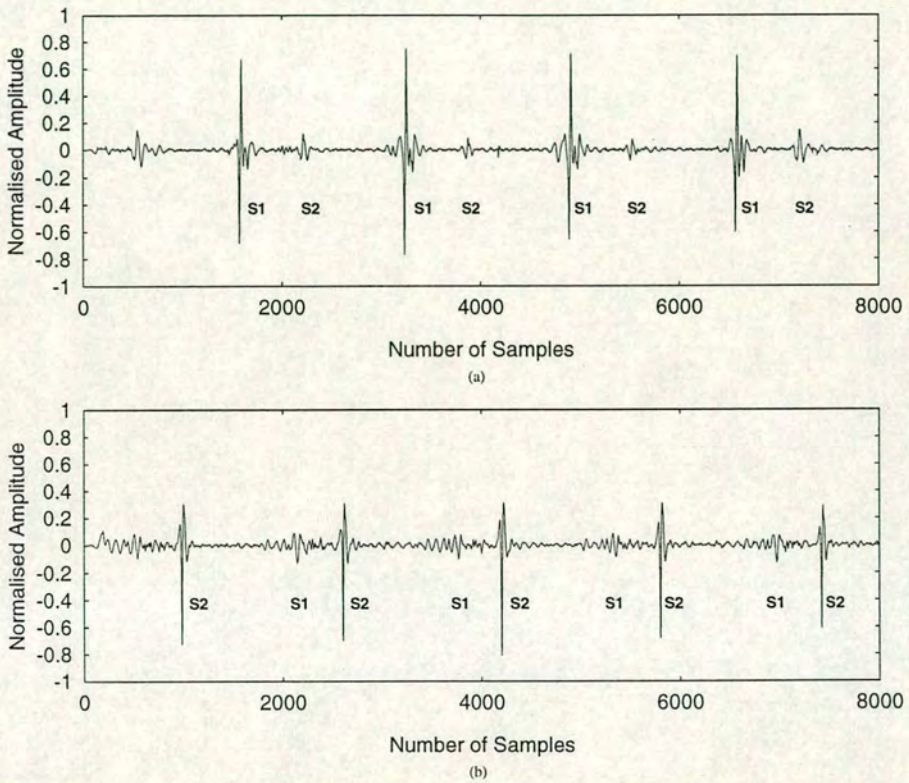

Figure 4.4: *Examples of PCG records where one principal heart sound is clearly the dominant signal event in each cardiac cycle, S1 is the first heart sound and S2 the second sound (a) Dominant first sound (source: dg4). (b) Dominant second sound (source: jg1).*

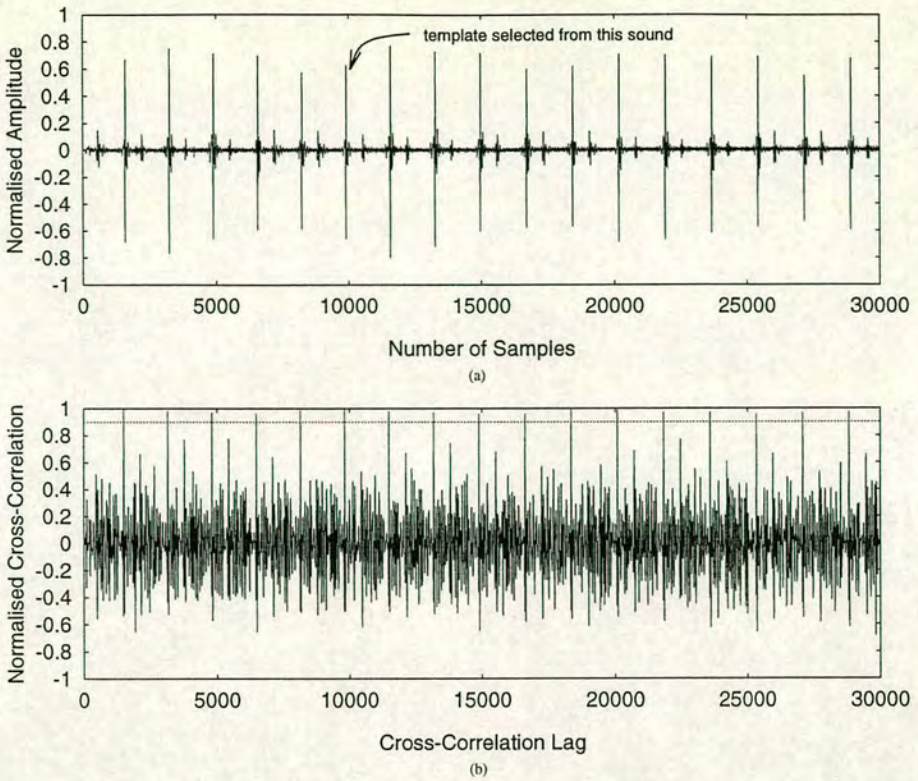

Figure 4.5: *Cross-correlation between a PCG with dominant first heart sounds and a representative mitral closing sound template selected from the sixth first sound. (a) Fifteen-second (30,000 data samples) filtered PCG (source: dg4), (b) Cross-correlation output: seventeen sounds are identified using a correlation threshold of 90%.*

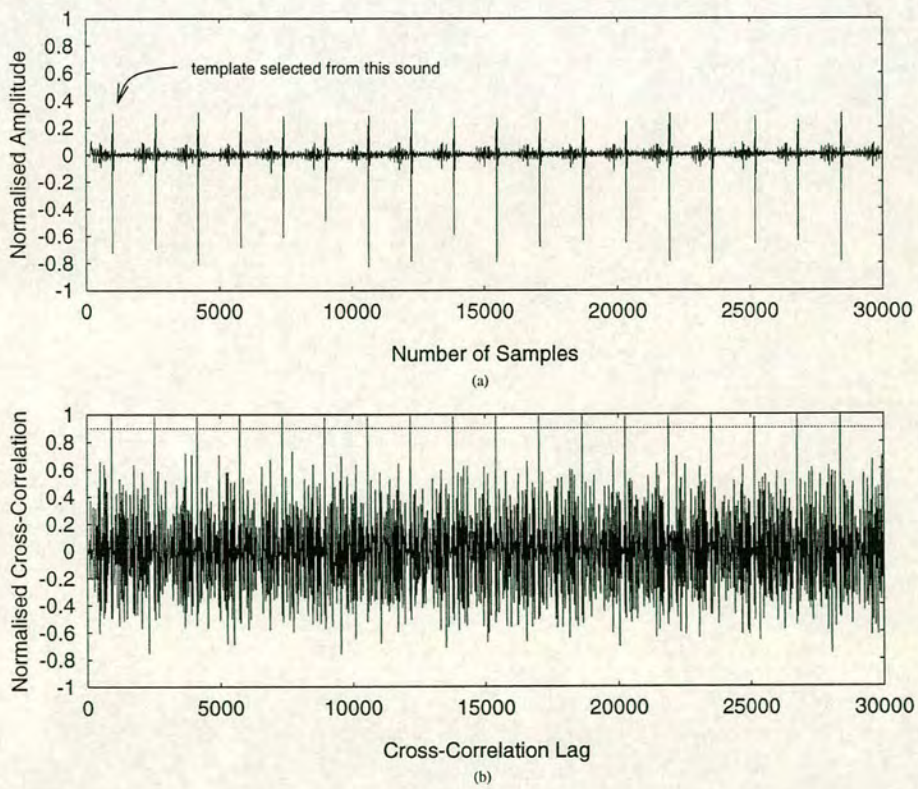

Figure 4.6: *Cross-correlation between a PCG with dominant second heart sounds and a representative aortic closing sound template selected from the first second sound. (a) Fifteen-second (30,000 data samples) filtered PCG (source: jg1), (b) Cross-correlation output: eighteen sounds are identified using a correlation threshold of 90%.*

Using a correlation threshold of 90%, the cross-correlation of the PCG with the mitral closing sound template shown in Figure 4.5 located sixteen[3] other mitral components. Likewise, the cross-correlation of the PCG with the aortic closing sound template shown in Figure 4.6 located seventeen other aortic components. A correlation threshold of 90% was selected on the basis that after having examined typical cross-correlation outputs from various subjects within the patient population, it was judged that a threshold of 90% was sufficiently large to truly identify the remaining principal components only, and reject the extraneous low-correlation output.

To facilitate the search of the sounds, two further processing operations were performed on the correlator output prior to the extraction of the identified components from the PCG: the output from the correlator is rectified, *i.e.* all negative values are made equal to zero, and the rectified output is squared. The result of this nonlinear operation is to further accentuate the points of very high correlation only (identified principal components), thus aiding discrimination from the remaining low-correlation output. The improvement in the interpretation and identification of the location of the remaining components between the standard bipolar cross-correlation output and the rectified squared unipolar output is clearly apparent from the examples shown in Figure 4.7. By rectifying and squaring the bipolar cross-correlation output, the comparison threshold of 90% was subsequently lowered to 81% prior to extraction.

When both principal heart sounds in each cardiac cycle have comparable structure as illustrated in Figure 4.8, the result of the cross-correlation operation can be to identify both components within each cycle as illustrated in Figure 4.9(b). The correlator output shown in Figure 4.9(b) locates seventeen mitral sounds within the PCG. Additionally, the cross-correlation operation identifies three aortic components which have a correlation of 81% or more with the mitral reference template. In total, twenty sounds were identified, seventeen correctly identified mitral components and three conflicting 'potentially hazardous' aortic components as illustrated in Figure 4.10.

The use of the PCG solely in automating the extraction of mitral and aortic components functions very well for one class of phonocardiographic signal, *i.e.* when one principal heart sound has very large structure relative to the other and is clearly the dominant signal event in each cardiac cycle. However, when both principal sounds have comparable structure, the resulting performance is clearly unsatisfactory and is a major shortcoming of this method. During the post-operative evaluation of bioprostheses, subsequent frequency analysis of incorrectly identified extracted sounds, which may originally have been produced by a native natural heart

[3]In total, seventeen mitral components are identified, sixteen from the remaining cardiac cycles as well as the sound chosen to be the representative template.

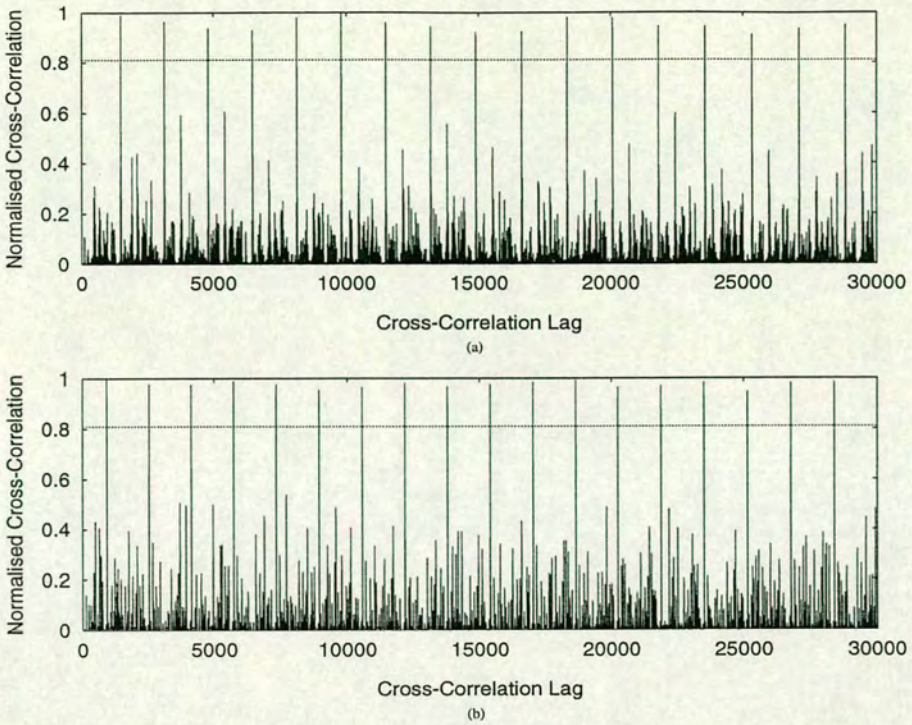

Figure 4.7: *Examples of rectified squared PCG cross-correlation output. (a) Equivalent output of Figure 4.4(b), (b) Equivalent output of Figure 4.5(b).*

valve or by another prosthetic valve, could result in an incorrect diagnosis being made of valvular heart disease. Such an outcome could be fatal. Therefore to overcome this potential hazard, an alternative method of automatically extracting mitral and aortic components from all types of phonocardiographic signals is required, regardless of the structure of one sound relative to the next.

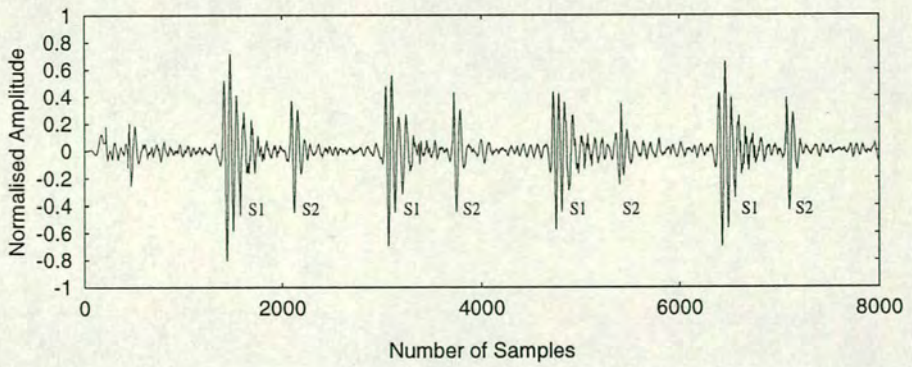

Figure 4.8: *Example of a PCG where both principal heart sounds have comparable structure (source: jp1).*

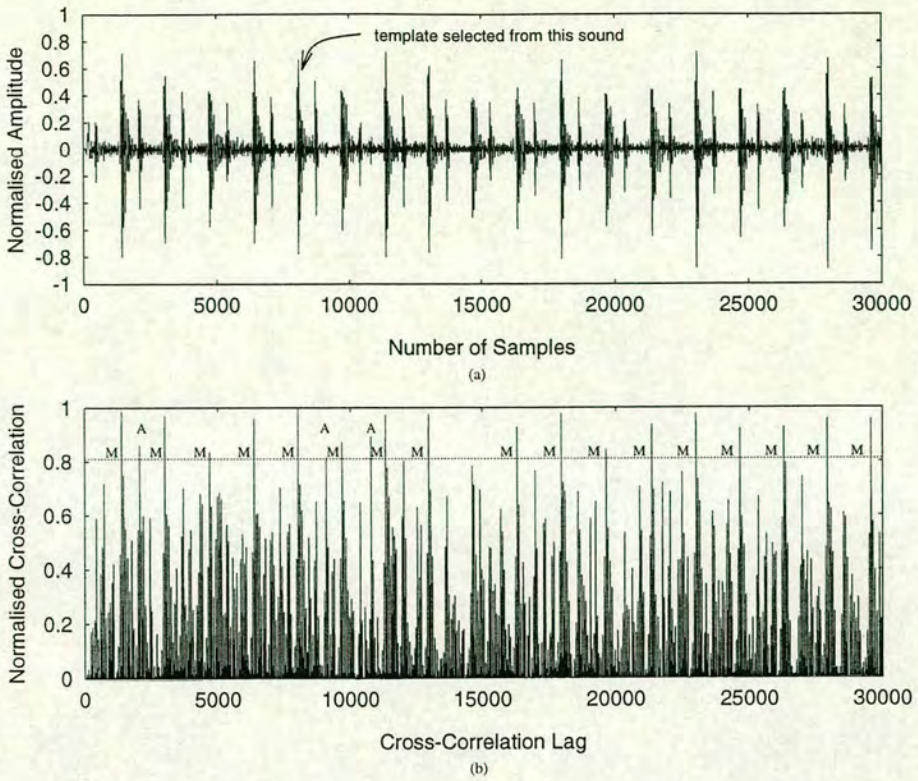

Figure 4.9: *Cross-correlation between the PCG illustrated in Figure 4.7 and a representative mitral closing sound template selected from the fifth first sound. The identified components are denoted as: M = Mitral and A = Aortic.*

4.6.2 Correlator Output Results: Method 2

To overcome the potential conflict of identifying and incorrectly extracting the wrong component when both S1 and S2 have similar structure, a second method is proposed, which utilises time-referenced PCG and ECG signals. The technique is based on the following methodology:

1. Locate the beginning of each cardiac cycle using the ECG. This involves initially manually selecting a representative QRS complex from each ECG record adopting the same template selection criterion as used for PCG.

2. Extract all the respective closing sound components from the PCG by repeating method 1.

3. Using the terminal points identified by the ECG cross-correlation and the *a priori* knowledge that S1 always occurs before S2, *i.e.* ventricular contraction occurs before ventricular relaxation, if the PCG correlation identifies two signal events within the same cardiac cycle, *i.e.* a mitral and an aortic component, reject the respective component and extract the appropriate component only.

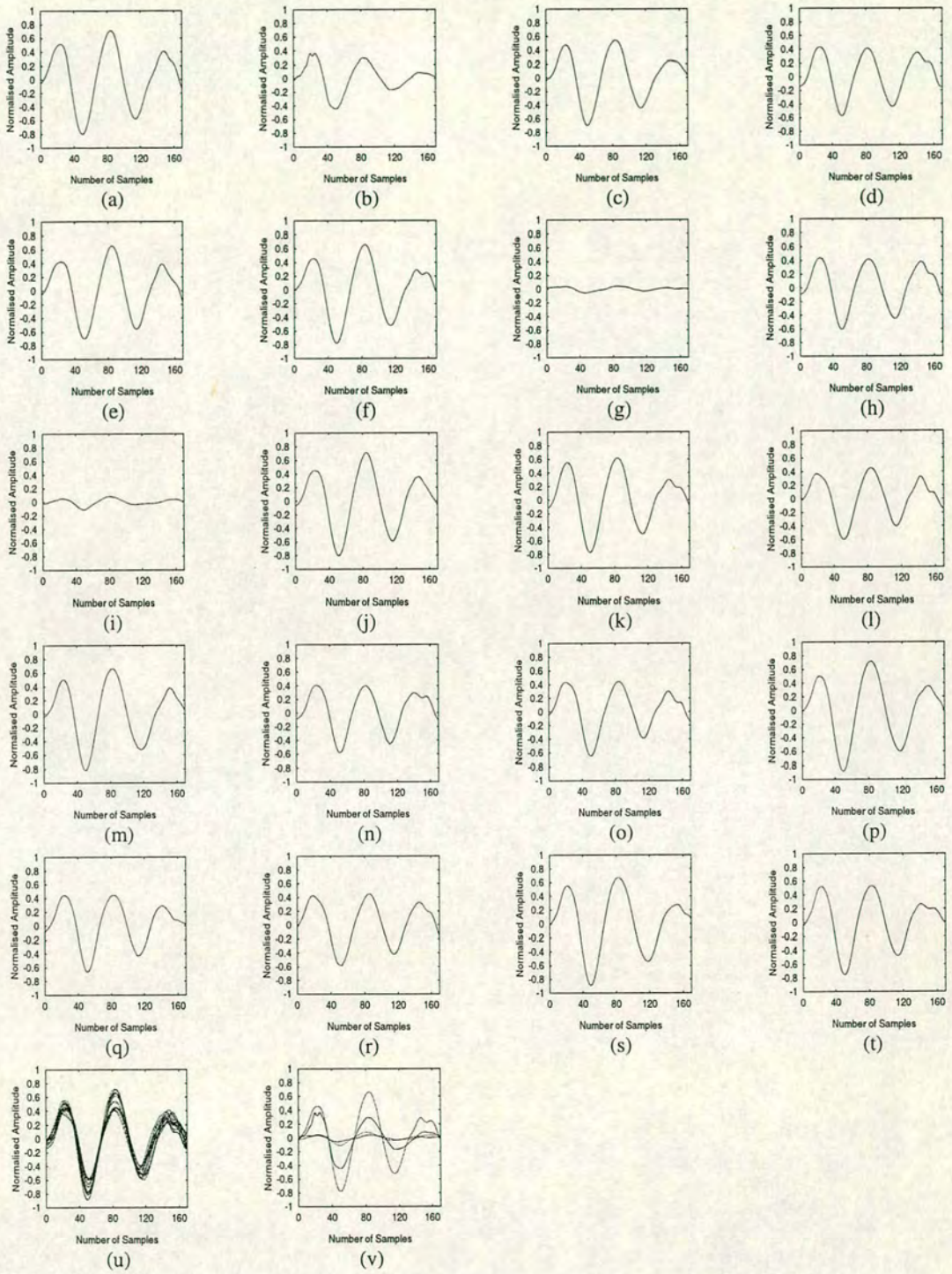

Figure 4.10: *The twenty sounds identified by the cross-correlation output of Figure 4.8(b). (a, c-f, h, j-t) Seventeen mitral components, (b, g, i) Three conflicting aortic components, (u) The seventeen extracted mitral components superimposed with the computed mean mitral sound, (v) The three conflicting aortic components superimposed with the computed mean mitral sound.*

As only one QRS complex occurs within each cardiac cycle, the result of the cross-correlation operation between the ECG and the QRS complex template is to locate the beginning of each cardiac cycle within the ECG. After careful inspection of all acquired ECG records, it was observed that in general, there is much less temporal variation and inconsistency between consecutive cardiac cycles within the ECG than typically can be present within a PCG. With only one QRS complex per cycle, and the fact that the practice of electrocardiography is much more standardised than phonocardiography, the result of the ECG correlation is to consistently identify the beginning of each cardiac cycle with a very high degree of fidelity, *i.e.* correlation coefficients typically in the range from 98% to 99.9% were commonly observed throughout the patient population as the examples illustrated in Figure 4.11 show. Even after rectifying and

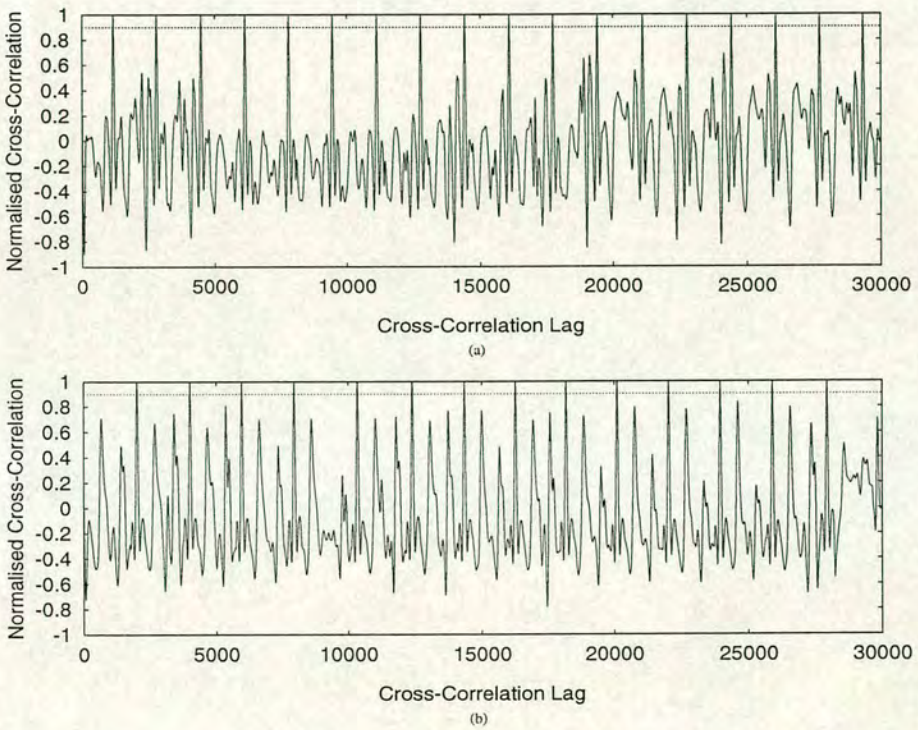

Figure 4.11: *Cross-correlation outputs computed from filtered ECG records and representative QRS complexes. (a) Eighteen identified cycles (source: jp1), (b) Fourteen identified cycles (source: jh6).*

squaring the standard bipolar cross-correlation output, correlation coefficients were observed typically ranging from 97% to 99.8%. Figure 4.12 shows the rectified, squared, equivalent ECG cross-correlation outputs originally illustrated in Figure 4.11. The use of the ECG and the subsequent cross-correlation identification of each cardiac cycle provides an excellent fiducial synchronising reference point for future analysis. Figure 4.13 illustrates the correlator output for the PCG shown in Figure 4.9(a) using method 2. The three aortic components originally identified as mitral components have now been rejected for further analysis. The only sounds

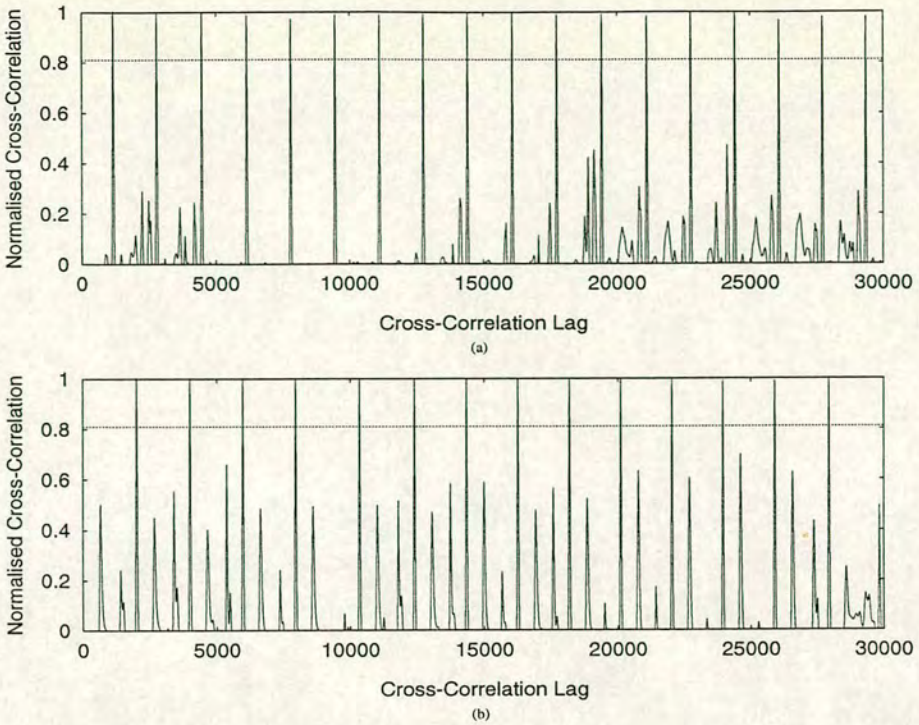

Figure 4.12: *Examples of rectified squared ECG cross-correlation output. (a) Equivalent output of Figure 4.10(a), (b) Equivalent output of Figure 4.10(b).*

now extracted are the actual seventeen mitral components.

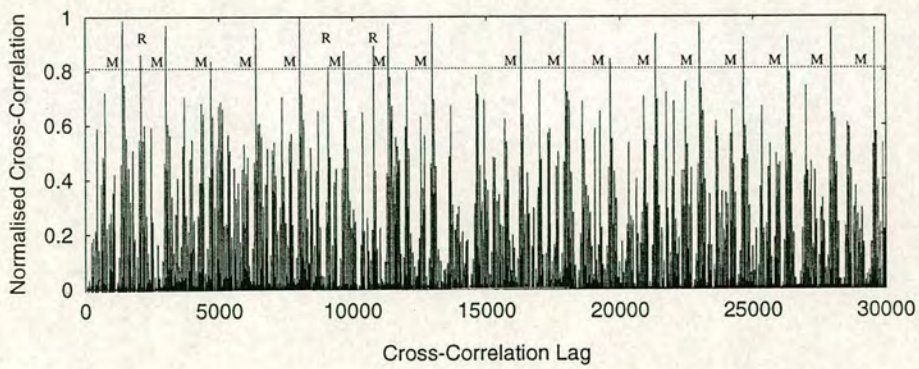

Figure 4.13: *Cross-correlation of the PCG illustrated in Figure 4.7 using method 2. The 'R' denotes a component rejected for further analysis.*

4.7 Summary and Conclusion

This chapter describes the preprocessing and signal conditioning operations applied to the acquired PCG prior to the subsequent analysis of the principal heart sound components. Effective preprocessing in the time domain greatly facilitates this analysis and produces more accurate results overall: through the enhancement of the principal heart sounds and the reduction of noise. The ultimate aim was the accentuation of the principal sounds to expedite the automated

extraction of mitral and aortic components from each PCG for subsequent frequency analysis.

The various stages of preprocessing are introduced, from the initial conditioning of the acquired PCG signal which involves the abstraction of the principal sounds from a low-frequency noise artifact, to the automated extraction of the principal components from the filtered PCG.

Two methods based on a cross-correlation, template-based matching approach were developed to automatically extract mitral and aortic components. The first method uses the PCG signal solely and matches a representative closing sound with similar successive occurrences, *i.e.* the respective closing sound in each of the remaining cardiac cycles. This method is shown to give good performance when one principal heart sound is clearly the dominant signal event in each cardiac cycle. However, when both principal sounds are evident and have similar temporal structure, method 1 can identify a mitral and an aortic component within the same cycle, resulting in the possible subsequent analysis of an incorrectly extracted sound. This is a major shortcoming of this method, the consequences of which could be fatal. To overcome this potential hazard, a second method was proposed which uses an ECG signal referenced to the PCG to initially locate the beginning of each cardiac cycle. Using this *a priori* information and the fact that S1 always occurs before S2, method 2 demonstrates that the appropriate closing sound only is correctly extracted for subsequent frequency analysis.

Chapter 5

Methods for the Frequency Analysis of Heart Sounds

The primary motivation for investigating the frequency spectrum of the sounds produced by the operation of mitral and aortic Carpentier-Edwards bioprostheses is to assess whether examination of the sound spectrum will reveal parameterising features that provide information of diagnostic significance concerning the functionality of the prosthesis. If such a relationship can be confirmed between the sound spectrum and the functionality of the Carpentier-Edwards bioprosthesis, this would allow for the identification of valvular heart disease and hence, an indication of impending valve failure. In addition, this would demonstrate the diagnostic potential of frequency analysis (spectral phonocardiography) as an alternative, clinical post-operative evaluation technique.

From the closing sounds produced by the operation of normally functioning, leaky and stiffening valves illustrated in section 2.3, some variations are apparent in the temporal characteristics of these sounds, *e.g.* leaky valves are often associated with a characterising backflow murmur. However, as discussed in section 4.4, there can be great variability in the structure and morphology of heart sounds from one recording to the next. Therefore a visual inspection solely in the time domain is inadequate to objectively discriminate between normally functioning, leaky and stiffening prostheses. Hence, it is in the frequency domain that less subjective discriminatory parameters are sought. During clinical auscultation, cardiologists use the sounds heard through the stethoscope to diagnose the functionality of bioprostheses. One of the key

attributes used is the frequency content of these sounds: identification of low-frequency sounds using a bell attachment to a stethoscope and high-frequency sounds, snaps and murmurs using a rigid diaphragm. Thus, the frequency domain (sound spectrum) is an appropriate domain from which to extract diagnostic features.

Mitral and aortic components produced by the operation of normally functioning and dysfunctioning bioprostheses were transformed into the frequency domain with a view to extracting heuristic parameters of diagnostic significance from the resulting sound spectrum. Specifically, the objective of the frequency analysis is to identify spectral features which uniquely characterise the acoustic components produced by the operation of mitral and aortic Carpentier-Edwards bioprostheses. It was envisaged that such parameters would include the identification of a number of characterising dominant frequency peaks, their relative intensities and metrics associated with the overall spectral profile and bandwidth of the sound spectrum. It was then the intention to classify these sounds by associating the derived spectral parameters with the functionality of prostheses.

This chapter investigates signal processing methods for the transformation of mitral and aortic components to the frequency domain, *i.e.* the sound spectrum. Particular attention is paid to the physiological transient-oscillatory nature of the heart sound signal and the suitability of the spectral estimation techniques when analysing such a temporal signature. The methods considered were: the periodogram, including a description describing its limitations; the Bartlett power spectral density estimate, which reduces the variance of a conventional periodogram estimate through ensemble averaging; ARMA-based, parametric linear modelling techniques, which attempt to synthesise the heart sound generation process; and Prony's method: a parametric modelling technique based on a damped sinusoidal model.

The number of modelling coefficients used by the parametric spectral estimation techniques, *i.e.* the model order, is a very important variable when analysing bioprosthetic heart valve closing sounds. As the precise order of a principal component time series is not known *a priori*, variations in spectra can occur with different orders. Therefore determining an accurate order is essential. Chapter 5 also investigates methods which determine the optimal model order of time series. The model order selection criteria considered were: hypothesis-based methods, decision-based techniques, the FPE, the AIC, the MDL and the CAT; and methods which attempt to extract the optimum model order from the heart sound time series by first removing the numerical ill-conditioning inherent with the use of linear-algebra-based spectral estimation techniques.

5.1 Classical Spectral Analysis of Heart Sounds

Classical methods of spectral estimation are based directly on the Fourier transform of the data sequence. The DFT can be used to transform a heart sound time series $x[n]$ of N data samples into the frequency domain, *i.e.* into a sequence, $X[k]$, of N frequency samples, defined to be:

$$X[k] = \sum_{n=0}^{N-1} x[n] \exp(-j2\pi kn/N) \qquad for\ k, n = 0, 1, \ldots, N-1 \tag{5.1}$$

The squared modulus of (5.1), $\hat{S}_{xx}[f]|_{f=k/N} = |X[k]|^2$, represents the distribution of signal energy as a function of frequency, and for this study of random bioprosthetic heart valve closing sounds, is referred to as the power spectral density (PSD) estimate. This method of directly transforming a time series of N data samples into the frequency domain is referred to as the **periodogram**, and is defined to be:

$$\hat{S}_{xx}[f]|_{f=k/N} = \frac{1}{N} \left| \sum_{n=0}^{N-1} x[n] \exp(-j2\pi kn/N) \right|^2 = \frac{1}{N} |X[k]|^2 \tag{5.2}$$

An efficient evaluation of the DFT hence the periodogram estimate can be computed using the FFT algorithms [78, 83, 94]. This approach to frequency analysis is robust, computationally efficient and produces reasonable results for a large class of signal processes [95]. However, in spite of these advantages, a number of inherent performance limitations are associated with the use of the DFT to accurately transform bioprosthetic heart valve closing sounds to the frequency domain. These limitations arise from the finite nature of mitral and aortic component time series records, and in particular, their relatively short duration. The steps commonly employed to overcome these shortcomings are discussed.

5.1.1 Windowing

Whenever mitral and aortic components are extracted from a PCG, an implicit windowing operation is performed on these components: data samples lying on either side of the sounds are ignored. This is equivalent to multiplying the extracted sound by a uniform rectangular (Dirichlet) window, with unit amplitude for the duration of the sound and zero amplitude before and after the sound, expressed as:

$$x_w[n] = x[n] w_{\text{rect}}[n] = \begin{cases} x[n] & for\ n = 0, 1, \ldots, N-1 \\ 0 & \text{otherwise} \end{cases} \tag{5.3}$$

where, $x_w[n]$, represents the implicitly windowed principal component extracted from the PCG. The multiplication of two sequences in the time domain is equivalent to convolution of the Fourier transforms of both sequences in the frequency domain, such that:

$$X_w[f] = X[f] \star W[f] \tag{5.4}$$

where $X_w[f]$, $X[f]$ and $W[f]$ are the Fourier transforms of the implicitly windowed principal component extracted from the PCG, the true desired component and the windowing function respectively, and where the '$\star$' denotes the convolution operator. A rectangular window in the time domain is equivalently represented in the frequency domain by the sinc function: $(\frac{\sin w}{w})$ [83]. Hence, the resulting sound spectrum will be the convolution of the spectral response of the desired principal component with the sinc function, *i.e.* the spectral response of the desired principal component will be filtered, producing a smoothed overall estimate $X_w[f]$. As a result of the sidelobes present in the frequency domain representation of the rectangular window, the convolution of $X[f]$ with the sidelobes of $W[f]$ spreads or 'leaks' energy from the desired response $X[f]$ across many bands producing sidelobe energy in $X_w[f]$ in frequency bands where the true principal component signal spectrum is zero. This energy might otherwise have been concentrated at a single point or in a narrow bandwidth of frequencies. This sidelobe energy is referred to as **'leakage'** [83] and is a direct consequence of the windowing inherent in the computation of the periodogram. The extraction of mitral and aortic components from a PCG results in discontinuities at the boundaries of the observation window, such that, the periodic extension of the extracted components are not commensurate with their natural period. If the signal being analysed has an integer number of continuous cycles within the finite record, the frequency bins coincide exactly with the points of zero magnitude within the windowing function. However, for a nonintegral number of cycles within the measurement interval, the main lobe of the windowing function and the points of zero magnitude are not coincident with the computed discrete spectral bins, resulting in sidelobe leakage. In addition to the distorting effects of leakage, the resultant spectral spreading has a further detrimental impact on the PSD estimate of bioprosthetic heart valve closing sounds: the detectability of responses. The spectral response of a weak signal can be completely masked by higher sidelobe leakage in the adjacent bins from a stronger spectral response, particularly if the weaker component is located close to the stronger response.

The effects of sidelobe leakage can be reduced by applying a weighting function to the signal before it is Fourier transformed. This function has a nonuniform weighting, producing a

smoother gradual termination in the time domain rather than the abrupt discontinuity inherent in rectangular window truncation. Hence, the extracted windowed component is smoothly brought to zero at the boundaries such that the periodic extension appears continuous.

The requirements for an ideal windowing function are that the central lobe should be narrow to give good spectral resolution and that the sidelobes are of insignificant magnitude relative to the main lobe to reduce the effects of leakage [96]. The ideal window is the impulse function, *i.e.* if $w[n] = \delta[n]$ then $W[f] = 1$, as this would exactly reproduce the spectral response of the desired principal component spectral response after convolution [97]. However, a windowing function of $\delta[n]$ cannot be readily realised in practice. Other windowing functions [98] reduce the overall sidelobe leakage as they have smaller spectral lobes than those of the implicit rectangular window. However, concomitant with a decrease in the level of sidelobe leakage is an increase in the broadening of the main lobe and hence the resulting smoothing effect, *i.e.* a reduction in spectral resolution. Therefore the selection of a suitable windowing function to gradually weight the extracted mitral and aortic principal components involves a compromise between two conflicting requirements: the width of the main lobe and the extent of sidelobe suppression. The implicit rectangular window has the narrowest main lobe of any window, but it also has the highest sidelobe level.

5.1.2 Hamming Window

A windowing function which provides a good compromise between frequency resolution and reduced leakage is the Hamming window [98–100]. The Hamming window was applied to the extracted principal component time series prior to zero padding, and followed by transformation to the frequency domain. This windowing function is a member of the family of raised cosine pulses and is defined to be:

$$w[n] = \alpha + (1.0 - \alpha) \cos\left(\frac{2\pi n}{N}\right) \qquad for\ n = 0, 1, \ldots, N-1 \tag{5.5}$$

where, α, is an adjustable parameter which allows the level of sidelobe cancellation to be tailored. Whenever $\alpha = 25/46 \approx 0.54$, such that:

$$w[n] = 0.54 + 0.46 \cos\left(\frac{2\pi n}{N}\right) \qquad for\ n = 0, 1, \ldots, N-1 \tag{5.6}$$

there is near perfect cancellation of the first sidelobe [99]. The application of the Hamming window to the principal component time series biases the amplitude of each resultant spectral

coefficients. Multiplication of the time series by a Hamming window reduces the magnitudes of the data samples at the taper reducing the total power of the principal component signal, resulting in modified DFT values and distortion of the amplitude response. In addition, windowing affects the mean of the data, resulting in the introduction of a d.c. component into the amplitude response and an apparent increase in the energy of the lower-frequency components [101]. Hence, to obtain an accurate measure of the amplitude response, a compensation factor is applied to the computed PSD estimate [96, 98]. For the Hamming window, the compensation which must be applied is:

$$\hat{S}_{xx}[f] = \frac{\hat{S}_{xx}[f]}{0.4} \tag{5.7}$$

5.1.3 Frequency Resolution

The extent to which two spectral responses can be distinguished from one another in the frequency domain is referred to as **frequency resolution**, Δf, defined to be:

$$\Delta f = \frac{\beta}{T_d} \tag{5.8}$$

where, β, is a coefficient always greater than unity which reflects the fact that a windowing function imposes an effective bandwidth on the spectral response of the principal component, and, T_d, is the duration of the signal under investigation [99]. Therefore the frequency resolution of the DFT is inversely proportional to the duration of the signal event under analysis. If frequency components present are closer than Δf Hz, the DFT is not able to resolve and represent these components as separate and distinct frequencies. As discussed in section 4.3, the duration of the principal components typically varies in the range from 20 to 80 ms (40 to 160 data samples). The corresponding DFT resolution ranges from $\frac{1}{80\text{ms}}$ = 12.5Hz to $\frac{1}{20\text{ms}}$ = 50Hz. The frequency resolution is also dependent on the choice of windowing function applied to the sounds. Regardless of which tapered function is used, the convolution of the Fourier transform of the window with that of the spectral response of the desired principal component means that the narrowest spectral response of the resultant transform is limited to the width of the main lobe of the window transform, independent of the data or its SNR [78].

5.1.4 The 'Picket-Fence' Effect

A consequence of the DFT transformation of a signal to the frequency domain is that the resultant spectrum is sampled in the frequency domain. The sample points (or bins) are spaced at integer multiples of f_s/N, where, f_s, is the temporal sampling frequency. If the signal being

analysed has an integer number of continuous cycles within the finite record, no error will occur in the measurement of magnitude or frequency [96]. However, if the signal frequency is not one of these discrete frequencies, this results in the 'Picket-Fence' effect, also referred to as scalloping loss [101, 102]. A spectral component between two distinct harmonic frequencies will be seen by the adjacent bins because of the leakage caused by the spectrum of the data window. In the worst case, where a spectral component lies midway between two bins, the amplitude is attenuated by 3.9dB and 3.1dB in the adjacent bins for rectangular and Hamming windowing functions respectively. This is judged to be analogous to viewing the spectrum through the gaps in a 'picket fence', where the pickets represent the inter-bin separation.

In this thesis, the primary aim is to compute the frequency spectrum of extracted mitral and aortic sounds. There is no *a priori* knowledge concerning the spectral composition of these sounds, and from their structure one can not accurately postulate a single stable frequency component [3]. However, scalloping loss can be reduced by decreasing the separation between the bins in the DFT spectrum. This is achieved by increasing the number of points in the transform by appending zeros to the principal component temporal record. This allows the interpolation of the values of the measured spectrum at more frequencies. The principal component finite records typically varied from 40 to 160 data samples in length. These were zero padded to construct a 1024-point data sequence which was subsequently transformed to the frequency domain.

5.1.5 Inconsistent Periodogram PSD Estimates

The periodogram does not produce a consistent estimate of the true power density, *i.e.* the variance of the estimate $\hat{S}_{xx}[f]$ does not decay to zero as $N \rightarrow \infty$, such that, $\hat{S}_{xx}[f]$ does not converge to the true power density spectrum. For finite data records, the mean periodogram spectral estimate $\hat{S}_{xx}[f]$ contains a bias defined to be:

$$E(\hat{S}_{xx}[f]) = S_{xx}[f] \star W_B[f] \tag{5.9}$$

where, E, is the expectation operator and $W_B[f]$, is the spectral characteristic of the Bartlett (triangular) window. The mean periodogram spectral estimate is the convolution of the true power density spectrum $S_{xx}[f]$ with the Fourier transform of the Bartlett window. This convolution results in a smoothed distorted version of the true spectrum and suffers from the same spectral leakage problems inherent when analysing finite data records using DFT-based techniques. The smoothing and leakage ultimately limit the ability to resolve closely spaced spectra.

The Bartlett method of spectral estimation reduces the variance in the conventional periodogram PSD estimate by subdividing the data record into smaller segments and averaging the resulting periodograms [103, 104]. Bartlett's method for reducing the variance can be summarised as follows:

1. the N-point finite data record is subdivided into K nonoverlapping segments, where each segment has length M.

2. For each segment, the periodogram is computed:

$$\hat{S}_{xx}^{i}[f] = \frac{1}{M}\left|\sum_{n=0}^{M-1} x[n]\exp(-j2\pi fn)\right|^2 \quad \textit{for } i = 0, 1, \ldots, K-1 \tag{5.10}$$

3. The periodograms for the K segments are averaged to obtain the Bartlett power spectrum estimate defined to be:

$$\hat{S}_{xx}^{B}[f] = \frac{1}{K}\sum_{i=0}^{K-1} \hat{S}_{xx}^{i}[f] \tag{5.11}$$

The effect of reducing the length of the finite record from N points to $M = N/K$ results in a window whose spectral width has been increased by a factor K. Consequently, the frequency resolution decreases by a factor K [83]. In return for this reduction in spectral resolution, the variance of the Bartlett PSD estimate, $\text{var}\{\hat{S}_{xx}^{B}[f]\}$, decreases by a factor K such that:

$$\text{var}\{\hat{S}_{xx}^{B}[f]\} = \frac{1}{K}\hat{S}_{xx}[f] \tag{5.12}$$

In an attempt to overcome the inherent performance limitations of the DFT approach to frequency analysis, the motivation for better methods of spectral analysis has resulted in alternative, more recent developments, which attempt to circumvent the fundamental limitations of classical spectral analysis methods by constructing a parametric model for the random process, and then calculating an associated spectrum. Many of the problems of the DFT approach to spectral estimation arise from the finite nature of the signal event under investigation and the accompanying windowing and leakage problems inherent with the analysis of finite data records. Furthermore, DFT-based methods require the availability of long data records to yield adequate frequency resolution; however, in this thesis, the signal under analysis is a short-transient oscillation. In addition, large variances are associated with the estimates of short-time data records, which necessitates the need for some sort of pseudo-ensemble averaging to obtain statistically consistent periodogram spectral estimates. Ultimately, such spectral smoothing invariably leads to a further reduction in frequency resolution. The utility of classical-based

methods assumes that either the unestimated autocorrelation sequence is implicitly zero outside the measurement interval or that the data is periodic or cyclic. Neither of these assumptions are realistic and severely limit the frequency resolution and quality of the resulting PSD estimate.

Section 5.2 discusses spectral estimation techniques which do not require any such assumptions. These methods extrapolate the autocorrelation sequence outside the measurement interval. In such cases, a parametric model for the signal generation process is constructed from the observed data, from which a PSD estimate is computed. This modelling approach to frequency analysis completely eliminates the need for windowing functions along with their distorting impact, as well as the need for assumptions concerning the nature of the data outside the measurement interval. This results in spectral estimation methods which provide superior frequency resolution, particularly for short-time finite data records such as transient heart sounds, where the amount of available stationary data is limited. Parametric methods accurately determine the frequencies in a multicomponent signal without the need for spectral smoothing techniques and their subsequent reduction in frequency resolution [105].

5.2 Parametric Spectral Analysis of Heart Sounds

Often there is some knowledge concerning the process that generated the time series from which data samples are used for frequency analysis, or at least, one is able to make a more realistic assumption regarding the nature of the observed process outside the measurement interval other than to assume that it is zero or cyclic. This allows for the selection of an accurate model for the process that generated the data samples, or at least, a model that is a good approximation to the underlying process. When using such a model by determining the parameters from time series observations, it is usually possible to obtain a better spectral estimate of short-time data records than that which would be obtained using DFT-based methods. Hence, in this context of time series modelling, the parametric approach to spectral analysis can be summarised as follows:

1. Select an appropriate parametric time series model that approximates the generated observed time sequence. In this thesis, the observed time sequence are the data samples of the principal heart sound components produced by the operation of the Carpentier-Edwards bioprosthetic heart valve.

2. Construct the model by estimating the parameters from the heart sound time series.

3. Compute the PSD estimate implied by the model by inserting the estimated model parameters into a theoretical PSD expression appropriate for that time series model.

The parametric methods of spectral analysis used in this thesis are based on a linear system or model which synthesises a principal heart sound time series $x[n]$ as the output of this linear equivalent causal filter (impulse response = $h[k] = 0$ for $k < 0$) when excited by an input signal, $w[n]$. These parametric time series models are characterised by stochastic and deterministic rational polynomial system transfer functions, $H[z]$, defined to be:

$$H[z] = \frac{B[z]}{A[z]} = \frac{\sum_{k=0}^{\hat{q}} b[k]z^{-k}}{\sum_{k=1}^{\hat{p}} a[k]z^{-k}} = 1 + \sum_{k=1}^{\infty} h[k]z^{-k} \tag{5.13}$$

where, $A[z]$, and, $B[z]$, are polynomials that have all of their roots (zeros) within the unit-circle of the z-plane to guarantee that H[z] is a stable minimum-phase causal filter, $a[k]$, and, $b[k]$, are the filter coefficients that determine the location of the poles and zeros of $H[z]$ respectively, and, $\hat{p}$, and, $\hat{q}$, are the number of $a[k]$ and $b[k]$ coefficients respectively, *i.e.* the **order** of the linear model.

With the modelling approach to frequency analysis, only the output process from the model is assumed available for analysis, *i.e.* the input driving sequence is not observable [78]. However, as a synthesised heart sound can be considered to be a realisation of a stationary random process, the exogenous input sequence may also be considered to be a stationary random process. The resulting PSD estimate of the modelled heart sound output, $\hat{S}_{xx}[f]$, is defined to be:

$$\hat{S}_{xx}[f] = \hat{S}_{ww}[f]\,|H[f]|^2 = \hat{S}_{ww}[f]\left|\frac{B[f]}{A[f]}\right|^2 \tag{5.14}$$

where, $\hat{S}_{ww}[f]$, is the PSD estimate of the input driving sequence and, $H[f]$, is the system transfer function of the linear model. A principal heart sound time series can be represented as the output of a linear causal filter when excited by a white-noise sequence of zero mean and a.c. power, σ_w^2, *i.e.* constant variance independent of frequency and having a flat PSD. The resulting PSD estimate of the principal heart sound output is defined to be:

$$\hat{S}_{xx}[f] = \sigma_w^2\,|H[f]|^2 = \sigma_w^2\left|\frac{B[f]}{A[f]}\right|^2 \tag{5.15}$$

It is conventional to assume that the white-noise sequence has unit variance, *i.e.* $\sigma_w^2 = 1$, with the filter providing any necessary gain. The resulting PSD estimate of the principal heart sound

is now completely characterised by the amplitude response of the filter and the variance of the white noise. As the shape of this estimate is dependant only upon the magnitude of the filter frequency response, a random process with almost any desired second-order statistics can be produced by applying white noise to an appropriate filter [103]. As the model is defined by a finite set of parameters, the resulting PSD estimate is also defined by these parameters. The overall effect of this process is to colour or shape the PSD estimate of a white-noise sequence by an appropriate filter frequency response to produce an estimate of a desired shape. In this thesis: the spectral profile of Carpentier-Edwards bioprosthetic heart valve closing sounds.

However, the hypothetical white-noise input sequence with PSD $\hat{S}_{ww}[f]$ is not realisable and the linear filter with system transfer function $H[z]$ cannot be readily identified. Nevertheless, an alternative approach is possible. If an inverse linear causal filter with system transfer function, $\frac{1}{H[z]}$, can be found which whitens the PSD estimate of the principal heart sound time series $x[n]$, then it too will also completely define or parameterise the PSD estimate of this heart sound time series, *i.e.* a stationary random process $x[n]$ with a PSD estimate $\hat{S}_{xx}[f]$ can be transformed into a white-noise sequence by passing $x[n]$ through a linear filter with system transfer function $\frac{1}{H[z]}$ such that:

$$\hat{S}_{ww}[f] = \sigma_w^2 = |H^{-1}[f]|^2 \hat{S}_{xx}[f] \tag{5.16}$$

where:

$$\hat{S}_{xx}[f] = \frac{\sigma_w^2}{|H^{-1}[f]|^2} \tag{5.17}$$

This inverse filter is as a noise whitening filter and its white noise output is known as the **'innovations process'** associated with the stationary random process $x[n]$ [83]. This approach of parametrically modelling heart sounds is shown in Figure 5.1. The representation of a stationary stochastic heart sound process $x[n]$ as the output of an linear filter with system transfer function $H[z]$ and excited by a white-noise sequence $w[n]$ is known as the **Wold representation** [83].

For linear models with a rational system transfer function $H[z]$, the corresponding linear difference equation relating the modelled heart sound output, $\hat{x}[n]$, to the input $w[n]$ is defined to be:

$$\hat{x}[n] = -\sum_{k=1}^{\hat{p}} a[k]x[n-k] + \sum_{k=0}^{\hat{q}} b[k]w[n-k] \tag{5.18}$$

where, $a[k]$, and, $b[k]$, are the autoregressive (AR) and moving average (MA) filter coefficients respectively and, $\hat{p}$, and, $\hat{q}$, are the orders of the AR and MA parts of the ARMA$[\hat{p}, \hat{q}]$ model respectively, *i.e.* the number of AR and MA parameters. This general model is known as the

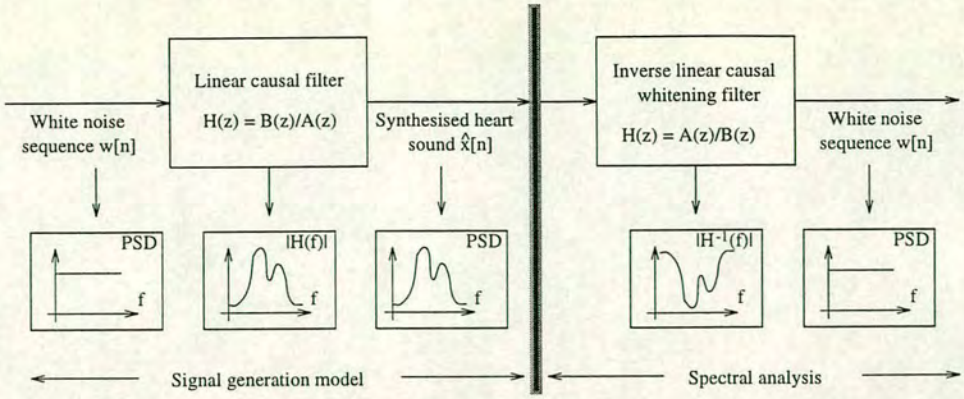

Figure 5.1: *Parametric modelling approach to spectral analysis.*

autoregressive-moving average (ARMA) model, denoted as ARMA[$\hat{p}, \hat{q}$].

If all the MA parameters are zero except $b[0] = 1$, *i.e.* $b[k] = 0$ for $k > 0$, the resulting linear filter $H[z] = \frac{1}{A[z]}$ is an all-pole filter. The difference equation relating input and output is strictly an AR process of order $\hat{p}$, *i.e.* AR[$\hat{p}$], and is defined to be:

$$\hat{x}[n] = -\sum_{k=1}^{\hat{p}} a[k]x[n-k] + w[n] \tag{5.19}$$

The resulting AR PSD estimate is:

$$\hat{S}_{xx}^{AR}[f] = \frac{\sigma_w^2}{|A[f]|^2} \tag{5.20}$$

Likewise, if all the AR parameters are zero except $a[0] = 1$, *i.e.* $a[k] = 0$ for $k \geq 0$, the resulting linear filter $H[z] = B[z]$ is an all-zero filter. The difference equation relating input and output is strictly an MA process of order $\hat{q}$, *i.e.* MA[$\hat{q}$], and is defined to be:

$$\hat{x}[n] = \sum_{k=1}^{\hat{q}} b[k]w[n-k] + w[n] \tag{5.21}$$

The MA PSD estimate is:

$$\hat{S}_{xx}^{MA}[f] = \sigma_w^2 |B[f]|^2 \tag{5.22}$$

The selection of one of these models requires some knowledge regarding the likely spectral shape of the process under investigation [106]. Of the three, the AR model is the most widely used. This is due to the fact that the AR model is particularly suitable for representing spectra with narrow sharp peaks (resonances) and that the estimation of the AR model parameters entails the solution of a set of linear equations. The MA model, however, is suited to representing spectra with deep nulls and requires many parameters to adequately model a narrow spectrum.

Furthermore, the estimation of the MA model parameters requires the solution of a set of nonlinear equations. By combining poles and zeros, the ARMA model is able to represent and characterise spectra with both sharp peaks and deep nulls, *i.e.* a composite of the AR and MA models. The ARMA model provides the most efficient representation from the viewpoint of the number of parameters, *i.e.* parsimony [83], however, it requires the solution of a set of nonlinear equations. The Wold decomposition theorem [103, 107] asserts that given an AR, MA or ARMA model of a finite number of parameters, it is possible to express that model in terms of the other two, *e.g.* an ARMA or MA process may be uniquely represented by an AR model of infinite order. Although such a model may not be parsimonious, an ARMA model can be approximated by a higher-order AR model, which involves the solution of a set of linear equations.

Thus far the parametric modelling of heart sounds has assumed a white-noise input. However, from the sounds shown in chapters two and four, the transient-oscillatory nature of these sounds suggests that a rational model excited by an impulse would be more appropriate. When $w[n] = \delta[n]$, the resulting PSD output is:

$$\hat{S}_{xx}[f] = |H[f]|^2 \tag{5.23}$$

An alternative ARMA parametric model was also investigated based on a deterministic exponential model known as Prony's method [103], where a $\hat{p}$-term complex exponential model is defined to be:

$$\hat{x}[n] = \sum_{k=1}^{\hat{p}} A[k] \exp\left[(\alpha[k] + j2\pi f[k])(n-1)T + j\theta[k]\right] \tag{5.24}$$

for $0 \leq n \leq N-1$, where, N, is the number of data samples, T, is the sampling interval in seconds, A_k, is the amplitude of the exponential, α_k, is the damping factor in second^{-1}, f_k, is the sinusoidal frequency in Hz, θ_k, is the sinusoidal initial phase in radians and $\hat{p}$ is the number of complex exponentials (model order). A modified version of Prony's method was implemented for this thesis. This modified version is based on a damped sinusoidal model, with the resulting Prony energy spectral density (ESD) estimate, $\hat{S}_{xx}^{P}[f]$, being particularly appropriate for transient signals such as valvular closing sounds [78]. The Prony ESD estimate is defined to be:

$$\hat{S}_{xx}^{P}[f] = \left| T \left(\sum_{k=1}^{\hat{p}} \frac{A[k] \exp(j\theta[k])}{1 - \exp[(\alpha[k] + j2\pi f[k])T] \exp(-j2\pi f T)} \right) \right|^2 \tag{5.25}$$

Evaluating the parameters of the Prony ARMA-based models and hence the PSD estimate is achieved by minimising the modelling approximation error between the synthesised heart sound output and the actual heart sound, *i.e.* between the impulse response $h[n]$ of the model and the actual heart sound time series.

5.2.1 Evaluation of ARMA Model Parameters

When the PSD estimate of a stationary random process is a rational function, a relationship exists between the autocorrelation sequence, $\hat{r}_{xx}[l]$, which is estimated from the heart sound time series, and the $a[k]$ and $b[k]$ parameters of the linear filter $H[z]$. Multiplying both sides of (5.18) by the complex conjugate of $x^*[n-l]$ and taking expected values yields the 'Yule-Walker' equations:

$$\hat{r}_{xx}[l] = \begin{cases} -\sum_{k=1}^{\hat{p}} a[k]\hat{r}_{xx}[l-k] & \text{for } l > \hat{q} \\ -\sum_{k=1}^{\hat{p}} a[k]\hat{r}_{xx}[l-k] + \sigma_w^2 \sum_{k=l}^{\hat{q}} b[k]h^*[k-l] & \text{for } l = 0, 1, \ldots, \hat{q} \\ \hat{r}_{xx}^*[-l] & \text{for } l < 0 \end{cases} \tag{5.26}$$

where the superscripted '*' denotes complex conjugation and $h[0] = 1$ [83, 106]. Inspection of (5.26) reveals that a nonlinear relationship exists between the autocorrelation lag estimates $\hat{r}_{xx}[l]$, the parameters $a[k]$ and $b[k]$ and the impulse response $h[n]$. A best least-squares evaluation with optimum $a[k]$ and $b[k]$ parameters involves the least mean-square solution of the highly nonlinear Yule-Walker equations. This entails the use of computationally intensive, nonlinear iterative programming algorithms with their attendant problems of nonconvergence or convergence to the wrong solution [95, 108–110]. In this thesis, the $a[k]$ and $b[k]$ parameters are evaluated separately: the AR parameters are first calculated followed by the MA parameters. This suboptimal approach results in a considerable easing in computational complexity with the evaluation of the AR parameters of an ARMA model requiring a linear solution. Although this approach is suboptimal (in the maximum likelihood sense), it provides for near-optimal modelling [108, 111].

5.2.1.1 Evaluation of AR ARMA Model Parameters

The first stage of the suboptimal approach to ARMA modelling is the evaluation of the AR parameters. Inspection of (5.26) reveals that the AR parameters of an ARMA model are related to the autocorrelation lag estimates by a set of linear equations, which may be expressed in

matrix form as:

$$\hat{\mathbf{R}}_{xx}\mathbf{a} = -\hat{\mathbf{r}}_{xx} \tag{5.27}$$

where:

$$\hat{\mathbf{R}}_{xx} = \begin{pmatrix} \hat{r}_{xx}[\hat{q}] & \hat{r}_{xx}[\hat{q}-1] & \dots & \hat{r}_{xx}[\hat{q}-\hat{p}+1] \\ \hat{r}_{xx}[\hat{q}+1] & \hat{r}_{xx}[\hat{q}] & \dots & \hat{r}_{xx}[\hat{q}-\hat{p}+2] \\ \vdots & \vdots & \ddots & \vdots \\ \hat{r}_{xx}[\hat{q}+\hat{p}-1] & \hat{r}_{xx}[\hat{q}+\hat{p}-2] & \dots & \hat{r}_{xx}[\hat{q}] \end{pmatrix}$$

$$\mathbf{a} = \begin{pmatrix} a[1] \\ a[2] \\ \vdots \\ a[\hat{p}] \end{pmatrix} \qquad \hat{\mathbf{r}}_{xx} = \begin{pmatrix} \hat{r}_{xx}[\hat{q}+1] \\ \hat{r}_{xx}[\hat{q}+2] \\ \vdots \\ \hat{r}_{xx}[\hat{q}+\hat{p}] \end{pmatrix}$$

This relationship is known as the 'Modified Yule-Walker' (MYW) equations, also referred to as the 'extended Yule-Walker equations', and evaluate the $\hat{p}$ AR parameters of an ARMA model from the autocorrelation estimates from lags $\hat{q}-\hat{p}$ to $\hat{q}+\hat{p}$. Hence, the AR $a[k]$ parameters of an ARMA model are obtained by evaluating the first $\hat{p}$ MYW equations ($\hat{q}+1 \leq n \leq \hat{q}+\hat{p}$) and solving the resulting $\hat{p}$ linear equations for the $\hat{p}$ $a[k]$ parameters. This approach is computationally attractive, however, only a subset of the autocorrelation lag estimates are used: $2\hat{p}$ estimates in total, from lags $\hat{q}-\hat{p}$ to $\hat{q}+\hat{p}$. Direct implementation of the MYW equations can result in poor performance, especially for short-time and noisy finite data records. For higher-order models, direct implementation of the MYW equations produces poor estimates of the AR parameters (large variance) due to the poor estimates of the autocorrelation sequence for large values of lag, or that the selected model is not correct, or both [83,112]. Improved performance can be achieved by using more than the minimal number of $\hat{p}$ MYW equation evaluations with more correlation estimates. The improvement in estimation accuracy results from the fact that there is valuable information in the high-lag autocorrelation estimates which is not exploited by the minimal direct implementation of the MYW equations. Increasing the number of equations is particularly effective for narrowband processes, where the autocorrelation estimates decay slowly [111]. The net result is a reduction in data-induced parameter sensitivity and a corresponding improvement in overall modelling performance: particularly suited for the generation of low-order high-quality spectral estimates from short-time heart sound data records. The $\hat{p}$ AR $a[k]$ parameters are evaluated using a least-squares fit to this overdetermined set of linear equations, referred to as the 'Least-Squares Modified Yule-Walker' method. In the

overdetermined modelling approach, if the autocorrelation estimates can be accurately evaluated to lag L, where $L > \hat{p}+\hat{q}$, this yields an overdetermined set of linear equations in the $\hat{p}$ unknown AR parameters, defined in matrix form to be:

$$\hat{\mathbf{R}}_{xx}\mathbf{a} = -\hat{\mathbf{r}}_{xx} \tag{5.28}$$

where:

$$\hat{\mathbf{R}}_{xx} = \begin{pmatrix} \hat{r}_{xx}[\hat{q}] & \hat{r}_{xx}[\hat{q}-1] & \dots & \hat{r}_{xx}[\hat{q}-\hat{p}+1] \\ \hat{r}_{xx}[\hat{q}+1] & \hat{r}_{xx}[\hat{q}] & \dots & \hat{r}_{xx}[\hat{q}-\hat{p}+2] \\ \vdots & \vdots & \ddots & \vdots \\ \hat{r}_{xx}[L-1] & \hat{r}_{xx}[L-2] & \dots & \hat{r}_{xx}[L-\hat{p}] \end{pmatrix}$$

$$\mathbf{a} = \begin{pmatrix} a[1] \\ a[2] \\ \vdots \\ a[\hat{p}] \end{pmatrix} \qquad \hat{\mathbf{r}}_{xx} = \begin{pmatrix} \hat{r}_{xx}[\hat{q}+1] \\ \hat{r}_{xx}[\hat{q}+2] \\ \vdots \\ \hat{r}_{xx}[L] \end{pmatrix}$$

5.2.1.2 Evaluation of MA ARMA Model Parameters

The second stage of the suboptimal approach to ARMA modelling is the evaluation of the MA parameters. Inspection of (5.26) reveals that a nonlinear relationship exists between the autocorrelation sequence, the impulse response and the MA parameters. However, as only a spectral estimate is required, there is no need to solve for the MA parameters, but only to estimate the autocorrelation function, as the MA PSD estimate, $\hat{S}_{xx}^{MA}[f]$, may be evaluated from:

$$\hat{S}_{xx}^{MA}[f] = \sum_{k=-q}^{q} \hat{r}_{xx}[k]exp(-j2\pi fk) \tag{5.29}$$

5.2.2 Evaluation of AR Model Parameters

For a pure AR model of order $\hat{p}$, *i.e.* AR[$\hat{p}$], a relationship exists between the autocorrelation sequence and the AR $a[k]$ parameters. This linear relationship is referred to as the 'AR Yule-Walker normal equations' [106] and can be expressed in matrix form as:

$$\begin{pmatrix} \hat{r}_{xx}[0] & \hat{r}_{xx}[-1] & \dots & \hat{r}_{xx}[-\hat{p}] \\ \hat{r}_{xx}[1] & \hat{r}_{xx}[0] & \dots & \hat{r}_{xx}[-\hat{p}+1] \\ \vdots & \vdots & \ddots & \vdots \\ \hat{r}_{xx}[\hat{p}] & \hat{r}_{xx}[\hat{p}-1] & \dots & \hat{r}_{xx}[0] \end{pmatrix} \begin{pmatrix} 1 \\ a[1] \\ \vdots \\ a[\hat{p}] \end{pmatrix} = \begin{pmatrix} \sigma_w^2 \\ 0 \\ \vdots \\ 0 \end{pmatrix} \tag{5.30}$$

Inspection of (5.30) reveals that estimating the autocorrelation sequence from the heart sound time series will subsequently yield the AR parameters and hence the AR PSD estimate $\hat{S}_{xx}^{AR}[f]$. This intuitive approach to AR PSD estimation is known as the 'Yule-Walker' method. However, better results are possible from methods which produce the AR model parameters directly from the data rather than indirectly via the autocorrelation sequence. For short-time data records, the Yule-Walker method produces low-resolution spectral estimates relative to these methods.

The matrix of autocorrelation estimates in (5.30) has a Toeplitz symmetry (elements along each diagonal are identical, *i.e.* $\hat{\mathbf{R}}_{xx}(i,j) = \hat{\mathbf{R}}_{xx}(i-j)$ as well as being Hermitian, *i.e.* $\hat{\mathbf{R}}_{xx}(i,j) = \hat{\mathbf{R}}_{xx}^{*}(j,i)$. This matrix can be evaluated efficiently using the Levinson-Durbin algorithm [78,83,113,114], which sequentially solves (5.30) without the need for matrix inversion: requiring only $\hat{p}^2$ operations in contrast to standard techniques such as Gauss elimination which typically involve $\hat{p}^3$ operations. The Levinson-Durbin algorithm recursively computes the AR $a[k]$ parameter sets: $\{a_1[1], \sigma_1^2\}, \{a_2[1], a_2[2], \sigma_2^2\}, \ldots, \{a_{\hat{p}}[1], a_{\hat{p}}[2], \ldots, a_{\hat{p}}[\hat{p}], \sigma_{\hat{p}}^2\}$ where the leading subscript denotes the iteration number, *i.e.* $a_k[\hat{p}]$ for $k = 1, 2, \ldots, \hat{p}$. The final set of parameters at order $\hat{p}$ is the desired solution. Hence, the Levinson-Durbin algorithm evaluates the AR parameters for all the lower-order AR model fits to the data. This property is particularly useful when analysing heart sounds, as the precise model order, p_{hs}, is not known *a priori*. The Levinson-Durbin algorithm can be used to generate successively higher-order models until σ_k^2 is reduced to a desired value. The variance of the excitation noise reaches a constant value for a model order equal to or greater than the correct order. Consequently, the order at which σ_k^2 does not change can be used as an indication of the correct model order, at which point, σ_k^2 reaches its minimum value, *i.e.* $\sigma_k^2 = \sigma_{\hat{p}}^2$ for $k > \hat{p}$. This Levinson-Durbin method of model order determination is discussed further in section 5.2.5.1.

5.2.3 Relationship of the AR Process to Linear Prediction

The one-step forward linear prediction estimate, $\hat{x}^f[n]$, of the future value of the data sample, $x[n]$, is defined to be:

$$\hat{x}^f[n] = -\sum_{k=1}^{\hat{p}} a^f[k]\, x[n-k] \tag{5.31}$$

where, $a^f[k]$, is the forward linear prediction coefficient at time index k of the one-step forward predictor of order $\hat{p}$. The prediction is forward, *i.e.* the prediction for the current data sample is a weighted linear combination of the $\hat{p}$ past samples $x[n-1]$, $x[n-2]$, $\ldots$, $x[n-\hat{p}]$. The difference between the actual data sample $x[n]$ and its predicted value $x^f[n]$ is the forward

prediction error, $e^f[n]$, also referred to as the 'residual', and is defined to be:

$$e^f[n] = x[n] - \hat{x}^f[n] = x[n] + \sum_{k=1}^{\hat{p}} a^f[k]\, x[n-k] \tag{5.32}$$

The mean-squared value or variance of the forward prediction error is defined as:

$$\xi^f = E\{|e^f[n]|^2\} \tag{5.33}$$

Similarly, the one-step backward linear prediction coefficient estimate, $\hat{x}^b[n-\hat{p}]$, of the data sample, $x^b[n-\hat{p}]$, is defined to be:

$$\hat{x}^b[n-\hat{p}] = -\sum_{k=0}^{\hat{p}-1} a^b[k]\, x[n-k] \tag{5.34}$$

where, $a^b[n]$, is the backward linear prediction coefficient at time index k of the one-step backward predictor of order $\hat{p}$. The prediction is backward, *i.e.* the prediction for the current data sample is a weighted linear combination of the $\hat{p}$ samples indexed later in time, $x[n], x[n-1], \ldots, x[n-\hat{p}+1]$. The difference between the actual data sample $x^b[n-\hat{p}]$ and its predicted value $\hat{x}^b[n-\hat{p}]$ is the backward prediction error, $e^b[n]$, and is defined to be:

$$e_p^b[n] = x[n-\hat{p}] - \hat{x}^b[n-\hat{p}] = x[n-\hat{p}] + \sum_{k=0}^{\hat{p}-1} a^b[k]\, x[n-k] \tag{5.35}$$

The mean-squared value (variance) of the backward prediction error is defined to be:

$$\xi^b = E(|e^b[n]|^2) \tag{5.36}$$

The forward linear prediction coefficients are evaluated by performing a least-squares minimisation of the mean-squared forward prediction error. Minimisation with respect to all of the prediction coefficients yields a set of linear equations structurally identical to the AR Yule-Walker equations [83, 106]. Likewise, minimisation of ξ^b with respect to all of the backward linear prediction coefficients yields normal equations structurally identical to the AR Yule-Walker equations. If the underlying process $x[n]$ is autoregressive, *i.e.* AR[$\hat{p}$], the $a[k]$ parameters of the AR process and the $a^{f/b}[k]$ prediction coefficients[1] of the order $\hat{p}$ predictor will be identical. Furthermore, the prediction error variance $\xi^{f/b}$ will be identical to σ_w^2, the variance of the white-noise sequence, *i.e.* the prediction-error filter is a whitening filter. For heart sounds,

[1] the superscript 'f/b' denotes that either forward or backward linear prediction may be used

i.e. a non-AR process, the prediction-error filter attempts to remove the correlation between the signal samples. As the order of the predictor is increased, the predicted output becomes a close approximation to its actual value, with the prediction error approaching a white-noise sequence [83, 115].

5.2.3.1 Separate Forward Linear Prediction Analysis

With a heart sound time series (N data samples indexed from $n = 0$ to $N - 1$), the forward prediction error $e^f[n]$ may be defined over the range from $n = 0$ to $n = N + \hat{p} - 1$. The total squared error (energy) to be minimised is defined to be:

$$\xi^f = \sum_n |e^f[n]|^2 \tag{5.37}$$

where a number of summation ranges may be selected. Selecting the range from $e^f[0]$ to $e^f[N + \hat{p} - 1]$ where:

$$\xi^f = \sum_{n=0}^{N+\hat{p}-1} |e^f[n]|^2 \tag{5.38}$$

is the windowed case, as it entails an implicit rectangular windowing of the data samples to extend the index range for $e^f[n]$ from $n = 0$ to $n = N + \hat{p} - 1$, *i.e.* unavailable data samples are set to zero. This windowed case is termed the 'autocorrelation' method of least-squares linear prediction analysis with the resulting matrix of autocorrelation estimates having a Toeplitz symmetry [113]. The autocorrelation method of linear prediction analysis is equivalent to the Yule-Walker method of AR parameter estimation, with the windowing of the data responsible for the reduction in resolution relative to other linear prediction-based methods. Therefore this approach is not suitable for short-time data records.

Selecting the range from $e^f[\hat{p}]$ to $e^f[N - 1]$ where:

$$\xi^f = \sum_{n=\hat{p}}^{N-1} |e^f[n]|^2 \tag{5.39}$$

is the nonwindowed case, as only available data samples are used, *i.e.* the limits are chosen to always remain within the measured data. This nonwindowed method is termed the 'covariance' method of least-squares linear prediction analysis with the resulting matrix of autocorrelation estimates having the properties of a covariance matrix [113, 116].

5.2.3.2 Combined Forward and Backward Linear Prediction

Both forward and backward linear prediction have similar statistical information and by combining the forward and backward linear prediction error statistics, twice as much data is available[2] The combined total error is defined to be:

$$\xi^{fb} = \sum_{n=\hat{p}}^{N-1} (|e^f[n]|^2 + |e^b[n]|^2) \tag{5.40}$$

The net result is a reduction in variance and hence an improved estimate of the AR parameters [103, 106]. This method is termed the 'forward-backward method' also known as the Modified covariance (MCV) method.

5.2.3.3 The Burg (Harmonic) Algorithm

An alternative method of AR parameter estimation based on the least-squares minimisation of the total forward and backward prediction errors is the Burg algorithm, sometimes also referred to as the maximum entropy method of spectral estimation. To obtain estimates of the predictor (or AR) parameters, at each order $\hat{p}$, the arithmetic mean of the combined forward and backward linear prediction error power is minimised. This combined error is defined to be:

$$\xi^{fb} = \sum_{n=\hat{p}}^{N-1} (|e^f[n]|^2 + |e^b[n]|^2) \tag{5.41}$$

The minimisation of ξ^{fb} is subject to the constraint that the AR parameters satisfy the Levinson-Durbin algorithm recursion. This constraint was motivated by the desire to ensure a stable AR filter, *i.e.* poles within the unit-circle. As with the MCV method, the summation ranges only over available data. However, with the Burg algorithm, the least-squares minimisation is with respect to a single parameter, namely, the reflection coefficient, $\hat{k}_{\hat{p}}$, defined in the equivalent lattice filter realisation of the linear prediction error filter [78, 83, 106]. For a heart sound time series (N data samples indexed from $n = 0$ to $N - 1$), at each order $\hat{p}$, $\hat{k}_{\hat{p}}$ is defined to be:

$$\hat{k}_{\hat{p}} = \frac{-2\sum_{n=\hat{p}}^{N-1} e^f_{\hat{p}-1}[n] e^{b*}_{\hat{p}-1}[n-1]}{\sum_{n=\hat{p}}^{N-1} |e^f_{\hat{p}-1}[n]|^2 + |e^b_{\hat{p}-1}[n]|^2} \tag{5.42}$$

[2] the superscript '*fb*' denotes combined forward-backward linear prediction.

The Burg algorithm is computationally efficient [78,103,117,118], yields a stable AR model and results in high frequency resolution. However, in spite of these advantages, a number of inherent performance limitations are associated with the use of the Burg algorithm to accurately transform time series to the frequency domain. Firstly, it exhibits spectral line splitting, where one actual peak in the sound spectrum is split into two or more closely spaced peaks [119, 120]; and secondly, at high model orders, it introduces spurious peaks and detail into the sound spectrum which is not actually present. In this thesis, correct interpretation of the sound spectrum is paramount before associating spectra with physiological and pathological functionality. In addition, for sinusoidal signals in noise, the Burg algorithm is known to exhibit a sensitivity to the initial phase of a sinusoid, especially for short-time data records. This sensitivity is manifest as a frequency shift from the true frequency resulting in a frequency bias that is phase dependant. In order to overcome these limitations, a modification has been proposed to the Burg algorithm. The modification involves the application of a weighting or windowing sequence, $w[n]$, to the squared forward and backward errors. The least-squares minimisation is now performed on the weighted combined squared errors defined to be:

$$\xi^{fb} = \sum_{n=\hat{p}}^{N-1} w[n] \left(|e^f[n]|^2 + |e^b[n]|^2 \right) \tag{5.43}$$

which when minimised, yields the reflection coefficient estimate:

$$\hat{k}_{\hat{p}} = \frac{-2 \sum_{n=\hat{p}}^{N-1} w_{\hat{p}-1}[n] e^f_{\hat{p}-1}[n] e^{b*}_{\hat{p}-1}[n-1]}{\sum_{n=\hat{p}}^{N-1} w_{\hat{p}-1}[n] \left(|e^f_{\hat{p}-1}[n]|^2 + |e^b_{\hat{p}-1}[n]|^2 \right)} \tag{5.44}$$

In this thesis, the weighting sequences used were: the Hamming windowing function and an optimum parabolic taper [121,122]. At each order $\hat{p}$, the recursive Hamming window function is defined to be:

$$W_{\hat{p}}[k] = 0.54 - 0.46 \cos\left(\frac{2\pi k}{N-\hat{p}} + \frac{\pi}{N-\hat{p}} \right) \quad \text{for } k = 0, 1, \ldots, N-1-\hat{p} \tag{5.45}$$

The optimum parabolic taper is defined to be:

$$W_{\hat{p}}[k] = \frac{6\,(k+1)(N-\hat{p}-k+1)}{(N-\hat{p}+1)(N-\hat{p}+2)(N-\hat{p}+3)} \quad \text{for } k = 0, 1, \ldots, N-1-\hat{p}. \tag{5.46}$$

These weighting sequences are particularly effective in reducing the occurrence of spectral line splitting, spurious peaks and frequency bias. In particular, the quadratic optimum parabolic taper was derived to minimise the frequency averaged variance of the estimated frequency of a real sinusoid over all possible phases. The net result is that both spectral line splitting and frequency bias are alleviated without any degradation in spectral resolution while maintaining stability [122].

Of all the least-squares linear prediction-based spectral estimation techniques, the Burg algorithm and the MCV method produce estimates with the least PSD variance. Moreover, as the MCV method is based on unconstrained forward-backward linear prediction, it results in superior performance over all other linear-predictive methods. The net result is an absence of spectral line splitting and less bias and variance in the frequency estimates of spectral components. Furthermore, the MCV method is almost as computationally efficient as the Burg algorithm with a complexity proportional to the order squared [123, 124].

5.2.4 Prony's Method

Prony's method is an ARMA parametric modelling technique based on a linear deterministic model, which synthesises sampled data as a linear combination of exponentials [78, 103, 125, 126]. The primary motivation for investigating the Prony model is that the modern least-squares version of Prony's method generalises to a damped sinusoidal model. The transient-oscillatory nature of heart sounds suggests that the utility of such a model would be more appropriate than the ARMA-based methods, providing a more accurate synthesis. Prony's method seeks to fit a deterministic exponential model to the data, in contrast to AR and ARMA methods which seek to fit a random model to the second-order statistics [106]. The Prony model is defined to be:

$$\hat{x}[n] = \sum_{k=1}^{\hat{p}} A[k] \exp\left[(\alpha[k] + j2\pi f[k])(n-1)T + j\theta[k]\right] \tag{5.47}$$

for $0 \leq n \leq N-1$, where N is the number of data samples, T, is the sampling interval in seconds, $A[k]$, is the amplitude of the exponential, $\alpha[k]$, is the damping factor in second^{-1}, $f[k]$, is the sinusoidal frequency in Hz, $\theta[k]$, is the sinusoidal initial phase in radians and $\hat{p}$ is the number of complex exponentials (model order). This $\hat{p}$-exponent discrete-time function can be expressed in the form:

$$\hat{x}[n] = \sum_{k=1}^{\hat{p}} h[k] z[k]^n \tag{5.48}$$

where the complex constants $h[k]$ and $z[k]$ are defined to be:

$$h[k] = A[k]\exp(j\theta[k]) \tag{5.49}$$

$$z[k] = \exp[(\alpha[k] + j2\pi f[k])T] \tag{5.50}$$

The constant $h[k]$ is time independent while $z[k]$ is a time-dependent parameter.

When analysing heart sounds, the squared modelling approximation error between the synthesised heart sound output and the actual sound, ξ, computed over the N data samples is defined to be:

$$\xi = \sum_{n=0}^{N-1} |\epsilon[n]|^2 \tag{5.51}$$

where

$$\epsilon = x[n] - \hat{x}[n] = x[n] - \sum_{k=1}^{\hat{p}} h[k]z[k]^n \tag{5.52}$$

with respect to the parameters $h[k]$ and $z[k]$ and the number of exponents $\hat{p}$. However, simultaneous evaluation of the order $\hat{p}$ and the parameters $h[k]$ and $z[k]$ for $k = 1$ to $k = \hat{p}$ that minimises the total, squared modelling approximation error ξ is a highly nonlinear operation, requiring the implementation of very computationally expensive algorithms [78]. Consequently, the complexity of these algorithms led to the development of a suboptimum minimisation of ξ based on a least-squares analysis. The least-squares version of Prony's method, also known as the 'Extended Prony Method', utilises a set of linear equations, with an intermediate step that concentrates the nonlinear aspects of the exponential model into one of polynomial factoring.

5.2.4.1 Evaluation of Prony Model Parameters

When analysing bioprosthetic heart valve closing sounds, the number of data samples N exceeds the minimum number needed to fit a model of $\hat{p}$ exponentials, *i.e.* $N > 2\hat{p}$. For this overdetermined case, the $\hat{p}$ equations of (5.48) for $1 \leq n \leq N$ can be expressed in matrix form as:

$$\mathrm{Zh} = \mathrm{x} \tag{5.53}$$

where:

$$\mathbf{Z} = \begin{pmatrix} 1 & 1 & \dots & 1 \\ z[1] & z[2] & \dots & z[\hat{p}] \\ \vdots & \vdots & \ddots & \vdots \\ z[1]^{N-1} & z[2]^{N-1} & \dots & z[\hat{p}]^{N-1} \end{pmatrix} \quad \mathbf{h} = \begin{pmatrix} h[1] \\ h[2] \\ \vdots \\ h[p] \end{pmatrix} \quad \mathbf{x} = \begin{pmatrix} x[1] \\ x[2] \\ \vdots \\ x[N] \end{pmatrix} \tag{5.54}$$

from which the time-indexed z elements are first evaluated followed by the solution of the linear simultaneous equations for the unknown vector of complex amplitudes. The subsequent parameters of each exponential, *i.e.* the $\alpha[k]$, $f[k]$, $A[k]$ and $\theta[k]$ terms, can then be computed from $h[k]$ and $z[k]$. Equation (5.48) represents the solution of a homogeneous linear difference equation which can be evaluated from a polynomial, $\phi[z]$, that has the $z[k]$ exponents as its roots, defined to be:

$$\phi[z] = \prod_{k=1}^{\hat{p}} (z - z[k]) \tag{5.55}$$

with complex coefficients, $a[m]$, when expanded into a power series becomes:

$$\phi[z] = \sum_{m=0}^{\hat{p}} a[m] z^{\hat{p}-m} \tag{5.56}$$

where $a[0] = 1$. For heart sounds, *i.e.* $N > 2\hat{p}$, the homogeneous linear difference equation whose solution is (5.48) is defined to be:

$$\hat{x}[n] = -\sum_{m=1}^{\hat{p}} a[m] x[n-m] + e^f[n] \tag{5.57}$$

for $\hat{p} + 1 \leq n \leq N$. This is the equation for the forward linear prediction estimate $\hat{x}[n]$ of $x[n]$ previously defined in section 5.2.3, where the term $e^f[n]$ represents the forward linear prediction approximation error, *i.e.* the difference between $x[n]$ and its linear prediction based on $\hat{p}$ past data samples. This in contrast to ϵ, which represents the Prony exponential modelling approximation error. Hence, each polynomial complex coefficient $a[m]$ is equivalent to a linear prediction parameter. The polynomial coefficients can now be evaluated as those that minimise the forward linear prediction squared error, $\sum_{n=\hat{p}}^{N-1} |e^f[n]|^2$, previously defined by equation (5.38) rather than the squared, exponential modelling approximation error ξ. This minimisation is equivalent to the covariance method of linear prediction as detailed in section 5.2.3.1. Thus, the extended Prony parameter estimation procedure reduces to that of an AR parameter estimation. Moreover, the number of exponentials $\hat{p}$ (number of poles in AR analysis) can be quantitatively

calculated from the heart sound time series using AR model order selection criteria to be presented in section 5.2.5. However, in terms of PSD estimation, the transient-oscillatory morphology of the heart sound signal suggests that the damped sinusoidal Prony model will result in a more accurate synthesis and overall better spectral estimate than the AR covariance method. The evaluation of the Prony parameters from a heart sound time series can be summarised as follows:

1. Estimate the order $\hat{p}_{hs}$ of the principal heart sound time series.

2. The linear prediction parameters are first computed from the heart sound time series, which are equivalent to the complex polynomial coefficients $a[m]$ defined in (5.56)

3. The linear prediction coefficients $a[m]$ are used to construct the polynomial defined in (5.56) from which the roots are calculated. The damping $\alpha[m]$ and sinusoidal frequency $f[m]$ terms of each exponential can be determined from each root $z[m]$ using the relationships:

$$\alpha[m] = \ln|z[m]| / T \tag{5.58}$$

$$f[m] = \tan^{-1}\left[\Im\{z[m]\}/\Re\{z[m]\}\right] / 2\pi T \tag{5.59}$$

4. The computed roots are used to construct the matrix of $z[k]$ elements of (5.54), which is then solved for the unknown vector $\boldsymbol{h}$. This matrix of time-indexed z elements has a Vandermonde structure, *i.e.* $(z_{ij} = z_j^{i-1})$. The amplitude $A[m]$ and initial phase $\theta[m]$ terms of each exponential can be determined from the $h[k]$ parameter using the relationships:

$$A[m] = |h[m]| \tag{5.60}$$

$$\theta[m] = \tan^{-1}\left[\Im\{h[m]\}/\Re\{h[m]\}\right] \tag{5.61}$$

The resulting Prony ESD estimate, $\hat{S}_P[f]$, is derived on the assumption that the discrete-time exponential sum of (5.48) is defined over the interval $-\infty < n < \infty$ as a one-sided function:

$$\hat{x}[n] = \begin{cases} \sum_{k=1}^{\hat{p}} h[k] z[k]^n & n \geq 0 \\ 0 & n < 0 \end{cases} \tag{5.62}$$

The z-transform of (5.62) is:

$$\hat{X}[z] = \sum_{k=1}^{\hat{p}} \left(\frac{h[k]}{1 - z[k] z^{-1}} \right) \tag{5.63}$$

and substitution of $z = \exp(j2\pi f T)$ yields the discrete-time Fourier transform of the deterministic finite-energy sequence:

$$\hat{S}_{xx}^{P}[f] = \left| T \left(\sum_{k=1}^{\hat{p}} \frac{A[k] \exp(j\theta[k])}{1 - \exp[(\alpha[k] + j2\pi f[k])T] \exp(-j2\pi f T)} \right) \right|^2 \tag{5.64}$$

defined over the frequency range $-1/2T \leq f \leq 1/2T$. This spectrum is particularly appropriate for transient heart sounds, with peaks that are linearly proportional to spectral power.

5.2.5 Model Order Selection

When analysing the spectral content of bioprosthetic heart valve closing sounds, correct interpretation of the sound spectrum is paramount before associating spectra with physiological and pathological functionality. This is particularly significant when analysing heart sounds using parametric spectral estimation techniques, as the precise model order of the principal component time series is not known *a priori* and variations in spectra can occur with different orders. Therefore accurate model order determination is essential.

As a result of the variability in the structure and duration of heart sounds across the patient population, the use was rejected of a single universal order for all sounds and universal orders for each principal component. An individual analysis of each sound will account for this variability and produce more accurate and reliable results. The model order, *i.e.* the number of poles $\hat{p}$ and zeros $\hat{q}$, is a very important parameter when using parametric techniques to assess the spectral characteristics of valvular closing sounds. Ideally, it is desirable to have the minimum values for $\hat{p}$ and $\hat{q}$ that are adequate to represent the process: to reduce computation and to minimise the possibility of numerical ill-conditioning which increases with $\hat{p}$ as the prediction error variance $\xi^{f/b}$ decreases. However, too low an order will result in a highly-smoothed spectrum with low frequency resolution, containing little or no information of diagnostic value concerning the integrity of prostheses. This is due to there being too few pole-zero coefficients to sufficiently model the sound spectrum. Moreover, it is required to have large enough values of $\hat{p}$ and $\hat{q}$ to adequately model the process, with the fit of the model improving as $\hat{p}$ and $\hat{q}$ increase. However, too high an order introduces spurious detail such as false peaks which are not actually present into the spectrum and can also lead to the modelling of background noise. This is a result of extra 'noise' poles situated close to the unit-circle [106, 108, 113].

5.2.5.1 AR Hypothesis-Based Model Order Selection

For the least-squares, linear predictive AR estimation techniques, examination of the computed prediction error variance can provide an indication of the optimal model order. The prediction error (residual) variance ξ^{flb} decreases monotonically with increasing order $\hat{p}$. The Burg algorithm, covariance and modified covariance methods all involve a relationship for the mean/least squared error defined to be:

$$\xi_{\hat{p}}^{flb} = \xi_{\hat{p}-1}^{flb}(1 - |\hat{k}_{\hat{p}}|^2) \tag{5.65}$$

As the reflection coefficient $\hat{k}_{\hat{p}}$ is nonzero and less than or equal to one, the prediction error variance decreases with increasing order $\hat{p}$, and being a squared error, always remains positive: where $0 \leq \xi_{\hat{p}}^{flb} \leq \xi_{\hat{p}-1}^{flb}$. If the signal spectrum is an all-pole spectrum with p poles, then theoretically the prediction error variance ξ^{flb} remains flat for $\hat{p} \geq p$. Therefore examination of the error curve reveals that the optimal order for the model is the order at which the curve becomes flat. However, if the signal is the output of a p-pole filter excited by white noise, then this test will not work, as the estimates of the poles are based on a finite number of samples with the error curve not being flat for $\hat{p} \geq p$. In practice; however, the error curve will be almost flat. For valvular closing sounds (quasi-periodic transients with background noise, *i.e.* a non-AR process), an indication of the optimal order for the model is obtained by directly monitoring the monotonically decreasing prediction error variance. The order at which the rate of change in error variance suddenly decreases or the order when the rate of change becomes relatively slow is taken to be the optimal order [127]. This method of determining the optimal model order is sometimes also referred to as the Levinson-Durbin method of model order selection [128].

In this thesis, the optimal number of poles and zeros was evaluated by computing the normalised root-mean-square error (NRMSE) between the closing sounds $x[n]$ and the impulse response $h[n]$ of the parametric models for different values of $\hat{p}$ and $\hat{q}$, where the NRMSE for the MCV method is defined to be:

$$\text{NRMSE} = \sqrt{\frac{\sum_{n=\hat{p}}^{N-1}(x[n] - h[n])^2}{\sum_{n=0}^{N-1} x[n]^2}} \tag{5.66}$$

5.2.5.2 AR Multiple Decision-Based Model Order Selection Criteria

The monitoring of the monotonically decreasing prediction error variance or NRMSE is based on hypothesis testing methods using maximum likelihood ratios, rather than on some quantitative procedure where multiple decisions are used. This has been the major reason for the criticism of the use of such techniques [129,130] and the development of alternative less subjective methods, where model fitting is regarded as an estimation problem with an associated measure of fit. These alternative methods adhere to the philosophy of monitoring the decreasing prediction error variance while accounting for the increase in variance of a spectral estimate based on an increasing number of parameters. The prediction error variance is central to model order selection, because, from the Levinson-Durbin recursion $\xi^{f/b}$ decreases monotonically with $\hat{p}$ and first reaches a minimum for $\hat{p} = p$ for an AR[p] process.

The criteria presented in this section can be used to determine the optimal order and are known to work well for computer-generated synthetic AR data. The performance of these methods when applied to physiological phenomena such as heart sound signals depends on how well the valvular closing sounds can be synthesised by the parametric modelling techniques. For each method, the range of AR model orders to be considered is first selected. For each value of p, the AR parameters are estimated under the assumption that p is the correct order. The prediction error variance is also obtained, from which, the selection criterion for the model is computed. The value of p yielding the lowest value of the selection criterion is chosen as the best estimate of the true model order.

5.2.5.2.1 Final Prediction Error

This criterion selects the order of an AR process so that the mean square error variance for a one-step predictor is minimised [131,132]. The Final Prediction Error (FPE) for an AR process is defined to be:

$$\mathrm{FPE}[\hat{p}] = \xi_{\hat{p}}^{f/b} \frac{N + (\hat{p} + 1)}{N - (\hat{p} + 1)} \tag{5.67}$$

where (5.67) assumes that the mean has been removed from the data. The term in parentheses increases as the order increases, reflecting the increase in the uncertainty of the prediction error variance. The order $\hat{p}$ selected is the one for which the FPE is a minimum.

5.2.5.2.2 Akaike Information Criterion

Akaike [129] extended the FPE method by using a maximum likelihood approach to derive a criterion known as the Akaike Information Criterion (AIC). The AIC determines the optimal

order by minimising an information theoretic function:

$$\mathrm{AIC}[\hat{p}] = -2\ \ln(\textit{maximised likelihood}) + 2\hat{p}$$

where $\hat{p}$ is the number of independent parameters within the model which are adjusted to attain the maximum of the likelihood. The AIC for an AR process is defined to be:

$$\mathrm{AIC}[\hat{p}] = N \ln(\xi_{\hat{p}}^{flb}) + 2\hat{p} \tag{5.68}$$

where the term $2\hat{p}$ represents the penalty for the use of extra AR coefficients that do not result in a substantial reduction in the prediction error variance [106, 133].

5.2.5.2.3 Minimum Description Length

The FPE and AIC have been found to be statistically inconsistent in that the probability of error in choosing the correct order does not tend to zero as $N \rightarrow \infty$ [106, 134]. This limitation of the FPE and AIC criteria prompted Rissanen [135] to develop a variant information theoretic criterion to the AIC known as the Minimum Description Length (MDL), which is defined to be:

$$\mathrm{MDL}[\hat{p}] = N \ln(\xi^{flb}) + \hat{p} \ln(N) \tag{5.69}$$

The MDL is statistically consistent because $\hat{p} \ln(N)$ increases with N faster than with $\hat{p}$ [106, 135].

5.2.5.2.4 Criterion Autoregressive Transfer

The Criterion Autoregressive Transfer (CAT) function selects the order $\hat{p}$ to be the one in which the estimate of the difference between mean square errors of the true prediction error filter and the estimated filter is a minimum [136]. This difference can be calculated without explicitly knowing the true prediction error filter. It is defined to be:

$$\mathrm{CAT}[\hat{p}] = \left(\frac{1}{N} \sum_{k=1}^{\hat{p}} \frac{1}{\bar{\xi}_k^{flb}} \right) - \frac{1}{\xi_{\hat{p}}^{flb}} \tag{5.70}$$

where $\bar{\xi}_k^{flb} = [N/(N-k)]\xi_k^{flb}$. As before, $\hat{p}$ is chosen to minimise $\mathrm{CAT}[\hat{p}]$.

5.2.5.3 Linear-Algebra-Based Model Order Selection

Information regarding the precise model order which should be used when analysing bioprosthetic heart valve closing sounds is implicitly contained within the autocorrelation and data

matrices which characterise linear-algebra-based spectral estimation techniques. This information may be obtained by first removing the numerical ill-conditioning inherent with the use of such techniques, *e.g.* the statistical errors associated with the autocorrelation estimation procedure and/or the ill-conditioning of data matrices as a result of background noise.

5.2.5.3.1 ARMA Modelling

When the ARMA modelling parameters $\hat{p}$ and $\hat{q}$ are not known *a priori*, it is usual to select the initial order of the model, $[p_e, q_e]$, to be much larger that the eventual order of the principal component time series p_{hs}. The $L \times (p_e + 1)$ overdetermined extended-order matrix of autocorrelation estimates, $\hat{\mathbf{R}}_{e(xx)}$, associated with this ARMA$[p_e, q_e]$ model is defined to be:

$$\hat{\mathbf{R}}_{e(xx)} = \begin{pmatrix} \hat{r}_{xx}[\hat{q}_e] & \hat{r}_{xx}[\hat{q}_e - 1] & \dots & \hat{r}_{xx}[\hat{q}_e - \hat{p}_e + 1] \\ \hat{r}_{xx}[\hat{q}_e + 1] & \hat{r}_{xx}[\hat{q}_e] & \dots & \hat{r}_{xx}[\hat{q}_e - \hat{p}_e + 2] \\ \vdots & \vdots & \ddots & \vdots \\ \hat{r}_{xx}[L-1] & \hat{r}_{xx}[L-2] & \dots & \hat{r}_{xx}[L - \hat{p}_e] \end{pmatrix} \tag{5.71}$$

When actual autocorrelation lag information is available for PSD estimation, the rank of this overdetermined, extended-order autocorrelation matrix $R_{e(xx)}$ equals the true order [108]. However, in this study, samples of acquired heart sounds, *i.e.* a time series with order p_{hs}, are used to form the autocorrelation estimate matrix $\hat{\mathbf{R}}_{e(xx)}$. The rank of $\hat{\mathbf{R}}_{e(xx)}$ will typically be full for all values of $\hat{p}$ due to the invariable statistical errors inherent in the estimation of the autocorrelation function. Even though $\hat{\mathbf{R}}_{e(xx)}$ will have full rank, it will generally be found that when $\hat{p} > p_{hs}$, this matrix will have $(\hat{p} - p_{hs})$ of its eigenvalues close to zero, *i.e.* the 'effective' rank of $\hat{\mathbf{R}}_{e(xx)}$ is still equal to p_{hs}. Therefore an order selection procedure which examines the eigenvalue behaviour of the autocorrelation estimate matrix $\hat{\mathbf{R}}_{e(xx)}$ as a function of $\hat{p}$, can be used to determine the optimal model order [90, 137]. A method for implementing this procedure based on the Singular Value Decomposition (SVD) operation is used to determine the precise order. SVD removes the statistical errors from the autocorrelation estimation procedure thereby eliminating the inherent numerical ill-conditioning and producing a rank p_{hs} optimum approximation, $\hat{\mathbf{R}}^{(p_{hs})}_{e(xx)}$, of the $L \times (p_e + 1)$ overdetermined, extended-order, autocorrelation estimate matrix $\hat{\mathbf{R}}_{e(xx)}$. The matrix $\hat{\mathbf{R}}^{(p_{hs})}_{e(xx)}$ is a better estimate of the true autocorrelation matrix than $\hat{\mathbf{R}}_{xx}$, and is defined to be:

$$\hat{\mathbf{R}}^{(p_{hs})}_{e(xx)} = U \Sigma_{p_{hs}} V^* \tag{5.72}$$

where $\mathbf{U}$ and $\mathbf{V}^*$ are unitary matrices associated with the SVD operation and $\mathbf{\Sigma}_{p_{hs}}$ is a diagonal matrix of ordered singular values such that: $\sigma_{11} \geq \sigma_{22} \geq ... \geq \sigma_{p_{hs},p_{hs}} \geq 0$. These singular values convey valuable information concerning the rank characterisation of $\hat{\mathbf{R}}_{e(xx)}$. The quality of this optimum approximation based on the standard matrix Frobenius norm, $\| \, . \, \|_2$, is given by:

$$\| \hat{\mathbf{R}}_{e(xx)} - \hat{\mathbf{R}}_{e(xx)}^{(p_{hs})} \| = \left[\sum_{k=p_{hs}+1}^{p_e} \sigma_{kk}^2 \right]^{1/2} \qquad 0 \leq p_{hs} \leq p_e \tag{5.73}$$

The degree to which $\hat{\mathbf{R}}_{e(xx)}^{(p_{hs})}$ approximates $\hat{\mathbf{R}}_{e(xx)}$ is dependent on the sum of the $(p_e - p_{hs})$ smallest singular values. As p_{hs} approaches p_e, this sum will become progressively smaller and will eventually go to zero at $p_{hs} = p_e$. A convenient measure for this behaviour based on the standard matrix norm, $\| \, . \, \|$, is the normalised ratio:

$$\nu(p_{hs}) = \frac{\| \hat{\mathbf{R}}_{e(xx)}^{(p_{hs})} \|}{\| \hat{\mathbf{R}}_{e(xx)} \|} = \left[\frac{\sigma_{11}^2 + \sigma_{22}^2 + ... + \sigma_{p_{hs},p_{hs}}^2}{\sigma_{11}^2 + \sigma_{22}^2 + ... + \sigma_{p_e,p_e}^2} \right]^{1/2} \qquad 1 \leq p_{hs} \leq p_e \tag{5.74}$$

where $1 \leq p_{hs} \leq p_e$, with the actual order p_{hs} being the smallest value of $\hat{p}$ for which $\nu(p_{hs})$ is considered adequately close to one. For matrices of low effective rank, as in this thesis, the quantity $\nu(p_{hs})$ will be close to one for values of p_{hs} significantly smaller than p_e. As $\hat{\mathbf{R}}_{e(xx)}^{(p_{hs})}$ is a less noisy version of $\hat{\mathbf{R}}_{e(xx)}$, the resulting estimate PSD will be better than that obtained from the direct solution of the extended Yule-Walker equations.

Therefore upon adopting an extended-order approach, the resultant parameter estimates will generally be found to be less sensitive to the errors contained in the autocorrelation lag estimates than for the minimal order choice of $\hat{p}$. This leads to a significant improvement in overall modelling performance: particularly suited for the generation of low-order, high-quality spectral estimates from short-time heart sound data records. Furthermore, the PSD estimate which is generated using this extended-order procedure will typically have much more sharply defined peaks at the $\hat{p}$ frequencies and better resolution than those obtained from the minimal order choice of $\hat{p}$ [138].

Hence as well as alleviating the numerical ill-conditioning of the autocorrelation estimate matrix, the relative magnitudes of the heart sound signal-related singular values are larger and dominate those related to noise [90]. This allows for the identification of the number of heart sound signal-related values (signal modes), *i.e.* the optimal model order p_{hs}, in relation to the remaining $(p_e - p_{hs})$ relatively insignificant-sized nonzero values.

5.2.5.3.2 AR Modelling

With AR modelling, information regarding the precise order which should be used can be extracted from the data matrix used by the linear prediction-based methods. The linear prediction equations in matrix form can be written as $\mathbf{A}\,\mathbf{c} \simeq \mathbf{b}$, where, $\mathbf{A}$, is the data matrix, $\mathbf{b}$, the data vector and, $\mathbf{c}$, the linear prediction coefficient vector. The minimum norm solution can be expressed in terms of the pseudoinverse, $\mathbf{A}^I$, of the data matrix $\mathbf{A}$, where $\mathbf{c} = \mathbf{A}^I\mathbf{b}$. This pseudoinverse matrix $\mathbf{A}^I$ is related to the SVD of $\mathbf{A}$ by $\mathbf{A}^I = \mathbf{V}\Sigma^I\mathbf{U}^*$, where Σ^I is obtained from Σ by replacing each positive entry by its reciprocal. With an ideal (noiseless) heart valve closing sound, the solution is good: the rank of the data matrix A is p_{hs} with only p_{hs} nonzero elements in the diagonal matrices Σ and Σ^I. In practice; however, background noise changes the situation, with the data matrix $\mathbf{A}$ taking on its full rank. The matrix Σ then has some (or likely all) of its formerly zero singular values becoming small nonzero values. The small diagonal values of Σ introduced by background noise, become large diagonal values in Σ^I causing large perturbations in the prediction coefficient vector. The main perturbation effects of a small amount of noise are due to the increase in rank of $\mathbf{A}$ over its rank in the noiseless case and the associated large perturbations in the directions of the rest of the columns of $\mathbf{U}$ and $\mathbf{V}$. This ill-conditioning of the data matrix $\mathbf{A}$ when analysing heart valve closing sounds can be alleviated by using SVD and replacing $\mathbf{A}$ with a lower rank optimum approximation, $\mathbf{A}^{p_{hs}}$, prior to calculating the prediction coefficients. The relative magnitudes of the heart sound signal-related singular values are larger and dominate those related to background noise and examination of these values permits identification of p_{hs} - the optimal model order [139].

5.2.5.3.3 Prony's Method

The least squares version of Prony's method requires the solution of the covariance linear prediction normal equations used in AR spectral analysis. With low levels of noise, the AR decision-based criteria, *i.e.* FPE, AIC, MDL and CAT may be used to estimate the number of exponentials $\hat{p}$ (number of poles in AR analysis). With higher levels of noise, the frequency and damping component estimates are usually inaccurate and biased due to the effects of noise. Distinguishing the roots of the Prony characteristic polynomial, *i.e.* the roots due to weak signal exponentials from those as a result of noise, is often difficult. With Prony's method, if too high an order is selected, extraneous poles are generated which cause the residues of the true signal poles to be inaccurate. Too low an order results in the returned poles deviating from the true signal poles [140, 141].

As discussed in section 5.2.4.1, the $\hat{p}$ exponentials are generated by forward linear predic-

tion. The same $\hat{p}$ exponentials may also be generated by backward linear prediction. Examining the roots of the forward and backward linear prediction filter polynomials can determine which order to use. The roots of the forward linear prediction characteristic polynomial, $A[z]$, fall inside the unit z-plane circle, whereas the roots of the backward linear prediction characteristic polynomial, $B[z]$, fall outside the unit-circle. With an ideal (noiseless) heart valve closing sound consisting of p_{hs} exponentials, p_{hs} zeros would be identified. In practice, however, background noise biases the estimates of the zeros. This bias can be reduced significantly by selecting a linear prediction order much larger than p_{hs}. The p_{hs} true signal zeros of $B[z]$ will fall outside the unit circle whereas the $(p - p_{hs})$ extraneous zeros fall inside the unit-circle. This allows for the identification of the number of p_{hs} heart sound signal zeros (optimal model order) from the $(p - p_{hs})$ extraneous zeros of $B[z]$ and is the primary reason for using the data backward linear prediction. Applying SVD to the data matrix can provide further improvement as it alleviates the ill-conditioning caused by selecting an order greater than p_{hs}. The p_{hs} eigenvectors associated with the p_{hs} largest singular values primarily span the p_{hs} exponential heart sound signal components. The $(p - p_{hs})$ eigenvectors of the remaining smaller singular values span the components of the background noise. The result of applying SVD is that extraneous zeros are much less perturbed and form a uniform pattern around the inside of the unit circle [106, 142, 143]. This allows for the identification of the number of zeros due to the signal exponentials, *i.e.* the optimal model order p_{hs}.

5.3 Summary and Conclusion

This chapter investigates signal processing methods for the transformation of mitral and aortic components to the frequency domain. Particular attention is paid to the physiological transient-oscillatory nature of the heart sound signal and the suitability of the spectral estimation techniques when analysing such a temporal signature. The methods considered were: the periodogram, including a description describing its limitations; the Bartlett power spectral density estimate, which reduces the variance of a conventional periodogram estimate through ensemble averaging; ARMA-based, parametric linear modelling techniques, which attempt to synthesise the heart sound generation process; and Prony's method: a parametric modelling technique based on a damped sinusoidal model.

The chapter concludes by addressing the important issue of selecting and determining the optimal model order when using parametric spectral estimation techniques. When analysing the spectral content of bioprosthetic heart valve closing sounds, correct interpretation of the

sound spectrum is paramount before associating spectra with physiological and pathological functionality. This is particularly significant when analysing heart sounds using parametric spectral estimation techniques, as the precise model order of the principal component time series is not known *a priori* and variations in spectra can occur with different orders. Too low an order produces a highly-smoothed spectrum containing little or no information of diagnostic value, whereas, too high an order, can introduce spurious detail and false peaks which are not actually present into the sound spectrum. The model order selection criteria considered were: hypothesis-based methods, which monitor the monotonically decreasing prediction error variance for a decrease in the rate of change; and more quantitative techniques based on the FPE, the AIC, the MDL and the CAT decision-based methods, and procedures which attempt to determine the optimum order from the heart sound time series by first removing the numerical ill-conditioning inherent with the use of linear-algebra-based spectral estimation techniques.

Chapter 6

Heart Sound Spectral Analysis

This chapter investigates the application of the methods for the frequency analysis of heart sounds to the full range of recorded mitral and aortic sounds: the periodogram, the Bartlett periodogram, AR and ARMA-based techniques and Prony's method. The aim is to compare the performance and suitability of these spectral estimation techniques in extracting from the frequency domain features which may be considered suitable for use as heuristic parameters. Results are also presented which assess the performance of model order selection criteria in determining the optimal model order when analysing principal heart sound component time series using parametric spectral analysis techniques. The overall objective is to identify optimum signal processing methods for this thesis.

6.1 Evaluation and Presentation of Frequency Spectra

Following the extraction of mitral or aortic components from a PCG, a PSD estimate was evaluated from each component. To minimise the variance between the resulting estimates, an ensemble spectral average was computed to represent the overall frequency spectrum for each recording. The resultant ensemble estimate was normalised (0dB) with respect to the frequency peak with the most dominant amplitude over all frequencies. This allows for a qualitative comparison of the spectra evaluated from the full range of recorded sounds, regardless of microphone coupling and the variability in the intensity of heart sounds resulting from different amplification gain factors from one recording to the next. All spectra were estimated from d.c. to 1kHz (Nyquist rate = 2kHz).

6.2 Performance of Methods for the Frequency Analysis of Heart Sounds: Results

Based on the investigation comparing the performance and suitability of the methods for the frequency analysis of heart sounds, the periodogram, the Bartlett periodogram, the AR and ARMA-based techniques and Prony's method were applied to the full range of recorded sounds. The major observations concerning the application and performance of these methods to mitral and aortic sounds were:

1. The superior resolution of Prony's method in identifying within the frequency domain a number of dominant spectral peaks over the full range of recorded sounds and valve conditions.

2. The covariance, MCV, Burg and weighted Burg (parabolic optimum taper and Hamming window) methods all produce almost identical spectra. The resulting estimates are able to identify the same features revealed by the Prony PSD estimate, however, the ability of these AR methods to completely resolve the same spectral detail is secondary to Prony's method.

3. For some sounds, a difference was observed between the spectra produced by the covariance method when compared to the estimates evaluated by the other AR techniques.

4. The application of the periodogram (with and without a Hamming window) produces smoothed spectra relative to the AR and Prony estimates.

5. The Bartlett periodogram produces very highly smoothed spectra, containing little or no information in the frequency spectrum which may be considered suitable for use as heuristic parameters.

Figures 6.1 and 6.2 illustrate these findings for typical mitral and aortic sounds respectively. These spectra were evaluated using Prony's method, the MCV method and the periodogram with the implicit rectangular window.

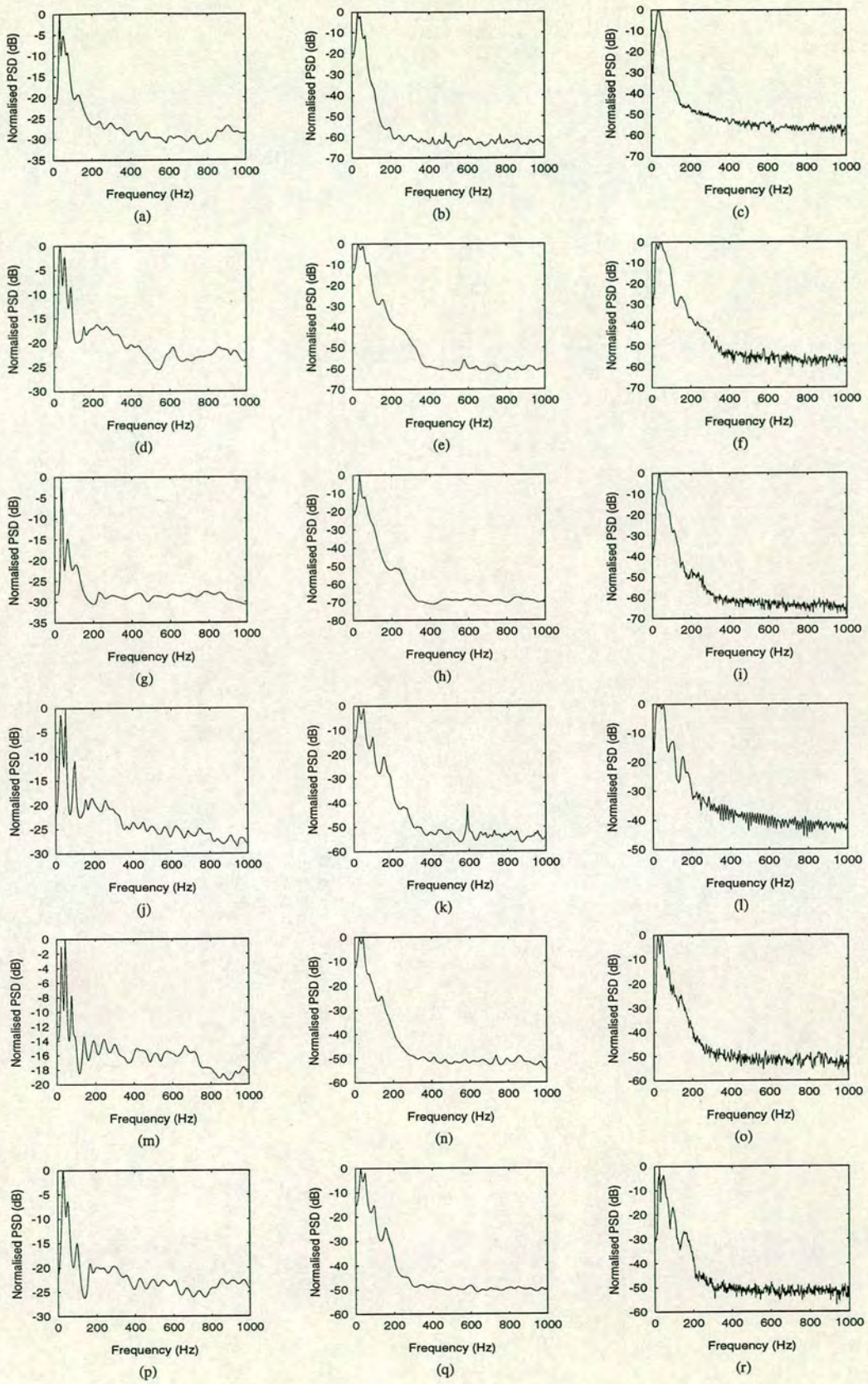

Figure 6.1: *Typical examples of Prony, MCV and periodogram ensemble PSD estimates respectively computed from mitral sounds. (a-c) source: mb3, (d-f) source: dg4, (g-i) source: tm5, (j-l) source: pw6, (m-o) source: jh2, (p-r) source: is6.*

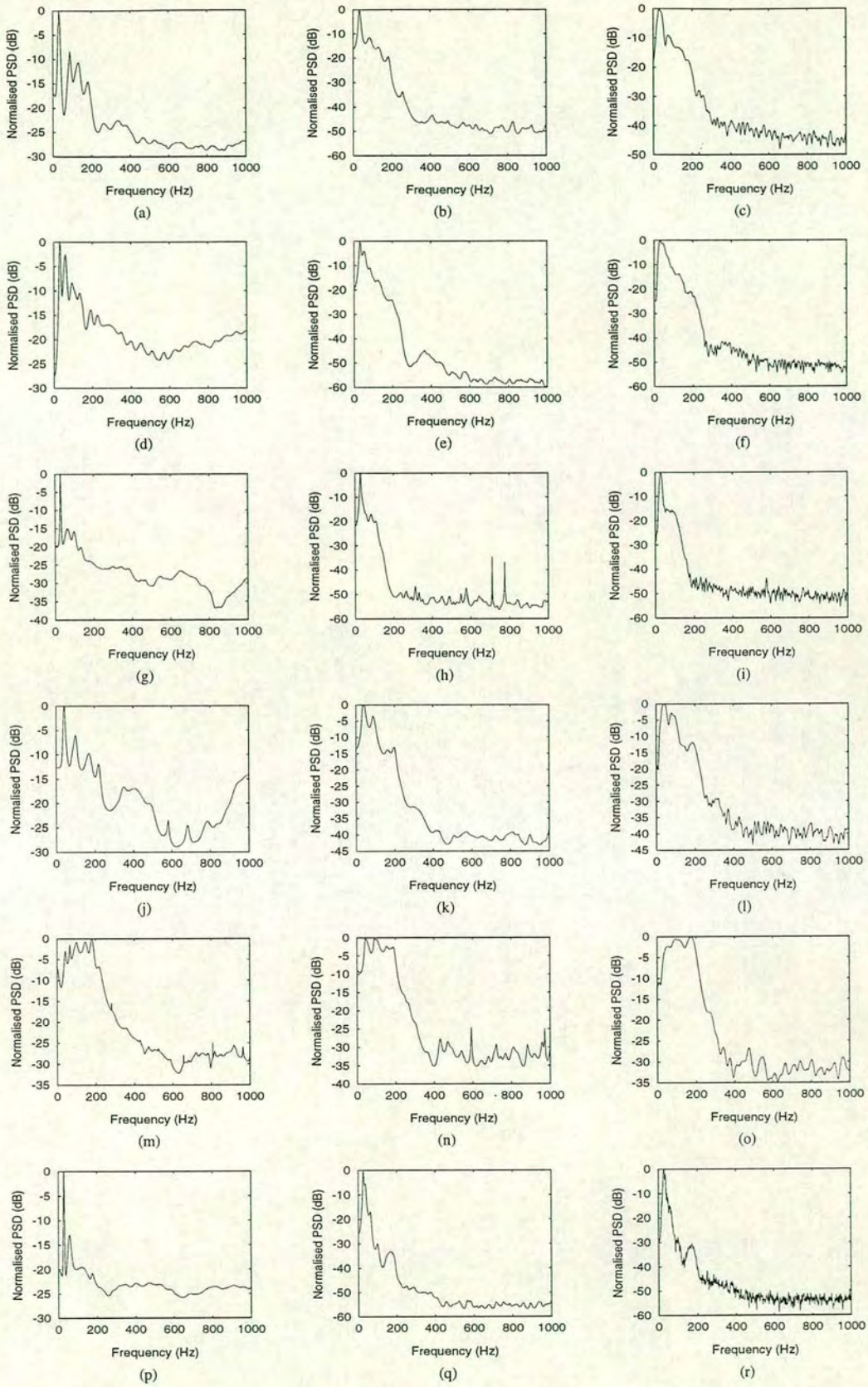

Figure 6.2: *Typical examples of Prony, MCV and periodogram ensemble PSD estimates respectively computed from aortic sounds. (a-c) source: em4, (d-f) source: an4, (g-i) source: eb4, (j-l) source: jm3, (m-o) source: mh4, (p-r) source: sh3.*

For most sounds, the AR covariance, MCV, Burg and weighted Burg methods all produce almost identical spectra. However, for some sounds, a difference was observed between the spectra produced by the covariance method when compared to the estimates evaluated by the other AR techniques. Figure 6.3 illustrates typical examples of PSD estimates computed using the covariance method, with corresponding MCV estimates shown in Figures 6.1 and 6.2. The frequency spectrum of Figure 6.3(a) reveals that the most dominant spectral peak originally identified by the spectra of Figure 6.1(k) is now the second most dominant peak. Similarly, the spectrum of Figure 6.3(d) reveals that the fourth dominant frequency peak identified by the spectra of Figure 6.2(b) is only just detected by the equivalent covariance estimate; however, the second most dominant spectral peak is better resolved as well as having a larger amplitude. In addition, a spurious peak is located at an amplitude of -28.86dB at 948Hz. Previous works [78, 106, 144–146] report on the limitations of the forward only prediction approach to AR spectral estimation when applied to processes consisting of sinusoids in white noise. It was observed that the AR parameters produced by the covariance method exhibit a greater sensitivity to noise and that the resulting PSD estimates can have more false peaks and greater perturbations of spectral peaks from their correct frequency location than other AR estimation approaches. Furthermore, spectral line splitting has been observed with the use of the covariance method [106, 147].

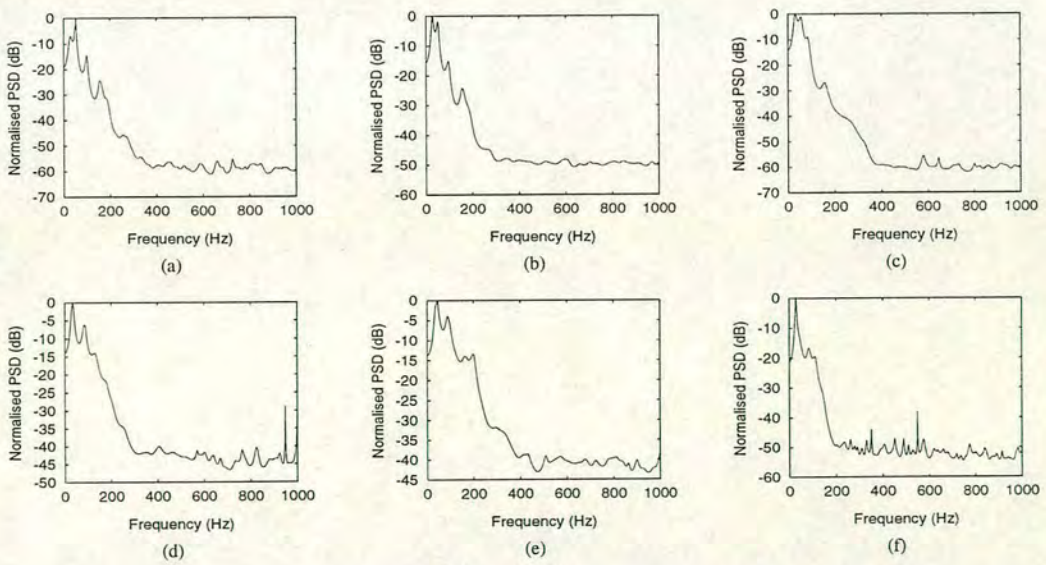

Figure 6.3: *Typical examples of ensemble spectra computed using the covariance method. (a-c) PSD estimates of mitral sounds; sources: pw6, is6 and dg4 respectively, (d-f) PSD estimates of aortic sounds; sources: em4, jm3 and eb4 respectively.*

The Burg algorithm and the weighted Burg methods produced almost identical spectra over the full range of recorded sounds and any differences between the resulting estimates are

negligible as illustrated in Figure 6.4. Corresponding MCV and covariance PSD estimates are shown in Figures 6.1, 6.2 and 6.3 respectively. When applied to processes consisting of sinusoids in white noise, the presence of spectral line splitting has been attributed to: high SNR, that the initial phase of the sinusoidal components is some odd multiple of 45° or that the time duration of the data sequence is such that sinusoidal components have an odd number of quarter cycles [119, 120, 147]. In this thesis, spectral line splitting was not observed over the full range of recorded sounds.

The periodogram produces smoothed spectra relative to the AR and Prony estimates as illustrated in Figures 6.1 and 6.2. The duration of mitral and aortic components typically varies in the range from 20 to 80mS. The corresponding periodogram resolution ranges from approximately $\frac{1}{80\text{ms}} = 12.5\text{Hz}$ to $\frac{1}{20\text{ms}} = 50\text{Hz}$. Figure 6.5 illustrates that the application of the periodogram with a Hamming window results in almost identical spectra to those evaluated using the implicit rectangular window as shown in Figures 6.1 and 6.2.

The spectra evaluated by the periodogram are similar in detail to those computed by the parametric methods; however, the resultant periodogram estimates are more erratic. The smoother, higher-resolution estimates computed by the parametric techniques result from the modelling of the mitral and aortic components, *i.e.* the parametric methods adapt to the characteristics of the signal and noise under investigation [97, 148]. A periodogram estimate may be viewed as a least-squares fit of a preassigned number of harmonically related sinusoidal frequencies to the data [78]. In addition, as the record length increases, the rapidity of the fluctuations in the periodogram estimate increases, as the variance of the periodogram becomes proportional to the square of the spectrum [104, 106]. The estimate then fluctuates about the true frequency spectrum.

The Bartlett method reduces the variance of the periodogram estimate through averaging. However, as illustrated in Figure 6.6, the Bartlett periodogram produces very highly smoothed spectral estimates, containing little or no information which may be considered suitable for use as heuristic parameters. Each sound was divided into sixteen nonoverlapping segments and then augmented to 1024 points by zero padding. A periodogram was evaluated for each segment and the resulting sixteen estimates were averaged to compute the Bartlett PSD estimate. This procedure was repeated for each sound extracted from a PCG, with a final ensemble average calculated for each recording. Figures 6.6(c and f) illustrate Bartlett PSD estimates for mitral and aortic sounds evaluated using four and eight nonoverlapping segments respectively. These estimates are still highly smoothed, with the increase in erratic behaviour corresponding to an increase in the variance of the estimate clearly apparent in Figure 6.6(c).

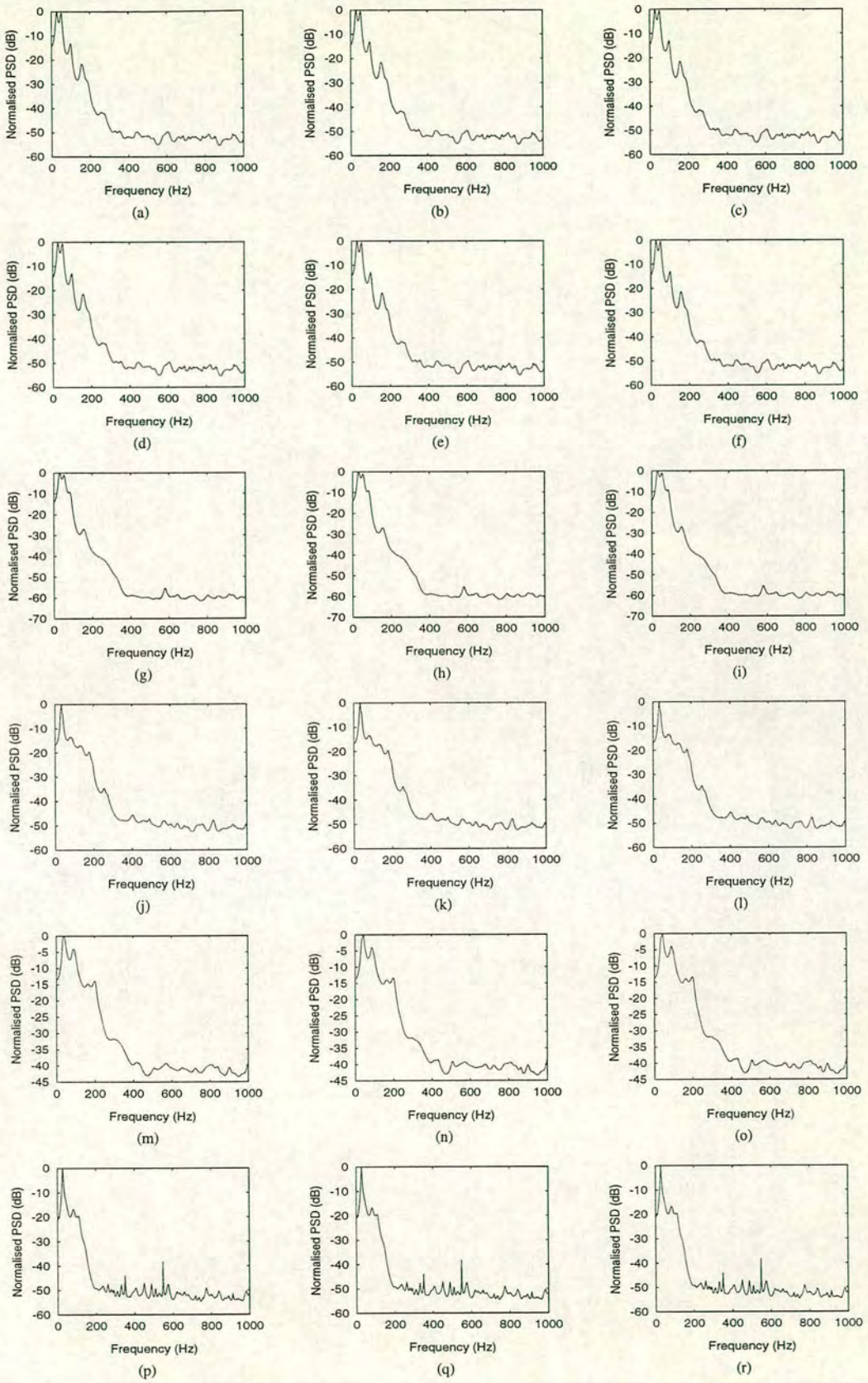

Figure 6.4: *Examples of ensemble spectra computed using the Burg algorithm, the Burg algorithm with a Hamming window and the Burg algorithm with an optimum parabolic taper respectively. (a-i) PSD estimates of mitral sounds; sources: pw6, is6 and dg4 respectively, (j-r) PSD estimates of aortic sounds; sources: em4, jm3 and eb4 respectively.*

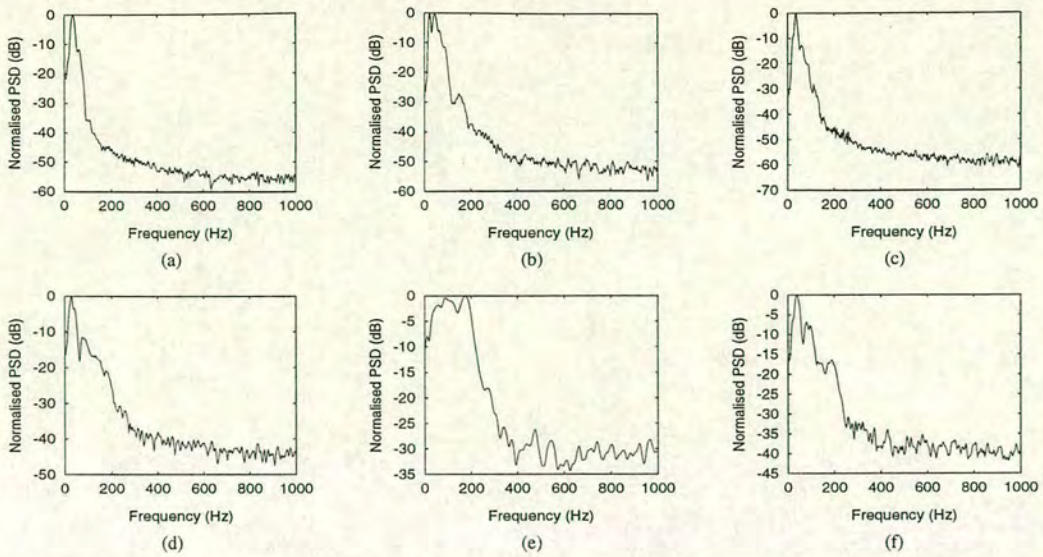

Figure 6.5: *Examples of ensemble spectra computed using the periodogram with a Hamming window. (a-c) PSD estimates of mitral sounds; sources: mb3, dg4 and tm5 respectively, (d-f) PSD estimates of aortic sounds; sources: em4, mh4 and jm3 respectively.*

Figures 6.1(k), 6.2(h), 6.2(n) and 6.4(p) illustrate examples of AR spectral estimates which contain spurious peaks as a result of selecting too high a model order relative to the number of data points. The orders chosen for these sounds were 36, 50, 28 and 50 for time series of 75, 82, 61 and 82 samples respectively. When actual autocorrelation lag information is available, the AR parameters $a_{\hat{p}}[k] = 0$ for $\hat{p} > p_{hs}$. However, when analysing heart sounds, estimation errors cause $a_{\hat{p}}[k] \neq 0$ for $\hat{p} > p_{hs}$. Consequently, there will be $\hat{p}$ - p_{hs} extra noise poles, and if located close to the unit circle, the result will be spurious peaks [146, 149, 150].

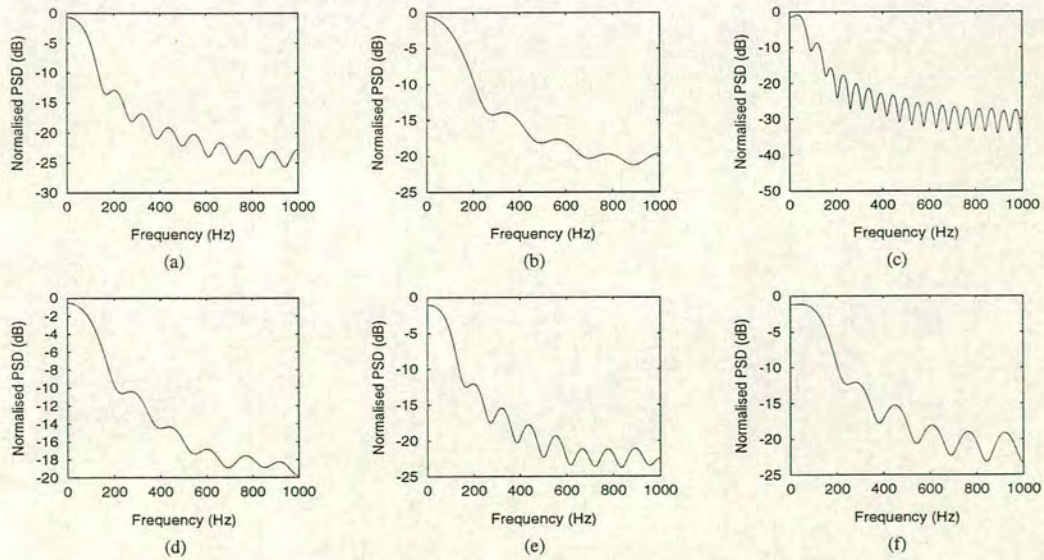

Figure 6.6: *Examples of ensemble spectra computed using the Bartlett periodogram. (a-c) PSD estimates of mitral sounds; sources: dg4, mb3 and pw6 respectively, (d-f) PSD estimates of aortic sounds; sources: jm3, eb4 and em4 respectively.*

When analysing sounds with low SNR (high levels of noise), the performance of the AR spectral estimation techniques can degrade significantly, resulting in low-resolution spectral estimates. This is due to the introduction of spectral zeros caused by noise, with the all-pole model assumed in AR spectral analysis no longer valid. The PSD estimate is now characterised by an ARMA[p_{hs}, p_{hs}] process [78, 151–153]. The effects of noise can be minimised by selecting a higher model order, as the ARMA[p_{hs}, p_{hs}] is equivalent to an AR[∞] model as asserted by the Wold decomposition theorem. As the order increases, the resulting estimate approaches the true PSD. In practice, a model order as large as possible should be used; however, the introduction of spurious peaks into the frequency spectrum by selecting too high an order imposes a 'maximum' limit of no more than half the number of data samples [146].

6.3 Performance of Methods for Optimal Model Order Selection: Results

From each PCG, the relevant closing sound was automatically extracted from within each cardiac cycle and a mean sound computed from this ensemble as described in section 4.5. This mean sound was used by the model order selection criteria to quantatively determine the optimal order for parametric spectral analysis.

6.3.1 AR Hypothesis-Based Model Order Selection

In general, it was observed that when monitoring the NRMSE for a decrease in the rate of change, the resulting model orders produce spectra with low-frequency resolution containing little or no information of diagnostic significance. Figure 6.7 illustrates typical plots of the monotonically decreasing NRMSE for mean mitral and aortic sounds and the resultant PSD estimates computed using the MCV method. Table 6.1 shows the orders selected when monitoring the NRMSE for all forty subjects. The mean NRMSE values computed for the mitral and aortic components are 14 and 8 respectively.

6.3.2 AR Decision-Based Model Order Selection Criteria

Likewise, in general, it was observed that the orders returned by the decision-based criteria produce low-frequency resolution spectral estimates. Figures 6.8 to 6.10 illustrate typical plots produced by the FPE, AIC, MDL and CAT criteria for mean mitral and aortic sounds and the resultant PSD estimates computed using the MCV method. Table 6.1 shows the orders

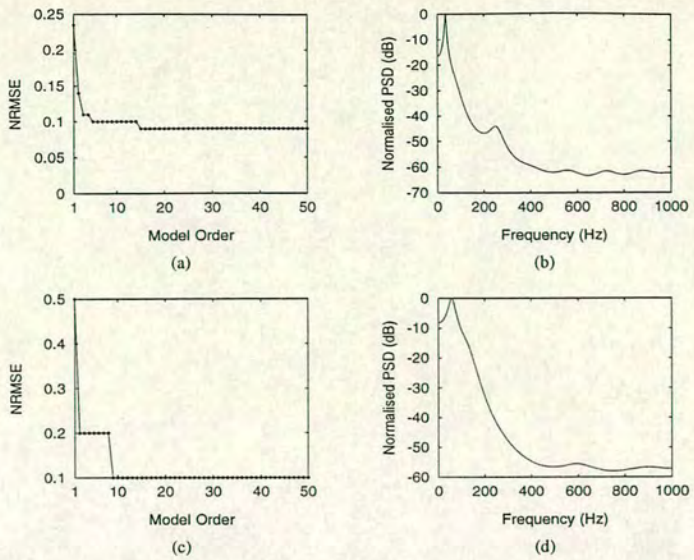

Figure 6.7: *Typical plots of the NRMSE for mean mitral and aortic sounds and the resultant PSD estimate. (a)* $\hat{p} = 15$ *for mean mitral sound (source: gc6.mean), (b) Spectrum of mean mitral sound when* $\hat{p} = 15$*, (source: gc6.mean), (c)* $\hat{p} = 9$ *for mean aortic sound (source: jg3.mean), (b) Spectrum of mean aortic sound when* $\hat{p} = 9$ *(source: jg3.mean).*

selected by these criteria for all forty subjects. The mean values computed for mitral and aortic components by the FPE, AIC, MDL and CAT criteria are 16 and 11, 16 and 11, 6 and 4 and 16 and 11 respectively.

For a pure AR process, the FPE is found to work well in selecting the correct order [106, 149, 154]. However, when applied to biomedical signals such as an electroencephalogram (EEG), the FPE is found to return orders which do not adequately model the EEG time series under investigation: producing highly smoothed spectral estimates [155]. As with the FPE, it was observed that the order selected by the AIC is often too low to adequately model the heart sound time series under investigation, *i.e.* practical, real non-AR data. This is primarily due to the fact that the assumptions of uncorrelated noise excitation and a Gaussian distribution do not apply to a principal component time series.

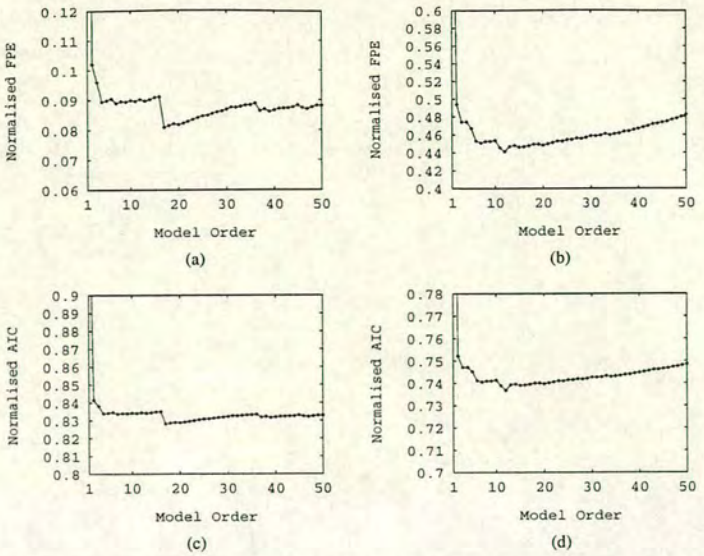

Figure 6.8: *Typical plots produced by the FPE and AIC model order selection criteria. (a) FPE = 17 for a mean mitral sound (source: gc6.mean), (b) FPE = 12 for a mean aortic sound (source: jg3.mean), (c) AIC = 17 for a mean mitral sound (source: gc6.mean), (d) AIC = 12 for a mean aortic sound (source: jg3.mean).*

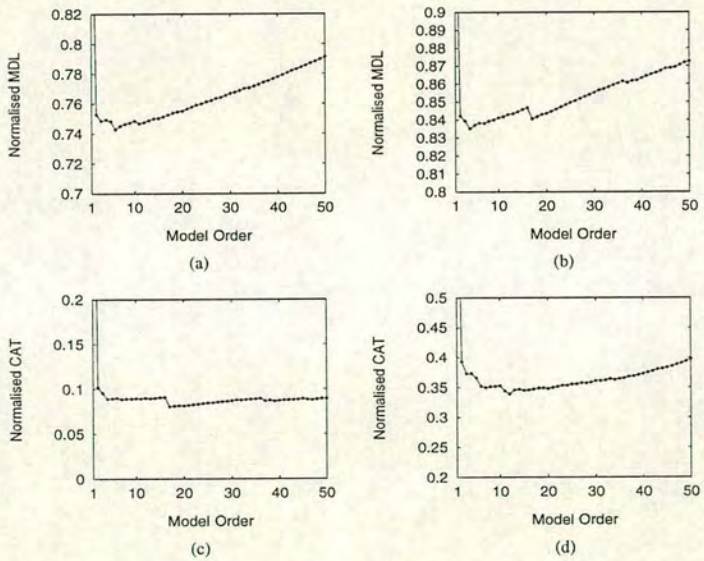

Figure 6.9: *Typical plots produced by the MDL and CAT model order selection criteria. (a) MDL = 6 for a mean mitral sound (source: gc6.mean), (b) MDL = 4 for a mean aortic sound (source: jg3.mean), (c) CAT = 17 for a mean mitral sound (source: gc6.mean), (d) CAT = 12 for a mean aortic sound (source: jg3.mean).*

Although the orders returned by the decision-based criteria are greater than or in the range suggested by theoretical values, *i.e.* to those expected from anatomical consideration of the mechanics and composition of heart sound generation, they are still too low to adequately model these sounds. The low orders returned produce spectra with low-frequency resolution containing little or no information of diagnostic value. This is as a result of the transient nature

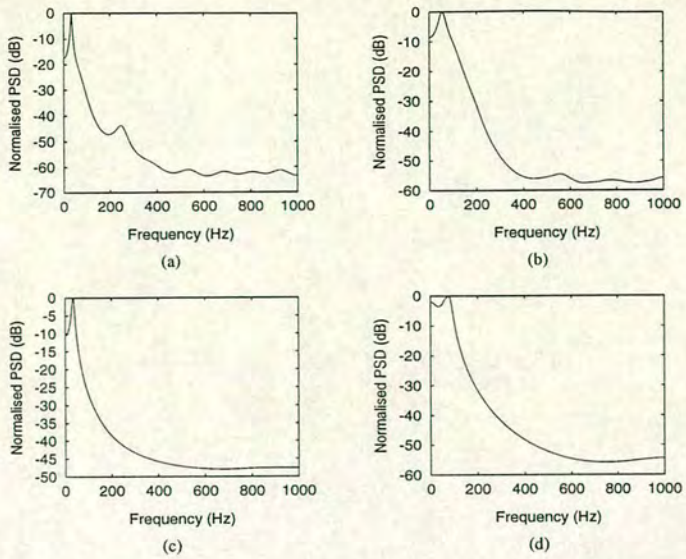

Figure 6.10: *Resultant spectra. (a) Spectrum of mean mitral sound when* $\hat{p} = 17$ *(source: gc6.mean). (b) Spectrum of mean aortic sound when* $\hat{p} = 12$ *(source: jg3.mean). (c) Spectrum of mean mitral sound when* $\hat{p} = 6$ *(source: gc6.mean) (d) Spectrum of mean aortic sound when* $\hat{p} = 4$ *(source: jg3.mean).*

of heart sounds, the presence of background noise and the fact that heart sounds do not satisfy the requirements of an AR model excited by white noise or a Gaussian distribution as required by some of these criteria. The orders selected by the FPE, AIC and CAT criteria are always identical and the orders selected by the MDL criterion, if not equal to those selected by the other methods, are always lower. The FPE, AIC and MDL are all asymptotically equivalent:

$$\lim_{N\to\infty} \frac{\mathrm{AIC}[\hat{p}]}{N} = \lim_{N\to\infty} \frac{\mathrm{MDL}[\hat{p}]}{N} = \lim_{N\to\infty} \ln \mathrm{FPE}[\hat{p}] \tag{6.1}$$

It was found that when empirically selecting orders, the optimum mean orders across the patient population for mitral and aortic components are 42 and 38 respectively. These values produced the best spectra, containing heuristic features, *e.g.* a number of distinct dominant frequency peaks as shown in Figure 6.11. The optimum empirical model order was selected on the basis that the resulting PSD estimate is consistent in detail with spectra evaluated using neighbouring values of order: consistent identification and localisation of features within the sound spectrum. Some of these features had not been identified by the spectra computed using the lower orders previously returned by the model order selection criteria. In addition, the resulting PSD estimate consistent in detail with an equivalent estimate evaluated using the fast Fourier transform. Table 6.1 shows the optimum empirical model orders chosen for all forty subjects. With some sounds, the orders selected by the decision-based criteria are often very close to and in some cases identical to or greater than that which is found to be most suitable

empirically. This inconsistency was observed throughout the patient population. In general, it was observed that mitral components require a higher order than aortic components, reflecting the more complex structure and longer duration of the mitral component relative to the aortic component.

Patient No.	NRMSE	FPE	AIC	MDL	CAT	EMP(AR)	ARMA	AR	Prony
Mitral									
1	4	18	18	10	18	32	6	6	6
2	13	12	12	7	12	36	6	6	6
3	17	9	9	5	9	34	4	4	4
4	9	16	16	4	16	44	4	4	4
5	21	15	15	5	15	36	4	4	4
6	12	11	11	6	11	40	4	4	4
7	15	12	12	4	12	42	4	6	6
8	10	30	30	7	30	38	4	4	4
9	23	15	15	8	15	44	4	4	4
10	15	14	14	5	14	40	4	4	4
11	20	29	29	6	29	48	6	6	6
12	21	23	23	5	23	36	6	6	6
13	14	11	11	6	11	38	4	4	4
14	12	17	17	6	17	52	6	6	6
15	9	13	13	7	13	40	4	4	4
16	10	13	13	7	13	48	6	6	6
Mean	14	16	16	6	16	40	5	5	5
Aortic									
1	7	4	4	4	4	42	4	4	2
2	11	22	22	7	22	44	4	4	2
3	8	17	17	4	17	40	6	4	4
4	10	13	13	5	13	32	6	4	4
5	7	2	2	2	2	38	4	4	4
6	8	20	20	3	20	44	4	4	4
7	9	19	19	3	19	42	6	6	6
8	18	20	20	5	20	28	6	6	6
9	7	11	11	2	11	36	6	6	6
10	7	9	9	5	9	40	4	4	4
11	14	12	12	4	12	42	6	6	6
12	8	10	10	3	10	32	4	4	4
13	8	12	12	5	12	38	6	6	6
14	9	8	8	4	8	40	4	4	4
15	7	10	10	3	10	42	4	4	4
16	9	8	8	3	8	36	4	4	4
17	8	13	13	4	13	30	6	6	6
18	7	6	6	6	6	38	4	4	4
19	10	8	8	4	8	44	4	4	4
20	6	10	10	5	10	42	6	6	6
21	7	13	13	6	13	36	4	4	4
22	6	8	8	6	8	32	4	4	4
23	5	10	10	8	10	40	4	4	4
24	4	6	6	3	6	32	4	4	4
Mean	8	11	11	4	11	38	5	5	5

Table 6.1: *Optimal model order selection. EMP = Best empirical order observed when using the MCV method. The ARMA and AR columns refer to the number of identified heart sound-related dominant singular values. For all forty patients, $v(p_{hs})$, i.e. equation (5.76), returned a value of 1 for both methods, demonstrating the quality of the lower rank optimal approximation and the low effective rank of matrices when analysing bioprosthetic heart valve closing sounds. The column for Prony's method refers to the number of identified heart sound signal-related zeros of the backward linear prediction polynomial. All mean values have been rounded to the nearest figure.*

Previous work by Foale *et al.* [39] uses the covariance method of AR/linear prediction analysis with an order of three or four to analyse the closing sounds produced by the operation

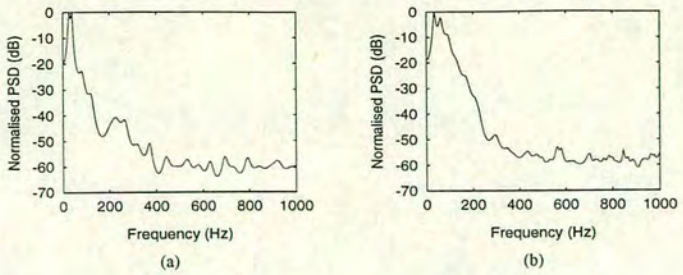

Figure 6.11: *Typical plots of PSD estimates evaluated by the MCV method. (a) source: gc6.mean;* $\hat{p} = 42$*, (b) source: jg3.mean;* $\hat{p} = 38$.

of aortic porcine xenografts. Although, theoretically an order of four may relate with that expected from consideration of the mechanics and composition of heart sound generation, from the results obtained in this study, an order of four initially appears too low to adequately model these sounds: firstly, the fact that an AR model is being used, and secondly, the numerical ill-conditioning inherent with the use of linear-algebra-based spectral estimation techniques was not removed. Figure 6.12 shows typical plots of PSD estimates of mitral and aortic components produced by the operation of Carpentier-Edwards bioprostheses computed using the covariance method with an order of $\hat{p} = 4$. The resultant PSD estimates are all highly smoothed, containing little or no information of possible diagnostic value.

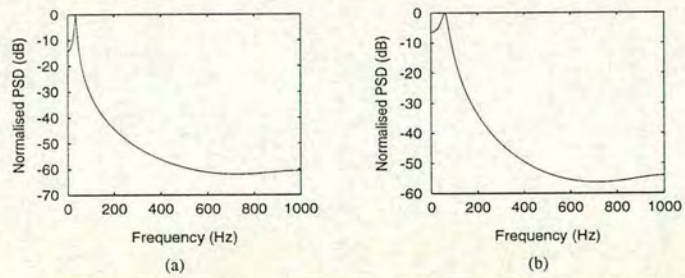

Figure 6.12: *Typical plots of ensemble PSD estimates evaluated by the covariance method using a model order of* $\hat{p} = 4$*. (a) source: gc6.mean, (b) source: jg3.mean.*

Previous work by Cloutier *et al.* [43,46] uses the NRMSE between mitral and aortic closing sounds and the impulse response of parametric models to calculate the optimal model order when analysing the acoustic output produced by the operation of bovine bioprostheses. Using the autocorrelation and covariance methods, they modelled both mitral and aortic closing sounds using 16 poles.

6.3.3 Linear-Algebra-Based ARMA Model Order Selection

It was observed that the ARMA method which uses the SVD operation to remove the statistical errors inherent with the estimation of an autocorrelation function from a heart sound time series, typically reveals four to six dominant singular values for mean mitral and aortic components.

Representative plots and examples of actual values obtained from mean mitral sounds are:

σ_{11} = 4670.84, σ_{22} = 4477.52, σ_{33} = 459.72, σ_{44} = 228.18,
σ_{55} = 78.52, σ_{66} = 32.28, σ_{77} = 14.9, σ_{88} = 7.89, $\cdots$, $\sigma_{50,50}$ = 0.013
(source: gc6.mean)

σ_{11} = 48519.78, σ_{22} = 46907.31, σ_{33} = 3502.03, σ_{44} = 1580.54, σ_{55} = 355.34, σ_{66} = 110.12, σ_{77} = 61.03, σ_{88} = 36.73, $\cdots$, $\sigma_{50,50}$ = 0.097
(source: ic5.mean)

σ_{11} = 16460.57, σ_{22} = 8918.23, σ_{33} = 451.37, σ_{44} = 117.17, σ_{55} = 20.11,
σ_{66} = 6.28, $\cdots$, $\sigma_{50,50}$ = 0.053
(source: jh4.mean)

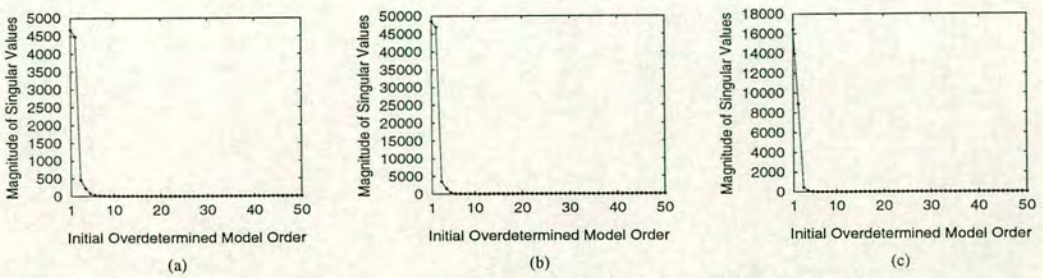

Figure 6.13: *Corresponding plots showing the relative magnitude of all fifty singular values. (a) gc6:mean, (b) ic5.mean, (c) jh4.mean.*

Representative plots and examples of actual values obtained from mean aortic sounds are:

σ_{11} = 260873.26, σ_{22} = 102702.39, σ_{33} = 5345.54, σ_{44} = 717.43,
σ_{55} = 12.97, σ_{66} = 0.58, $\cdots$, $\sigma_{50,50}$ = 0.003
(source: jg1.mean)

σ_{11} = 262688.06, σ_{22} = 234993.34, σ_{33} = 7284.22, σ_{44} = 2040.16,
σ_{55} = 194.98, σ_{66} = 53.98, $\cdots$, $\sigma_{50,50}$ = 0.184
(source: jp3.mean)

σ_{11} = 61953.55, σ_{22} = 22241.42, σ_{33} = 587.35, σ_{44} = 87.51,
σ_{55} = 19.67, σ_{66} = 3.96, $\cdots$, $\sigma_{50,50}$ = 0.117
(source: ad1.mean)

The relative magnitudes of these values clearly show that the first four to six values are related to the heart sound signal and that the extraneous relatively insignificant-sized nonzero values are related to background noise. Examination of these values reveals the number of dominant singular values, *i.e.* the optimal model order for subsequent parametric spectral analysis. For all subjects, an initial overdetermined order was chosen of $p_e = q_e = 50$ on the knowledge that this would be much larger than any eventual value of p_{hs}. This allows for easier discrimination between the heart sound signal-related singular values and the remaining superfluous values related to background noise. Table 6.1 shows the number of dominant values identified for all forty subjects using this method.

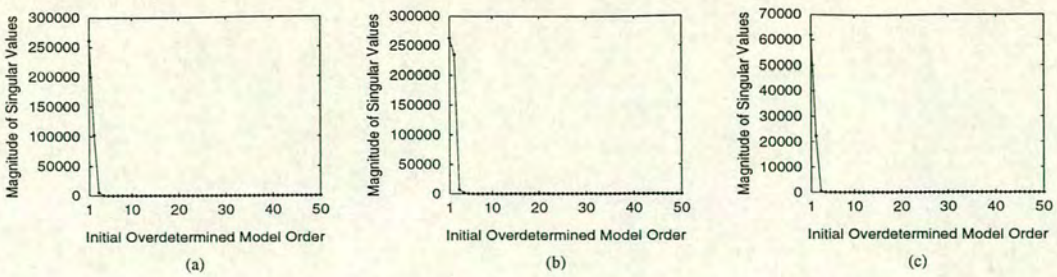

Figure 6.14: *Corresponding plots showing the relative magnitude of all fifty singular values. (a) jg1:mean, (b) jp3.mean, (c) ad1.mean.*

6.3.4 Linear-Algebra-Based AR Model Order Selection

Likewise, it was observed that the MCV method which uses SVD to eliminate the effects of noise from the heart sound time series, typically reveals four to six dominant values for mean mitral and aortic components. Representative plots and examples of actual values obtained from mean mitral sounds are:

$\sigma_{11} = 894.51,\ \sigma_{22} = 368.42,\ \sigma_{33} = 43.29,\ \sigma_{44} = 16.16,$

$\sigma_{55} = 9.81,\ \sigma_{66} = 5.02,\ \sigma_{77} = 2.86,\ \sigma_{88} = 2.47,\ \cdots\ , \sigma_{12,12} = 2.19$

(source: gc6.mean)

$\sigma_{11} = 2873.51\ \sigma_{22} = 971.96,\ \sigma_{33} = 132.23,\ \sigma_{44} = 37.57,$

$\sigma_{55} = 15.68,\ \sigma_{66} = 12.93,\ \sigma_{77} = 12.07,\ \sigma_{88} = 11.27,\ \cdots\ , \sigma_{12,12} = 9.99$

(source: ic5.mean)

$\sigma_{11} = 2653.26,\ \sigma_{22} = 1097.17,\ \sigma_{33} = 249.41,\ \sigma_{44} = 106.58,$

$\sigma_{55} = 47.71,\ \sigma_{66} = 25.95,\ \sigma_{77} = 16.05,\ \sigma_{88} = 13.89,\ \cdots\ , \sigma_{12,12} = 9.12$

(source: jh4.mean)

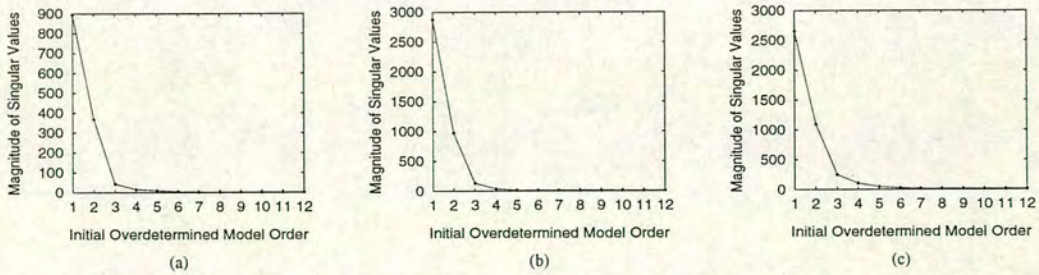

Figure 6.15: *Corresponding plots showing the relative magnitude of all twelve singular values. (a) source: gc6.mean, (b) source: ic5.mean, (c) source: jh4.mean.*

Representative plots and examples of actual values obtained from mean aortic sounds are:

$\sigma_{11} = 5287.19,\ \sigma_{22} = 515.85,\ \sigma_{33} = 21.11,\ \sigma_{44} = 0.68,$

$\sigma_{55} = 0.02,\ \sigma_{66} = 0.01,\ \cdots\ , \sigma_{12,12} = 0.0001$

(source: jg1.mean)

$\sigma_{11} = 5161.46,\ \sigma_{22} = 1894.85,\ \sigma_{33} = 116.61,\ \sigma_{44} = 26.08,$

$\sigma_{55} = 8.43,\ \sigma_{66} = 3.95,\ \cdots\ , \sigma_{12,12} = 2.22$

(source: jp3.mean)

$\sigma_{11} = 3531.11,\ \sigma_{22} = 1354.21,\ \sigma_{33} = 220.09,\ \sigma_{44} = 94.17,$

$\sigma_{55} = 36.57,\ \sigma_{66} = 16.17,\ \cdots\ , \sigma_{12,12} = 8.38$

(source: ad1.mean)

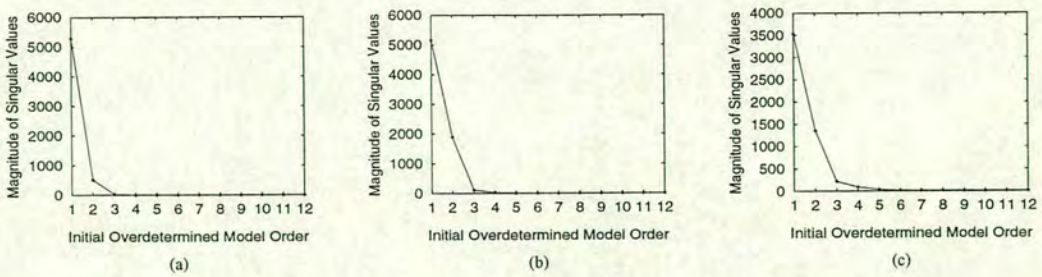

Figure 6.16: *Corresponding plots showing the relative magnitude of all twelve singular values. (a) source: jg1.mean, (b) source: jp3.mean, (c) source: ad1.mean.*

The application of SVD reduces the noise contribution within the data matrix effectively enhancing the signal-to-noise ratio. Table 6.1 shows the number of dominant values identified for all forty patients using this method.

6.3.5 Linear-Algebra-Based Prony Model Order Selection

With Prony's method, it was observed that examining the roots of the backward linear prediction polynomial typically reveals two to six signal zeros for mean mitral and aortic components, as illustrated by the unit-circle plots of Figures 6.17 and 6.18. After removing the effects of noise from the heart sound time series using the SVD operation, an initial overdetermined order was chosen of $\hat{p} = 12$ on the knowledge that this would be much larger than the eventual value of p_{hs}. The extraneous zeros resulting from selecting a model order greater than the number of heart sound signal components are less perturbed and form a uniform pattern around the inside of the unit-circle as shown in Figures 6.17 and 6.18. Examination of the signal zeros reveals the optimal model order for subsequent analysis using Prony's method. Table 6.1 shows the number of heart sound signal zeros identified for all forty patients.

In general, it was observed that after having removed the numerical ill-conditioning associated with the use of linear-algebra-based spectral estimation techniques, the Prony, ARMA and AR methods all report comparable model orders. These methods are able to identify the number of signal components within each sound accurately and consistently throughout the patient population and return model orders which relate closely to those expected from anatomical considerations of the mechanics of heart sound generation.

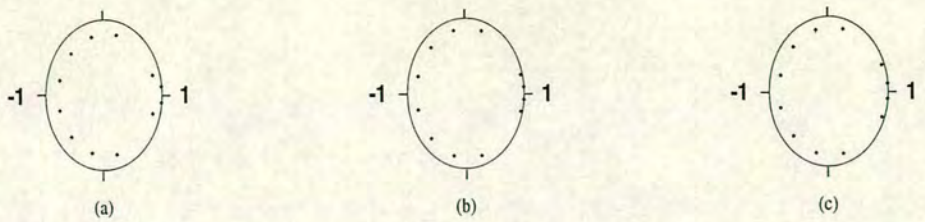

Figure 6.17: *Typical examples of the zeros of the backward linear prediction polynomial evaluated from mean mitral components. The unit-radius circle of the z-plane is shown for reference. (a) gc6:mean, (b) ic5.mean, (c) jh4.mean.*

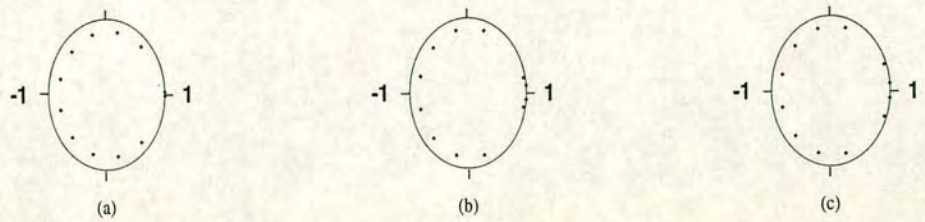

Figure 6.18: *Typical examples of the zeros of the backward linear prediction polynomial evaluated from mean aortic components. The unit-radius circle of the z-plane is shown for reference. (a) jg1.mean, (b) jp3.mean, (c) ad1.mean.*

6.4 Summary and Conclusion

This chapter investigates the application of the methods for the frequency analysis of heart sounds to the full range of recorded mitral and aortic sounds: the periodogram, the Bartlett periodogram, AR and ARMA-based techniques and Prony's method. The aim is to compare the performance and suitability of these spectral estimation techniques in extracting from the frequency domain features which may be considered suitable for use as heuristic parameters. The major observations concerning the performance of these methods were:

1. The superior resolution of Prony's method in identifying within the frequency domain a number of dominant spectral peaks over the full range of recorded sounds and valve conditions.

2. The covariance, MCV, Burg and weighted Burg (parabolic optimum taper and Hamming window) methods all produce almost identical spectra. The resulting estimates are able to identify the same features revealed by the Prony PSD estimate, however, the ability of these AR methods to completely resolve the same spectral detail is secondary to Prony's method.

3. For some sounds, a difference was observed between the spectra produced by the covariance method when compared to the estimates evaluated by the other AR techniques.

4. The application of the periodogram (with and without a Hamming window) produces smoothed spectra relative to the AR and Prony estimates.

5. The Bartlett periodogram produces very highly smoothed spectra, containing little or no information in the frequency spectrum which may be considered suitable for use as heuristic parameters.

The optimal model order is a very important parameter when analysing bioprosthetic heart valve closing sounds using parametric spectral estimation techniques, as variations in spectra can occur with different orders. Accurate model order determination is thus paramount before associating spectra with the physiological and pathological functionality of the Carpentier-Edwards bioprostheses. It was observed that monitoring the NRMSE for a decrease in the rate of change, the FPE, the AIC, the MDL and the CAT decision-based model order selection criteria returned orders that were too low to adequately model heart sounds, producing spectra with low-frequency resolution containing little or no information. The mean values observed by these methods were: 14 and 8, 16 and 11, 16 and 11, 6 and 4 and 16 and 11 for mitral and aortic components respectively. Although these orders are greater than or in the range suggested by theoretical values, as a result of the transient nature of heart sounds, the presence of background noise, and the fact that heart valve closing sounds do not satisfy the requirements of an AR model excited by white noise or a Gaussian distribution, these values are still too low to adequately model the sounds. It was found empirically that mean optimum orders of 40 and 38 for mitral and aortic components respectively produced the best spectra, containing features which may be considered for use as heuristic parameters.

Consistent determination of the model order was achieved by first removing the numerical ill-conditioning inherent with the use of linear-algebra-based spectral estimation techniques. Examining the relative magnitudes of singular values or the roots of the backward linear prediction polynomial used in Prony's method, produced model orders that relate closely to those expected from consideration of the mechanics of heart sound generation. Four to six dominant singular values and two to six signal zeros are consistently identified throughout the patient population.

Chapter 7

Physiological Interpretation of the Frequency Spectrum

Based on the heuristic parameters identified by the application of the frequency analysis techniques to mitral and aortic components in chapter six, the aim of this chapter is to first select appropriate features from the sound spectrum and then to examine whether these features convey any information of diagnostic significance concerning the functionality of prostheses. If a unique relationship can be confirmed, whether the spectral parameters can be utilised to distinguish between normally functioning and dysfunctioning prostheses and ultimately predict impending valve failure.

7.1 Diagnostic Feature Selection

Features considered to be of physiological and pathological significance were extracted from the frequency spectrum with a view to investigating the discriminatory ability of these parameters to distinguish between normally functioning and dysfunctioning prostheses. During clinical auscultation, cardiologists use the sounds heard through the stethoscope to diagnose the functionality of bioprostheses. One of the key attributes used is the frequency content of these sounds: identification of low-frequency sounds using a bell attachment to a stethoscope and high-frequency sounds, snaps and murmurs using a rigid diaphragm. Therefore the frequency domain (sound spectrum) is an appropriate domain from which to extract diagnostic parameters.

The selection of features from the frequency spectrum of mitral and aortic sounds was based on previous work on the mathematical modelling of semi-lunar valve vibration [156–159], as well as a visual examination of spectra estimated over the full range of recorded sounds and valve conditions. The models of valve sound vibration show that the natural resonance modes of bioprosthetic heart valves increase with stiffening of the leaflets. Based on the results of chapter six, a visual examination of all the spectra within each of the three population groups revealed certain metrics that were consistently identified throughout the patient population. Therefore using the *a priori* knowledge concerning the natural resonance modes of bioprosthetic heart valves, as well as the visual examination of all spectra, certain features were extracted from the frequency spectrum which highlight the structure, composition and morphology of the sound spectrum. A complete description defining these features is given in Table 7.1. These parameters are based on identifying the dominant frequency peaks to quantify the natural resonance modes of bioprosthetic heart valves, as well as characterising the distribution of energy in the sound spectrum by evaluating bandwidth, area and root mean square (RMS) measurements over the entire spectral profile.

No.	Feature	Description
1	$F1$	Dominant frequency peak (0dB)
2	$F2$	Second dominant frequency peak
3	$F3$	Third dominant frequency peak
4	$F4$	Fourth dominant frequency peak
5	$F5$	Fifth dominant frequency peak
6	$F6$	Sixth dominant frequency peak
7	F_{-3}	Highest frequency found at -3dB
8	F_{-10}	Highest frequency found at -10dB
9	F_{-20}	Highest frequency found at -20dB
10	F_{-30}	Highest frequency found at -30dB
11	*Energy*	Energy/Area in each interval
12	*RMS*	RMS value in each interval

Table 7.1: *Description of diagnostic features extracted from the frequency spectrum of mitral and aortic sounds.*

The most dominant frequency, $F1$, is defined as the frequency peak with the maximum intensity (0dB). $F2$, is the frequency of the peak with the second highest intensity, where the magnitude of $F1 > F2 > ... > F6$. Up to six major peaks were observed in many of the spectra. F_{-3}, F_{-10}, F_{-20} and F_{-30} are parameters associated with the frequency bandwidth of the sound spectrum, and denote the highest frequencies observed at the -3dB, -10dB, -20dB and -30dB amplitude levels respectively. These bandwidth measures were observed to be very prominent in many of the spectra. To completely characterise the distribution of the frequency spectrum, the spectrum was subdivided into a number of equal width frequency bands as discussed in section 7.2. The energy (area) in each band was evaluated by numerical integration using a

trapezoidal method based on Simpson's Rule, and then normalised with respect to the total spectral energy and expressed as a relative percentage of this total. This provides a measure of the relative proportion of mitral and aortic component energy associated with each frequency band. The RMS value in each band was obtained by summing the squared values of the spectral coefficients in each band, dividing by the number of coefficients included in the computation and taking the square root of this mean value. Similarly, the RMS value in each band was normalised with respect to the total spectral RMS and expressed as a relative percentage of this total.

7.2 Frequency Spectrum of Valve Sounds: Results

Based on the performance of the methods for the frequency analysis of heart sounds results presented in section 6.2, the physiological significance of the spectral characteristics derived from mitral and aortic sounds were investigated using Prony's method and the MCV method. Examination of spectra from each of the three population groups verifies the superior resolution of Prony's method in extracting spectral peaks from the frequency domain. Therefore Prony's method was used to identify and characterise the dominant peaks.

The sound spectrum produced by the MCV method was subdivided into 40 bands each of 25Hz (Nyquist rate = 2kHz). With AR spectral estimation, the amplitudes of the spectral peaks are nonlinearly related to energy, with the peak values being proportional to the square of the energy and the area under the curve proportional to energy [97]. Therefore subdividing the frequency spectrum produced by the MCV method provides a quantitative measure of the relative proportion of mitral and aortic component energy associated with each band. From the results illustrated in section 6.2, spectra estimated by the MCV method are consistent with Prony's method in the identification and localisation of features within the sound spectrum.

7.2.1 Sound Spectrum of Mitral Components

For the sounds produced by the operation of normally functioning mitral prostheses, Prony's method yields spectra which are similar throughout this population of subjects: group 1. Two to three dominant frequency peaks and one to two weaker secondary peaks are consistently identified. The mean frequencies and amplitudes of the observed peaks within this group were computed to be:

$F1$ = 31.6Hz @ 0dB $F4$ = 169.9Hz @ -19.79dB

$F2$ = 48.9Hz @ -6.82dB $F5$ = 252.8Hz @ -22.13dB

$F3$ = 95.1Hz @ -14.38dB $F6$ = 284.1Hz @ -21.19dB

Table 7.2 provides complete details of the observed peaks for all subjects with normally functioning mitral bioprostheses. The major concentration of spectral energy occurs in the region between d.c. and 100Hz, where mean relative energies and RMS energies within this population group were computed to be 39.22% and 36.62% respectively. These values are significant, as the remainder of the energy is evenly distributed throughout the other thirty-six frequency bands as illustrated in Figure 7.1. Figure 7.1 shows typical examples of spectra and the accompanying distributions of spectral energy estimated from the sounds produced by the operation of normally functioning Carpentier-Edwards mitral bioprostheses. A complete summary of observed results for all subjects with implanted mitral bioprostheses is given in Table 7.2.

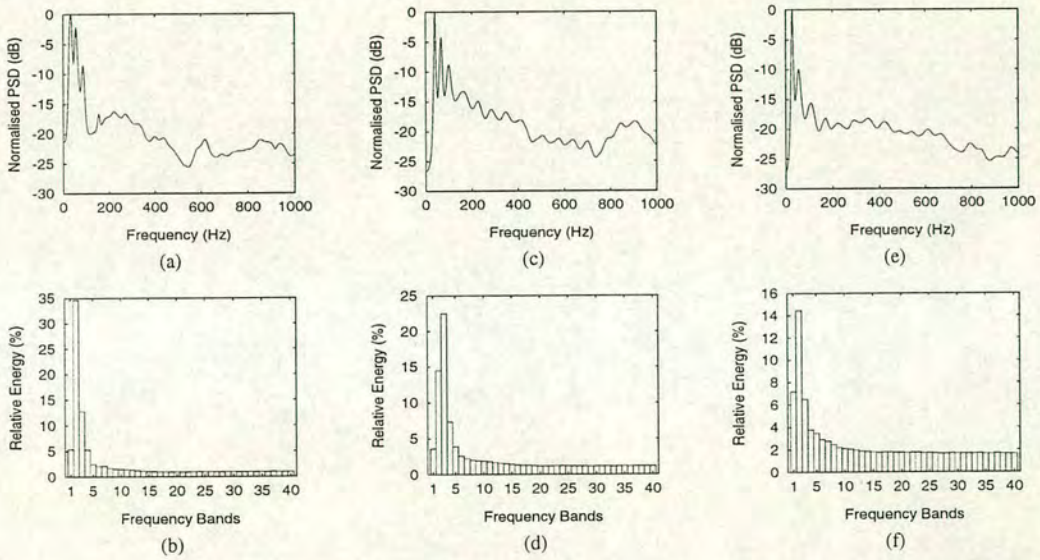

Figure 7.1: *Characteristics of sounds produced from the operation of normally functioning Carpentier-Edwards mitral bioprostheses. (a-b) Prony PSD estimate and energy distribution respectively of patient three, (c-d) Prony PSD estimate and energy distribution respectively of patient five, (e-f) Prony PSD estimate and energy distribution respectively of patient four.*

For the sounds produced by the operation of leaky mitral prostheses (group 2), Prony's method yields spectra which identify two to three dominant peaks and one to two weaker secondary peaks. The mean frequencies and amplitudes of observed peaks within this group were computed to be:

$F1$ = 44.75Hz @ 0dB $F4$ = 142.6Hz @ -14.5dB

$F2$ = 35.0Hz @ -3.22dB $F5$ = 196.6Hz @ -17.16dB

$F3$ = 78.0Hz @ -9.85dB $F6$ = 225.0Hz @ -17.78dB

Table 7.2 provides complete details of the observed peaks for all subjects diagnosed as having leaky mitral bioprostheses. The major concentration of spectral energy occurs in the region between d.c. and 75Hz, where mean relative energies and RMS energies within this population group were computed to be 42.75% and 38.25% respectively. Figure 7.2 illustrates typical examples of spectra and the accompanying distributions of spectral energy estimated from the sounds produced by the operation of leaky Carpentier-Edwards mitral bioprostheses.

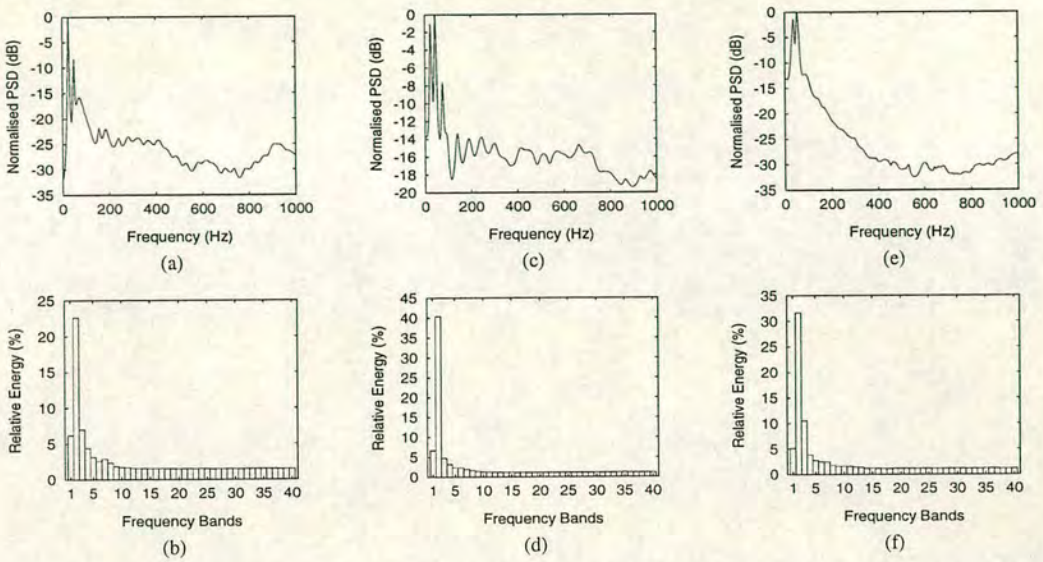

Figure 7.2: *Characteristics of sounds produced from the operation of leaky Carpentier-Edwards mitral bioprostheses. (a-b) Prony PSD estimate and energy distribution respectively of patient thirteen, (c-d) Prony PSD estimate and energy distribution respectively of patient fourteen, (e-f) Prony PSD estimate and energy distribution respectively of patient sixteen.*

Patient No.	$F1$	$F2$	$F3$	$F4$	$F5$	$F6$	F_{-3}	F_{-10}	F_{-20}	F_{-30}	*Energy*	*RMS*
Group 1												
1	28	34	42	93	137	194	32.5	50	N/P	N/P	38	33
2	24	54	107	219	267	N/P	25.0	29.37	307.5	N/P	31	30
3	34	56	86	154	221	271	58.12	89.37	350.0	N/P	58	53
4	28	55	106	169	351	292	31.25	59.37	N/P	N/P	31	30
5	41	68	101	162	226	283	40.62	105	440.6	N/P	47	46
6	35	49	105	131	218	372	40.62	58.75	440.6	N/P	61	50
7	35	41	68	115	188	269	40.62	43.75	48.75	426.25	36	35
8	34	52	73	129	238	298	34.37	75	133.12	N/P	46	43
9	32	47	127	259	355	N/P	31.25	33.12	68.75	N/P	33	33
10	31	48	150	264	356	N/P	34.47	36.25	65.62	N/P	33	30.5
11	30	44	113	237	324	383	31.25	32.5	58.12	N/P	27	27
12	28	39	64	107	153	195	28.75	40.62	71.87	N/P	29.75	29
Mean	31.6	48.9	95.1	169.9	252.8	284.1	35.7	54.4	198.4	N/C	39.22	36.62
Group 2												
13	27	52	98	187	159	330	31.25	53.12	193.75	N/P	36	34
14	45	24	77	141	243	190	45.62	81.25	N/P	N/P	51	46
15	54	28	49	100	188	155	56.25	59.37	270.62	N/P	37	33
16	53	36	88	N/P	N/P	N/P	59.37	66.87	188.75	N/P	47	40
Mean	44.7	35.0	78.0	142.67	196.67	225.0	48.12	65.15	217.7	N/C	42.75	38.25

Table 7.2: *Results obtained from the frequency analysis of mitral sounds: All sounds were recorded at the apex, where maximum PCG signal strength was observed (best signal-to-noise ratio). N/P = Not Present, N/C = Not Calculated. The Energy and RMS values are percentages within regions d.c. to 100Hz and d.c. to 75Hz for groups one and two respectively.*

7.2.2 Sound Spectrum of Aortic Components

For the sounds produced by the operation of normally functioning aortic prostheses, Prony's method yields spectra which are similar throughout this population of subjects: group one. Four to five dominant frequency peaks and one to two weaker secondary peaks are consistently identified. The mean frequencies and amplitudes of observed peaks within this group were computed to be:

$F1$ = 37.4Hz @ 0dB	$F4$ = 171.1Hz @ -14.17dB
$F2$ = 77.8Hz @ -7.66dB	$F5$ = 245.8Hz @ -16.59dB
$F3$ = 116.5Hz @ -10.04dB	$F6$ = 292.4Hz @ -17.0dB

Table 7.3 provides complete details of the observed peaks for all subjects with normally functioning aortic prostheses. The major concentration of spectral energy occurs in the region between 25Hz and 125Hz, where mean relative energies and RMS energies within this population group were computed to be 36.26% and 34.25% respectively. The remainder of the energy is evenly distributed throughout the other thirty-six frequency bands as illustrated in Figure 7.3. Figure 7.3 shows typical examples of spectra and the accompanying distributions of spectral energy estimated from the sounds produced by the operation of normally functioning aortic Carpentier-Edwards bioprostheses. A complete summary of observed results for all subjects with implanted aortic prostheses is given in Table 7.3.

For the sounds produced by the operation of leaky aortic prostheses (group 2), Prony's method yields spectra which identify two dominant peaks and two to three weaker secondary peaks. The mean frequencies and amplitudes of the observed peaks within this group were computed to be:

$F1$ = 30.6Hz @ 0dB	$F4$ = 149.2Hz @ -19.21dB
$F2$ = 55.3Hz @ -7.54dB	$F5$ = 210.7Hz @ -22.05dB
$F3$ = 114.0Hz @ -17.69dB	

Table 7.3 provides complete details of the observed peaks for all subjects diagnosed as having leaky aortic bioprostheses. The major concentration of spectral energy occurs in the region between d.c. and 75Hz, where mean relative energies and RMS energies within this population group were computed to be 28.67% and 26.3% respectively. Figure 7.4 shows typical examples of spectra and the accompanying distributions of spectral energy estimated from the sounds produced by the operation of leaky Carpentier-Edwards aortic bioprostheses.

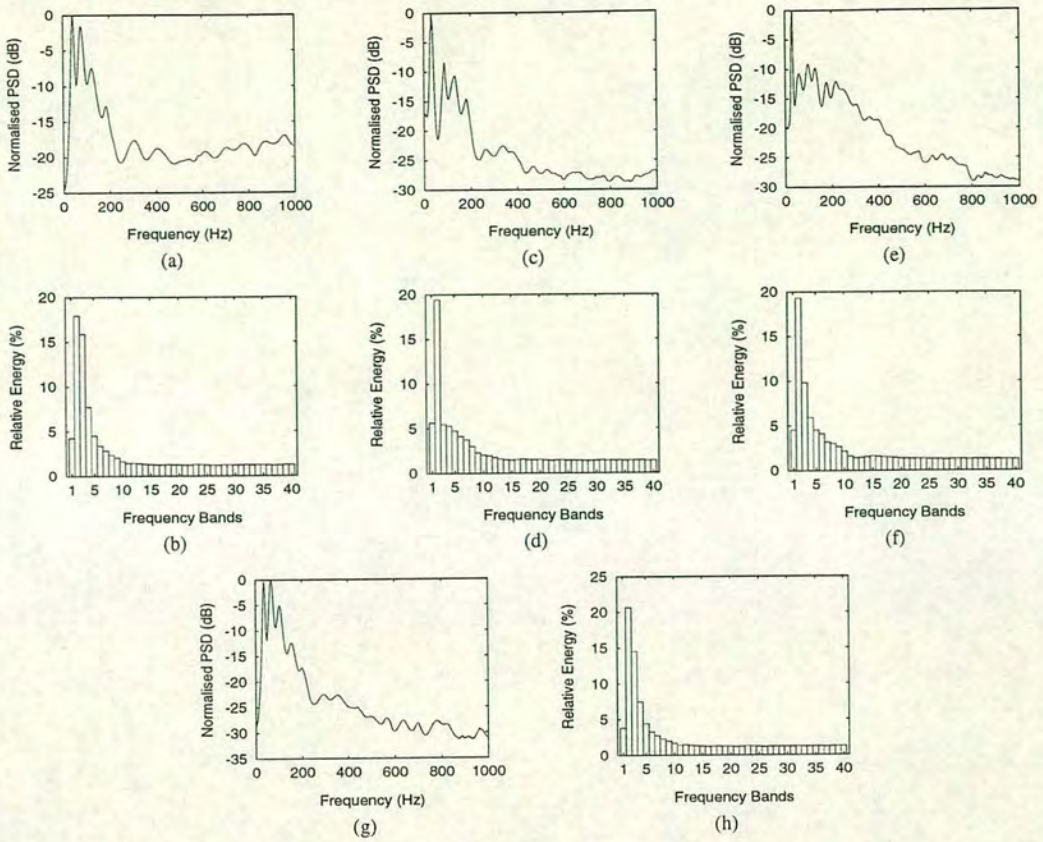

Figure 7.3: *Characteristics of sounds produced from the operation of normally functioning aortic Carpentier-Edwards bioprostheses. (a-b) Prony PSD estimate and energy distribution respectively of patient one, (c-d) Prony PSD estimate and energy distribution respectively of patient three, (e-f) Prony PSD estimate and energy distribution respectively of patient ten, (g-h) Prony spectral estimate and energy distribution respectively of patient twelve.*

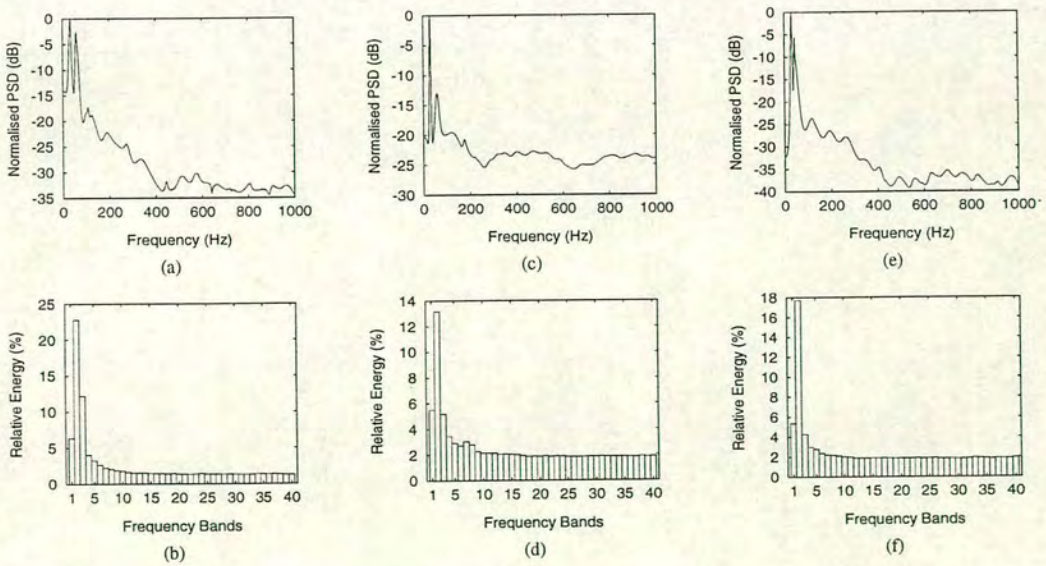

Figure 7.4: *Characteristics of sounds produced from the operation of leaky aortic Carpentier-Edwards bioprostheses. (a-b) Prony PSD estimate and energy distribution respectively of patient fourteen, (c-d) Prony PSD estimate and energy distribution respectively of patient sixteen, (e-f) Prony PSD estimate and energy distribution respectively of patient nineteen.*

For the sounds produced by the operation of aortic prostheses diagnosed as having stiffening calcified cusps (group 3 - patients 20 to 23), a shift was observed in spectral energy, with the higher-frequency peaks containing the most energy. The mean frequencies and amplitudes of the observed peaks within this group were computed to be:

$F1$ = 186.2Hz @ 0dB	$F4$ = 75.0Hz @ -1.49dB
$F2$ = 146.7Hz @ -0.77dB	$F5$ = 44.2Hz @ -2.97dB
$F3$ = 81.0Hz @ -0.82dB	$F6$ = 216.2Hz @ -6.68dB

Table 7.3 provides complete details of the observed peaks for all subjects diagnosed as having stiffening aortic bioprostheses. The major distribution of spectral energy occurs in the region between 50Hz and 200Hz, where mean relative energies and RMS energies within this population group were computed to be 62% and 61% respectively. Figures 7.5(a-d) show typical examples of spectra and the accompanying distributions of spectral energy estimated from the sounds produced by the operation of stiffening Carpentier-Edwards aortic bioprostheses.

One subject (patient twenty-four) had a prosthesis diagnosed as being both leaky and stiffening. The dominant frequencies and amplitudes of these peaks were observed to be:

$F1$ = 30.0Hz @ 0dB	$F4$ = 159.0Hz @ -22.8dB
$F2$ = 58.0Hz @ -9.27dB	$F5$ = 216.0Hz @ -26.7dB
$F3$ = 107.0Hz @ -16.52dB	$F6$ = 267.0Hz @ -28.7dB

The major concentration of spectral energy occurs in the region between d.c. and 75Hz, where relative energy and RMS energies were observed to be 26% and 24% respectively. Figures 7.5(e and f) show the spectra and the accompanying distribution of spectral energy respectively evaluated for this valve.

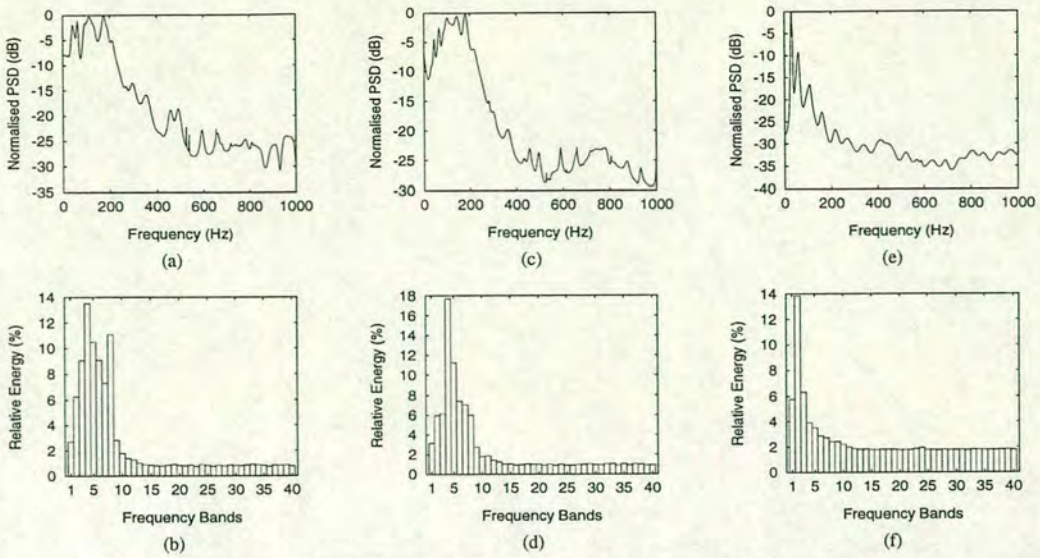

Figure 7.5: *Characteristics of sounds produced from the operation of stiffening aortic Carpentier-Edwards bioprostheses. (a-b) Prony PSD estimate and energy distribution respectively of patient twenty, (c-d) Prony PSD estimate and energy distribution respectively of patient twenty-one, (e-f) Prony PSD estimate and energy distribution respectively of patient ten, (g-h) Prony spectral estimate and energy distribution respectively of patient twenty-four.*

Patient No.	RS	*F1*	*F2*	*F3*	*F4*	*F5*	*F6*	F_{-3}	F_{-10}	F_{-20}	F_{-30}	*Energy*	*RMS*
Group 1													
1	2RIS	42	77	123	184	306	405	85.9	139.2	237	N/P	46	43
2	2RIS	46	89	148	209	386	N/P	48.7	234.3	N/P	N/P	47	44
3	2RIS	33	88	132	181	263	337	34.3	88.7	201.8	N/P	35	30
4	2RIS	43	85	131	164	200	317	43.7	221.8	N/P	N/P	46	39
5	2RIS	29	42	77	223	173	310	85	96.8	523.7	N/P	33.5	33
6	2RIS	27	55	96	115	164	200	27.1	30.5	35.2	316.6	30	27.5
7	3LIS	29	64	98	133	302	343	30	32.5	150	N/P	29	29
8	2RIS	25	118	72	250	N/P	N/P	25	30.6	36.8	190.6	21	22
9	2RIS	32	73	184	226	282	N/P	36.8	81.2	N/P	N/P	27	24
10	2RIS	31	98	129	59	218	178	25	134.3	425	N/P	39	37
11	2RIS	44	101	170	220	350	405	46.8	175	N/P	N/P	44	41
12	2RIS	68	37	105	155	199	293	73.7	117.5	220.6	N/P	46	46
13	2RIS	37	84	49	105	106	136	73.7	94.4	N/P	N/P	28	30
Mean	-	37.4	77.8	116.5	171.1	245.8	292.4	48.9	113.6	N/C	N/C	36.26	34.25
Group 2													
14	2RIS	33	59	108	124	190	N/P	57.5	66.2	137.5	375	41	38
15	2RIS	30	48	114	148	230	N/P	37.5	61.2	166.2	N/P	21	19
16	2RIS	29	59	122	176	N/P	N/P	30	33.7	143.7	N/P	24	22
17	2RIS	34	69	144	101	178	N/P	65.85	81.73	219.83	N/P	34.5	30.5
18	2RIS	27	53	89	153	193	262	26.25	30.0	162.5	N/P	24	23
19	2RIS	31	44	117	193	262	337	32.5	49.37	65.62	290.62	27.5	25.5
Mean	-	30.6	55.3	115.6	149.2	210.7	N/C	41.6	53.7	149.13	N/C	28.67	26.3
Group 3													
20	2RIS	175	113	63	95	42	210	193.75	233.12	506.87	N/P	60	60
21	2RIS	181	144	102	66	44	215	190.62	232.5	318.75	N/P	55	54
22	2RIS	248	167	95	64	37	244	181.58	233.66	N/P	N/P	69	74
23	2RIS	141	163	64	42	54	196	201.25	253.12	367.5	N/P	54	55
24	2RIS	30	58	107	159	216	267	31.25	34.37	73.75	446.8	26	24
Mean	-	186.25	146.75	81.0	75.0	44.25	216.25	191.8	238.1	N/C	N/C	59.5	60.75

Table 7.3: *Results obtained from the frequency analysis of aortic sounds: RS = Recording site where maximum PCG signal strength was observed (best signal-to-noise ratio and good separation of aortic and pulmonary components), 2RIS is the second right intercostal space (aortic area) and 3LIS is the third left intercostal space (Erb's point, auxiliary aortic area). N/P = Not Present, N/C = Not Calculated. The Energy and RMS values are percentages within regions 25Hz to 125Hz, d.c. to 75Hz and 50Hz to 200Hz for groups one, two and three respectively. Patient twenty-four was not included when evaluating the means for group three.*

7.3 Physiological Significance of Results

From the results presented in the preceding two subsections, it was observed that the sounds produced by the operation of normally functioning, leaky and stiffening Carpentier-Edwards bioprostheses each exhibit unique spectral characteristics. Normally functioning mitral valves are characterised by two to three dominant frequency peaks, with the major concentration of spectral energy occurring in the region between d.c. and 100Hz, whereas, normally functioning aortic prostheses are characterised by four to five dominant peaks, with the major distribution of spectral energy occurring in the region between 25Hz and 125Hz. For leaky mitral and aortic prostheses, a shift was observed in spectral energy: the major concentration of energy now occurs in the region between d.c. and 75Hz. Likewise, for aortic prostheses diagnosed as having stiffening calcified cusps, a shift was observed in spectral energy, with the higher-frequency peaks containing the most energy. The major distribution of energy now occurs in the region between 50Hz and 200Hz. It was observed that the frequency occurring at -10dB level can be used to identify and discriminate between normally functioning, leaky and stiffening aortic prostheses, where mean frequencies for these conditions at the -10dB level were computed to be 113.6Hz, 53.7Hz and 238.1Hz respectively. A single discriminating parameter was not observed from the analysis of mitral sounds.

For leaky mitral and aortic prostheses, in general the computed mean frequencies are lower than those obtained from the sounds produced by the operation of normally functioning prostheses. For leaky mitral prostheses; however, the amplitudes and energies of the observed lower-frequency peaks are greater. In particular, the second most dominant peak, $F2$, which characterises the sounds produced by the operation of normally functioning mitral prostheses assumes much more energy and becomes the most dominant frequency peak for three of the four subjects in this population group. The dominant frequency peak which characterises the sounds produced by the operation of normally functioning prostheses has slightly less energy and now becomes the second most dominant peak. For leaky aortic prostheses, there is a reduction in the amplitude of the higher-frequency peaks $F3$ to $F6$. Peaks $F3$ to $F6$, which characterise the sounds produced by the operation of normally functioning aortic prostheses, now have less energy, with the remainder of the energy having been evenly distributed throughout the other frequency bands of the sound spectrum as illustrated in Figure 7.4.

The concentration of energy in the lowest frequency regions of the sound spectrum for leaky prostheses can be explained by consideration of the aetiological composition of sounds produced by the operation of leaky bioprostheses. For leaky mitral prostheses, this is due

primarily to the presence of backward-flow systolic murmurs produced by an incompetent regurgitant valve, which coalesce with the mitral closing sound. As soon as the pressure in the left ventricle is greater than that in the left atrium, a driving force exists causing a backward flow of blood through an incompetent prosthesis resulting in a murmur. The usual pansystolic regurgitant murmur associated with leaky mitral prostheses begins with the first sound and remains more constant than forward midsystolic ejection murmurs as illustrated in Figure 2.6 [160]. Likewise, for leaky aortic prostheses, diastolic murmurs are produced by the incompetent regurgitant prosthesis. With mild aortic regurgitation, the early diastolic 'rumble' continues throughout diastole (pandiastolic), in contrast to the relatively short decrescendo associated with severe regurgitation as shown in Figure 2.7 [12, 160].

A previous study of heart valve sounds [128] expresses concern regarding the inconsistencies of past analyses of porcine valve sounds [38, 39], " ... it was not clear whether the peak frequencies changed or whether the peaks of higher frequencies assumed more power." In this thesis, it has been observed that the overall structure and composition of the sound spectrum effectively remains the same for normally functioning, leaky and stiffening prostheses. However, for leaky prostheses, peaks $F3$ to $F6$ have proportionally less energy when compared to peaks $F3$ to $F6$ produced by the operation of normally functioning valves. With stiffening prostheses, the higher frequency peaks assume more power. The frequencies observed in this thesis are in the range reported by previous researchers in chapter two.

A distinction exists between the frequencies which characterise the sounds produced by the operation of normally functioning mitral and aortic prostheses. Mitral sounds are characterised by two to three dominant peaks whereas aortic sounds are characterised by four to five dominant peaks. The mean computed frequencies, amplitudes and energies of these peaks are in general observed to be lower for mitral sounds. As the same microphone and instrumentation were used for both mitral and aortic sound recordings, the difference between the resulting spectra is attributed to the variations in the spectral characteristics of different transmission paths between the valves and the recording sites on the thorax.

7.4 Summary and Conclusion

This chapter examines whether a relationship exists between the heuristic parameters derived from the sound spectrum of mitral and aortic sounds and the functionality of Carpentier-Edwards bioprostheses. Results demonstrate that the sounds produced by the operation of normally functioning, leaky and stiffening prostheses from different subjects each exhibit unique spectral

characteristics.

Normally functioning mitral valves are characterised by two to three dominant frequency peaks with the major concentration of spectral energy occurring in the region between d.c. and 100Hz, whereas, normally functioning aortic prostheses are characterised by four to five dominant peaks with the major distribution of spectral energy occurring in the region between 25Hz and 125Hz. For leaky mitral and aortic prostheses, a shift was observed in spectral energy: the major concentration of spectral energy now occurs in the region between d.c. and 75Hz. Likewise, for aortic prostheses diagnosed as having stiffening calcified cusps, a shift was observed in spectral energy: the major distribution of energy was seen to occur in the region between 50Hz and 200Hz. It was observed that the frequency occurring at the -10dB level may be used to identify and discriminate between normally functioning, leaky and stiffening aortic prostheses, where mean frequencies for these conditions at the -10dB level were computed to be 113.6Hz, 53.7Hz and 238.1Hz respectively. A single discriminating parameter was not observed from the analysis of mitral sounds.

The results reported in this chapter demonstrate the diagnostic potential of frequency analysis as an alternative physiological measurement technique capable of assisting physicians in their evaluation of the post-operative performance and functional integrity of the Carpentier-Edwards bioprosthetic heart valve.

Chapter 8

Summary and Conclusions

In collaboration with the Cardiovascular Research Unit of The University of Edinburgh and The Royal Infirmary of Edinburgh, the motivation for the research described in this thesis was to investigate whether a principle based on noninvasive testing, using signal processing and analysis methods, could be applied to the acoustic output produced by the operation of the Carpentier-Edwards bioprosthesis. The overall objective of the research was to assess whether a relationship existed between the frequency spectrum of this acoustic output and the functionality of the Carpentier-Edwards bioprostheses, with a view to identifying and distinguishing between normally functioning and dysfunctioning prostheses by examination of the frequency spectrum, and ultimately, to predict impending valve failure. If a unique relationship can be found, this would demonstrate the diagnostic potential of frequency analysis as an alternative physiological measurement technique capable of assisting physicians in their post-operative evaluation of the Carpentier-Edwards bioprosthetic heart valve.

The following sections summarise the methods used in this thesis for the acquisition, conditioning, processing and analysis of the principal heart sound components contained within the phonocardiographic signals produced by the operation of the Carpentier-Edwards bioprostheses. The conclusions and achievements drawn from the research are also given. Finally, suggestions are proposed for possible extensions to the research undertaken.

8.1 Summary and Conclusions

Chapter 2 introduces the area of 'Heart Sound Processing' by first describing the function of the human heart, followed by a discussion detailing the origin of heart sounds and the physiological events which constitute a single heartbeat. The chapter also provides background material for this thesis by reviewing previous work reporting on the analysis and processing of the sounds produced by the operation of prosthetic heart valves.

In chapter 3, the design and development is discussed of a data-acquisition system comprising a battery-powered portable computer, analogue-to-digital conversion circuitry and a cardiac microphone, to digitise and record the acoustic output produced by the operation of the Carpentier-Edwards bioprostheses. The design of the data-acquisition system was based on a number of significant hardware, software and ergonomic factors to ensure high-quality reproduction. After a review of portable computers, analogue-to-digital conversion circuitry and cardiac transducers commercially available in 1991, the Elonex LT-320X laptop personal computer, the ADC-42 input/output expansion card marketed by Blue Chip Technology and the Hewlett-Packard HP-21050A contact sensor were selected for this research. The specification of this microphone includes a flat-frequency response from 0.02Hz to 2kHz, appropriate for this thesis; as well as being insensitive to extraneous ambient noise.

Particular attention was paid to the conditioning of the PCG prior to digitisation to maintain the characteristics of this signal. A PCG preamplifier was designed to amplify the output from the HP-21050A contact sensor to a level suitable for input to the data-acquisition system. The design of the preamplifier was based on a high-performance, low-noise, low-power operational amplifier, the TL064 marketed by Texas Instruments; ideal for battery-powered portable instrumentation. An 800Hz, low-pass, sixth-order, Bessel anti-aliasing filter was designed to bandlimit the phonocardiographic signal prior to digitisation. A Bessel filter is characterised by a constant time delay with frequency, thus preserving the relative phasing of all signal events. This is an important point which has not been addressed in any of the previous published works in this field.

A database of heart sounds produced by the operation of the Carpentier-Edwards bioprosthesis and recorded from a range of valve conditions now exists in the Department of Electrical Engineering at The University of Edinburgh. Details are provided of the breakdown of this database and the recording procedure implemented for this thesis.

A recorded phonocardiographic signal consists of relatively high-frequency principal heart sounds superimposed on a low-frequency respiration 'carrier'. Chapter 4 describes the pro-

cessing of this acquired signal in the time domain with a view to accentuating the principal heart sounds from the low-frequency artifact, followed by the automated extraction of mitral or aortic components from the PCG under investigation for further analysis. A 20Hz, 320 tap high-pass FIR filter (linear-phase characteristic) was implemented to abstract the principal heart sounds from the low-frequency artifact.

Two methods based on a cross-correlation, template-based matching approach were developed to automatically extract mitral and aortic components from the PCG. The first method uses the PCG solely and matches a representative closing sound with similar successive occurrences, *i.e.* the respective closing sound in each of the remaining cardiac cycles. This method is shown to give good performance when one principal heart sound is clearly the dominant signal event in each cardiac cycle. However, when both principal sounds are evident and have similar temporal structure, method 1 can identify mitral and aortic components within the same cycle resulting in the possible subsequent analysis of an incorrectly extracted sound. This is a major shortcoming of this method, the consequences of which could be fatal. To overcome this potential hazard, a second method was developed which uses an ECG signal referenced to the PCG to initially locate the beginning of each cardiac cycle. Using this *a priori* information and the fact that S1 always occurs before S2, method 2 demonstrates that the appropriate closing sound only is correctly extracted for further analysis.

Methods for the frequency analysis of heart sounds are discussed in chapter 5. Particular attention was directed towards the physiological transient-oscillatory nature of the heart sound signal and the suitability of the frequency analysis techniques when analysing such a temporal signature. The emphasis was on refining the application of spectral estimation techniques with the aim of identifying optimum methods for this thesis. Algorithms considered for the frequency analysis of valvular closing sounds were: the periodogram, the Bartlett power spectral density estimate, which reduces the variance of the conventional periodogram estimate through ensemble averaging; ARMA-based, parametric linear modelling techniques, which attempt to synthesise the heart sound generation process; and Prony's method: a parametric modelling technique based on a damped sinusoidal model.

The number of modelling coefficients used by the parametric spectral estimation techniques, *i.e.* the model order, is a very important variable when analysing bioprosthetic heart valve closing sounds, as the precise order of a principal component time series is not known *a priori* and variations in spectra can occur with different orders. Chapter 5 also investigates methods which determine the optimal model order of time series. Model order selection criteria considered were: hypothesis-based methods, decision-based techniques, the FPE, the

AIC, the MDL and the CAT; and methods which attempt to extract the optimum model order from the heart sound time series by first removing the numerical ill-conditioning inherent with the use of linear-algebra-based spectral estimation techniques.

Chapter 6 presents the results from the frequency analysis of heart sounds. From a signal processing perspective, the major observations concerning the application and performance of these methods were:

1. The superior resolution of Prony's method in identifying within the frequency domain a number of dominant spectral peaks over the full range of recorded sounds and valve conditions.

2. The covariance, MCV, Burg and weighted Burg (parabolic optimum taper and Hamming window) methods all produce almost identical spectra. The resulting estimates are able to identify the same features revealed by the Prony PSD estimate, however, the ability of these AR methods to completely resolve the same spectral detail is secondary to Prony's method.

3. For some sounds, a difference was observed between the spectra produced by the covariance method when compared to the estimates evaluated by the other AR techniques.

4. The application of the periodogram (with and without a Hamming window) produces smoothed spectra relative to the AR and Prony estimates.

5. The Bartlett periodogram produces very highly smoothed spectra, containing little or no information in the frequency spectrum which may be considered suitable for use as heuristic parameters.

It was observed that monitoring the NRMSE for a decrease in the rate of change, the FPE, the AIC, the MDL and the CAT decision-based model order selection criteria returned orders that were too low to adequately model heart sounds, producing spectra with low-frequency resolution containing little or no information. The mean values observed by these methods were: 14 and 8, 16 and 11, 16 and 11, 6 and 4 and 16 and 11 for mitral and aortic components respectively. Although these orders are greater than or in the range suggested by theoretical values, as a result of the transient nature of heart sounds, the presence of background noise, and the fact that heart valve closing sounds do not satisfy the requirements of an AR model excited by white noise or a Gaussian distribution, these values are still too low to adequately model the sounds. It was found empirically that mean optimum orders of 40 and 38 for mitral

and aortic components respectively produced the best spectra, containing features which may be considered for use as heuristic parameters.

Consistent determination of the model order was achieved by first removing the numerical ill-conditioning inherent with the use of linear-algebra-based spectral estimation techniques. Examining the relative magnitudes of singular values or the roots of the backward linear prediction polynomial used in Prony's method, produced model orders that relate closely to those expected from consideration of the mechanics of heart sound generation. Four to six dominant singular values and two to six signal zeros are consistently identified throughout the patient population.

By selecting appropriate features derived from the sound spectrum, chapter 7 identifies a relationship between these spectral parameters and the functionality of the Carpentier-Edwards bioprostheses. It was observed that the sounds produced from the operation of normally functioning, leaky and stiffening prostheses each exhibit unique spectral characteristics.

Normally functioning mitral valves are characterised by two to three dominant frequency peaks with the major concentration of spectral energy occurring in the region between d.c. and 100Hz, whereas, normally functioning aortic prostheses are characterised by four to five dominant peaks with the major distribution of spectral energy occurring in the region between 25Hz and 125Hz. For leaky mitral and aortic prostheses, a shift was observed in spectral energy: the major concentration of spectral energy now occurs in the region between d.c. and 75Hz. Likewise, for aortic prostheses diagnosed as having stiffening calcified cusps, a shift was observed in spectral energy: the major distribution of energy was seen to occur in the region between 50Hz and 200Hz. It was observed that the frequency occurring at the -10dB level may be used to identify and discriminate between normally functioning, leaky and stiffening aortic prostheses, where mean frequencies for these conditions at the -10dB level were computed to be 113.6Hz, 53.7Hz and 238.1Hz respectively. A single discriminating parameter was not observed from the analysis of mitral sounds.

The range of frequencies and that stiffening valves are characterised by a relative increase in higher-frequency energy, agree with previous analyses of the sounds produced by the operation of porcine bioprostheses reported in chapter 2 [37, 38]. However, the research detailed in this thesis has extended previous work by showing that effective and high-quality data acquisition, preprocessing and signal processing of bioprosthetic heart valve closing sounds offer the potential of being able to identify and discriminate between different states of valvular function: normally functioning, leaky and stiffening prostheses.

The objective of all the foregoing research has been to examine whether a relationship exists

between the acoustic output produced by the operation of the Carpentier-Edwards bioprosthesis and the functionality of this prosthesis, and the application of methods for the frequency analysis of heart sounds. The proposition of this thesis is that analysing the frequency spectrum of this acoustic output successfully meets this objective.

An automated diagnostic system has been developed which records heart sounds, and then, using signal analysis algorithms, processes and analyses the principal components over the full range of recorded sounds and valve conditions. Results demonstrate the diagnostic potential of frequency analysis as an alternative physiological measurement technique capable of assisting physicians in their post-operative assessment of the Carpentier-Edwards bioprosthetic heart valve. As a clinical technique for periodically monitoring patients with implanted prostheses, frequency analysis of valve sounds is particularly attractive as it is noninvasive, atraumatic, passive, reliable and sensitive. The very low-cost, repeatability and portability of this technique are added benefits.

The application of signal processing methods to the PCG signal has quantified the analysis of the PCG, which in turn is directly related to auscultation. Processing the PCG reveals valuable information such as the timing instants of heart sounds and their components, the structure of sounds, their frequency content and their location in the cardiac cycle. Frequency analysis can be used to complement other traditional post-operative techniques such as echocardiography, with one method providing supplementary information to the other.

8.2 Areas of Further Research

To conclude this thesis, several areas of research are discussed which could possibly extend the work undertaken. A prototype system based on the application of signal processing methods to the sounds produced by the operation of Carpentier-Edwards bioprostheses is now operational. This automated diagnostic system first records the sounds, and then, using signal analysis algorithms, processes and analyses the principal components contained within these sounds. For this system to be more comprehensively tested and its routine clinical value assessed, there is a requirement for a dedicated instrument for the recording and realtime implementation of the algorithms. Although computational efficiency was not an issue which was specifically addressed during system development, the algorithms can process and analyse a fifteen-second PCG record in approximately two minutes on a Sun 4 workstation. The major proportion of the computation is absorbed by the automated mitral or aortic component extraction algorithm developed in chapter 4 (Method 2), the frequency analysis of each extracted sound, followed

by the calculation of an ensemble spectral average for each recording. With the availability of high-speed digital signal processing chips, it would be possible to undertake a recording followed by a realtime analysis of the acquired phonocardiographic signal.

From a signal processing perspective, there exist a number of techniques whose application to heart sounds could possibly extend the research reported in this thesis:

Joint time-frequency approaches to signal analysis such as the short-time Fourier transform [161], the Wavelet Transform [162, 163], the Wigner-Ville [164], Choi-Williams [165] and the reduced interference distributions [166] offer the potential for better analysis of dynamic, nonstationary biomedical processes. Conventional classical and parametric methods of spectral estimation assume that the signal under investigation is locally stationary, *i.e.* the signal frequency is assumed to remain constant during the transform interval. However, such an assumption is not valid for many physiological processes [167]. Joint time-frequency methods of signal analysis produce a 3D-representation of time, frequency and spectral amplitude. This interpretation provides a more general perspective, and information such as the time-frequency evolution would become apparent of cardiac events, *e.g.* the regurgitant murmurs which characterise leaky mitral and aortic Carpentier-Edwards bioprostheses. Recent work by Bentley *et al.* [168] reports that the application of time-frequency methods to the sounds produced by the operation of native heart valves is able to distinguish between normally functioning and stenosed valves. In a number of personal communications received from Professor T. E. Posch of the Hughes Aircraft Company in the United States (US) (see appendix B), Professor Posch informed me that several US heart valve manufacturers are currently considering providing a sound spectrum with each valve made. This unique signature would characterise the function of a valve *in vitro*, and would allow for a direct comparison with the spectral characteristics of the sounds obtained after implantation. Professor Posch also informed me that the US Army are currently assessing the potential of phonocardiography as a screening procedure to evaluate the condition of the heart valves of all new potential recruits.

Recent advances in the technique and application of artificial neural networks have made possible the use of these classifiers for pattern recognition [169–171]. When a neural network is used to perform a pattern recognition task, there is no need for assumptions regarding the underlying probability distributions [172–174]. In addition, the parallel architecture of neural networks provides the potential for fast data processing. Features derived from the frequency analysis of the heart sounds produced by the operation of the Carpentier-Edwards bioprostheses may be used as input parameters to a neural network. The diagnostic potential of artificial neural networks in the classification of bioprosthetic heart valve sounds is an area which remains to

be investigated.

The application of homomorphic blind deconvolution approaches to signal analysis offer the potential to minimise the conditioning effect of the thorax as the transmitted sounds travel from within the chambers of the heart to the chest surface. Recent work [175, 176] reports a strong correlation between the surface PCGs and the intracardiac PCGs recorded from dogs. By eliminating the conditioning effect of the thorax on the sounds recorded at the chest surface, this would allow for a direct comparison of the spectral characteristics of the sounds before and after implantation. This would be particularly significant if the manufacturers of heart valves decide to provide a unique spectral signature with each valve made.

References

[1] E. Braunwald, *Heart Disease: A Textbook of Cardiovascular medicine.* ISBN 0721630979, W. B. Saunders Company, 1992.

[2] R. M. Rangayyan and R. J. Lehner, "Phonocardiogram Signal Analysis: A Review," *CRC Critical Reviews in Biomedical Engineering*, vol. 15, no. 3, pp. 211–236, 1988.

[3] R. B. Randall, *Frequency Analysis.* ISBN 8787355078, Brüel Kjaer, 1987.

[4] D. E. Harken, H. S. Soroff, W. J. Taylor, A. A. Lefemin, S. K. Gupta and S. Lunzer, "Partial and complete prostheses in aortic insufficiency," *Journal of Thoracic and Cardiovascular Surgery*, vol. 40, pp. 744–762, 1960.

[5] H. L. Edmunds, "Thrombotic and bleeding complications of prosthetic heart valves," *Annals of Thoracic Surgery*, vol. 44, pp. 430–445, October 1987.

[6] A. Starr and G. L. Grunkemeier, "The Expected Lifetime of Porcine Valves," *Annals of Thoracic Surgery*, vol. 48, pp. 317–318, 1989.

[7] D. J. Magilligan, J. W. Lewis, P. D. Stein and M. Alam, "The Porcine Bioprosthetic Heart Valve: Experience at 15 Years," *Annals of Thoracic Surgery*, vol. 48, pp. 324–330, 1989.

[8] A. Leatham, "Auscultation of the heart," *Lancet*, vol. 2, pp. 703–708, October 1958.

[9] M. B. Rappaport and H. B. Sprague, "Physiologic and physical laws that govern auscultation, and their clinical application - the acoustic stethoscope and the electrical amplifying stethoscope and stethograph," *American Heart Journal*, vol. 21, no. 3, pp. 257–318, March 1941.

[10] H. Fletcher and W. A. Munson, "Loudness, Its Definition, Measurement and Calculation," *Journal Aocustic Society of America*, vol. 5, pp. 82–108, October 1933.

[11] L. P. Feigen, "Physical characteristics of sound and hearing," *American Journal of Cardiology*, vol. 28, pp. 130–139, August 1971.

[12] A. Leatham, *Auscultation of the Heart and Phonocardiography.* ISBN 0700015140, J. & A. Churchill, 1970.

[13] A. A. Luisada, *From Auscultation to Phonocardiography.* ISBN 009661536, The C.V. Mosby Company, 1965.

[14] R. B. Urquhart, J. McGhee, J. E. S. Macleod, S. W. Banham and F. Moran, "The Daignostic Value of Pulmonary Sounds: A Preliminary Study by Computer-Aided Analysis," *Computers in Biology and Medicine*, vol. 11, no. 3, pp. 129–139, 1981.

[15] R. J. Dobrow, J. B. Calatayud, S. Abraham and C. A. Caceres, "A study of physician variation in heart-sound interpretation," *Annals of Medicine*, vol. 33, pp. 305–311, 1964.

[16] J. S. Butterworth and E. H. Reppert, "Auscultatory acumen in the general medical population," *Journal of the American Medical Association*, vol. 174, pp. 114–118, 1960.

[17] W. N. Bloch, J. M. Felner, R. C. Schlant, P. N. Symbas and E. L. Jones, "The echocardiogram of the porcine bioprosthesis in the aortic position," *Chest*, vol. 72, no. 5, pp. 640–646, November 1977.

[18] J. N. Schapira, R. P. Martin, R. E. Fowles, H. Rakowski, E. B. Stinson, J. W. French, N. E. Shumway and R. L. Popp, "Two dimensional echocardiographic assessment of patients with bioprosthetic valves," *American Journal of Cardiology*, vol. 43, pp. 510–519, March 1979.

[19] H. S. Rosman, M. Alam, J. B. Lakier, S. R. Kemp, H. N. Sabbah, D. J. Magilligan and P. D. Stein, "Utility of Physical Examination and Noninvasive Tests in the Diagnosis of Degeneration of Porcine Bioprosthetic Valves in the Mitral Position," *American Journal Noninvasive Cardiology*, vol. 2, pp. 48–51, 1988.

[20] M. E. DeBakey, *Advances in Cardiac Valves*. ISBN 013271231, Yorke Medical Books, 1982.

[21] R. J. C. Hall and D. G. Julian, *Diseases of the Cardiac Valves*. ISBN 013262503, Churchill Livingstone, 1989.

[22] A. F. White, R. E. Dinsmore and M. J. Buckley, "Cineradiographic evaluation of prosthetic cardiac valves," *Circulation*, vol. 48, pp. 882–889, 1973.

[23] A. A. Luisada, *The Sounds of the Normal Heart*. ISBN 002977459, Warren H. Green, Inc., 1972.

[24] A. Leatham and G. J. Leech, "Auscultation of the Heart," in *The Heart*. ISBN number not recorded. McGraw-Hill, 1982.

[25] A. Leatham and G. J. Leech, "The Generation of Heart Sounds and Murmurs," in *Scientific Foundations, Cardiology*. ISBN number not recorded. William Heinemann Medical Books Ltd, 1983.

[26] S. Laniado, E. L. Yellin, H. Miller and R. W. Frater, "Temporal relation of the first heart sound to closure of the mitral valve," *Circulation*, vol. 47, pp. 1006–1014, May 1973.

[27] S. Laniado, E. L. Yellin, M. Kottler, L. Levy, J. Stadler and R. Terdiman, "A study of the dynamic relation between the mitral valve echogram and phasic mitral flow," *Circulation*, vol. 51, pp. 104–113, February 1975.

[28] G. J. Leech, N. Brooks, A. Green-Wilkinson and A. Leatham, "Mechanism of the influence of PR interval on loudness of the first heart sound," *British Heart Journal*, vol. 43, pp. 138–142, 1980.

[29] E. Craige, "On the genesis of heart sounds," *Circulation*, vol. 53, pp. 207–209, 1976.

[30] E. Craige, "Echocardiography in studies of the genesis of heart sounds and murmurs," *Progress in Cardiology*, vol. 4, no. 1, pp. 1–18, 1975.

[31] J. C. Hylen, F. E. Kloster, R. H. Herr, A. Starr and H. E. Griswold, "Sound spectrographic diagnosis of aortic ball variance," *Circulation*, vol. 34, pp. 849–858, 1969.

[32] R. F. Gordon, M. Najmi, B. Kingsley, B. L. Segal and J. W. Linhart, "Spectroanalytic evaluation of aortic prosthetic valves," *Chest*, vol. 66, pp. 44–49, 1974.

[33] Y. Kagawa, N. Sato, S. Nitta, K. Saji, M. Tanaka, Y. Shibota and T. Horiuchi, "Sound Spectroanalytic Diagnosis of Malfunctioning Prosthetic Valves," *Tokohu Journal of Experimental Medicine*, vol. 123, pp. 77–89, 1977.

[34] Y. Kagawa, N. Sato, S. Nitta, T. Hongo, M. Tanaka, H. Mohri and T. Horiuchi, "Real-time sound spectroanalysis for diagnosis of malfunctioning prosthetic valves," *Journal of Cardiovascular Surgery*, vol. 79, no. 5, pp. 671–679, May 1980.

[35] N. Sato, H. Mohri, Y. Kagawa, T. Horiuchi and M. U. ans S. Nitta, "Real-time sound spectral analysis of thrombosed prosthetic valves," *Transactions American Society of Artifical Internal Organs*, vol. 34, pp. 831–834, 1988.

[36] P. D. Stein, *A Physical and Physiological Basis for the Interpretation of Cardiac Auscultation*. ISBN 0879930659, Futura Publishing Company, 1981.

[37] P. D. Stein, H. N. Sabbah, J. B. Lakier, D. J. Magilligan and G. S, "Frequency of the First Heart Sound in the Assessment of Stiffening of the Mitral Bioprosthetic Valves," *Circulation*, vol. 63, no. 1, pp. 200–203, 1981.

[38] P. D. Stein, H. N. Sabbah, J. B. Lakier, S. R. Kemp and D. J. Magilligan, "Frequency Spectra of the First Heart Sound and of the Aortic Component of the Second Heart Sound in Patients with Degenerated Porcine Bioprosthetic Valves," *The American Journal of Cardiology*, vol. 53, pp. 557–561, February 1984.

[39] R. A. Foale, T. H. Joo, J. H. McClellan, R. W. Metzinger, G. L. Grant and G. S. Myers, "Detection of aortic porcine valve dysfunction by maximum entropy spectral analysis," *Circulation*, vol. 68, no. 1, pp. 42–49, July 1983.

[40] T. H. Joo, J. H. McClellan, R. A. Foale, G. S. Myers and R. S. Lees, "Pole-Zero Modelling and Classification of Phonocardiograms," *IEEE Transactions on Biomedical Engineering*, vol. BME-30, no. 2, pp. 110–117, 1983.

[41] M. Brais, L. G. Durand, M. Blanchard, J. D. Guise, R. Guardo and W. J. Keon, "Frequency analysis of Ionescu-Shiley prosthetic closing sounds in patients with normally functioning prostheses," *Medical and Biological Engineering and Computing*, vol. 24, pp. 637–642, November 1986.

[42] L. G. Durand, J. D. Guise, G. Cloutier, R. Guardo and M. Brais, "Evaluation of FFT-Based and Modern Parametric Methods for the Spectral Analysis of Bioprosthetic Valve Sounds," *IEEE Transactions on Biomedical Engineering*, vol. BME-33, pp. 572–578, November 1986.

[43] G. Cloutier, R. Guardo and L. G. Durand, "Spectral analysis of closing sounds produced by Ionescu-Shiley bioprosthetic aortic heart valves: Part 1 - Optimal number of poles and zeros for parametric spectral analysis," *Medical and Biological Engineering and Computing*, vol. 25, pp. 487–491, September 1987.

[44] G. Cloutier, R. Guardo and L. G. Durand, "Spectral analysis of closing sounds produced by Ionescu-Shiley bioprosthetic aortic heart valves: Part 2 - Computer simulation of aortic closing sounds and estimation of their truncation level and signal-to-noise ratio," *Medical and Biological Engineering and Computing*, vol. 25, pp. 492–496, September 1987.

[45] G. Cloutier, R. Guardo and L. G. Durand, "Spectral analysis of closing sounds produced by Ionescu-Shiley bioprosthetic aortic heart valves: Part 3 - Performance of FFT-based and paramatric methods for extracting diagnostic spectral parameters," *Medical and Biological Engineering and Computing*, vol. 25, pp. 497–503, September 1987.

[46] G. Cloutier, L. G. Durand, R. Guardo, H. Sabbah and P. D. Stein, "Bias and Variability of Diagnostic Spectral Parameters Extracted from Closing Sounds Produced by Bioprosthetic Valves Implanted in the Mitral Position.," *IEEE Transactions on Biomedical Engineering*, vol. BME-36, no. 8, pp. 815–825, August 1989; correction in vol. BME-36, p. 1142, November 1989.

[47] L. G. Durand, M. Blanchard, H. N. Sabbah, M. S. Hamid, S. R. Kemp and P. D. Stein, "A Bayes Model for Automatic Detection and Quantification of Bioprosthetic Valve Degeneration," *Mathematical Computer Modelling*, vol. 11, pp. 158–163, 1988.

[48] L. G. Durand, M. Blanchard, G. Cloutier, H. Sabbah and P. D. Stein, "Comparison of Pattern Recognition Methods for Computer-Assisted Classification of Spectra of Heart Sounds in Patients with a Porcine Bioprosthetic Valve Implanted in the Mitral Position.," *IEEE Transactions on Biomedical Engineering*, vol. 37, no. 12, pp. 1121–1129, December 1990.

[49] P. Rolfe, *Non-invasive Physiological Measurement.* ISBN not recorded, Academic Press, 1979.

[50] E. V. Vollenhoven and J. Wallenburg, "Calibration of Air Microphones for Phonocardiography," *Medical Biological Engineering*, vol. 8, pp. 309–313, 1970.

[51] E. V. Vollenhoven, "Calibration of Contact Microphones Applied to the Human Chest Wall," *Medical Biological Engineering*, vol. 9, pp. 365–373, 1971.

[52] K. Ikegaya, N. Suzumura and T. Funada, "Absolute Calibration of Phonocardiographic Microphones and Measurements of Chest Wall Vibration," *Medical Biological Engineering*, vol. 9, pp. 683–692, 1971.

[53] N. Suzmura and K. Ikegaya, "Characteristics of the air cavities of phonocardiographic microphones and the effects of vibration and room noise," *Medical Biological Engineering and Computing*, vol. 15, pp. 240–247, May 1977.

[54] D. Groom, "Standardization in Phonocardiography: The Microphone Pickup," *Cardiology*, vol. 55, pp. 129–135, 1970.

[55] A. A. Luisada and J. G. Bernstein, "Better Resolution and Quantitation in Clinical Phonocardiography," *Cardiologia*, vol. 47, no. 3, pp. 113–126, 1965.

[56] V. Padmanabhan, R. Fischer, J. L. Semmlow and W. Welkowitz, "High Sensitivity PCG Transducer for Extended Frequency Applications," *Proceedings 11th Annual International Conference IEEE Engineering in Medicine and Biology Society*, pp. 57–58, 1989.

[57] V. Padmanabhan, J. L. Semmlow, W. Welkowitz and J. Kostis, "Comparative Evaluation of Cardiac Microphones," *Proceedings 10th Annual International Conference IEEE Engineering in Medicine and Biology Society*, pp. 167–169, 1988.

[58] R. S. Schwartz, J. T. Reeves, I. E. Sodal and F. S. Barnes, "Improved phonocardiogram system based on acoustic impedance matching," *American Journal of Physiology*, vol. 238, pp. 604–609, 1980.

[59] V. Padmanabhan, J. L. Semmlow and W. Welkowitz, "Accelerometer Type Cardiac Transducer for Detection of Low-Level Heart Sounds," *IEEE Transactions on Biomedical Engineering*, vol. 40, no. 1, pp. 21–28, January 1993.

[60] *Editor* A. Wald, "Special Edition on Biomaterials," *IEEE Engineering in Medicine and Biology Magazine*, vol. 8, no. 2, June 1989.

[61] A. Carpentier, E. Lane, S. Carpentier, A. Deloche, S. Chauvaud and S. Maxwell, "Continuing improvements in valvular bioprostheses," *The Journal of Thoracic and Cardiovascular Surgery*, vol. 83, no. 1, pp. 27–42, January 1982.

[62] W. R. Jamieson, A. I. Munro, R. T. Miyagishima, P. Allen, M. T. Janusz, A. N. Gerein, L. H. Burr, H. ling, R. I. Hayden, H. Tutassura, J. MacNab, F. Chan and G. F. Tyers, "The Carpentier-Edwards Supra-Annular Porcine Bioprosthesis: New Generation Low Pressure Glutaraldehyde Fixed Prosthesis," *Journal of Cardiac Surgery*, vol. 3, no. 4, pp. 507–521, December 1988.

[63] R. J. Levy, F. J. Shoen and G. Golomb, "Bioprosthetic Heart Valve Calcification: Clinical Features, Pathobiology, and Prospects for Prevention," *CRC Critical Reviews in Biocompatibility*, vol. 2, no. 2, pp. 147–187, 1986.

[64] P. J. Arnott, G. W. Pfeiffer and M. E. Tavel, "Spectral Analysis of Heart Sounds: Relationships between some physical characteristics and frequency spectra of first and second heart sounds in normals and hypertensives.," *Journal of Biomedical Engineering*, vol. 6, pp. 121–128, 1984.

[65] M. A. Dietz, A. O. Grant and C. F. Starmer, "An Object Oriented User Interface for Analysis of Biological Data," *Computers and Biomedical Research*, vol. 23, pp. 82–96, 1990.

[66] N. Instruments, "PC-Based Data Acquisition," *Instrumentation Newsletter*, vol. 5, no. 1, Autumn 1991.

[67] J. Barber and R. Almgren, "Building Virtual Instruments that Meet the Changing Demands of Scientific and Engineering Applications," *Canadian Chemical News*, pp. 17–19, May 1993.

[68] Measurements and Data Corporation, *Medical Electronics*, September 1991. Issue 130.

[69] Pan European Publishing Company, *International Hospital Equipment*, December 1991.

[70] Keithley Instruments Ltd, *Data Acquisition and Control Catalog*, 1991.

[71] Keithley Instruments Ltd, *Data Acquisition Catalog and Reference Guide*, 1992.

[72] National Instruments, *Data Acquisition Reference Guide*, 1991.

[73] Advantech, *Total Solution for PC-based Industrial and Lab Automation Catalog*, 1991.

[74] Strawberry Tree, *Data Acquisition and Control Catalog*, 1991.

[75] Dataq Instruments, Inc., *Real Time, PC-Based Instrumentation Catalog*, 1991.

[76] Borland International, Inc., *Turbo C User's Guide*, 1988.

[77] W. C. S. Smith, H. Tunstall-Pedoe, I. K. Crombie and R. Tavendale, "Concomitants of Excess Coronary Deaths - Major Risk Factor and Lifestyle Findings From 10,359 Men and Women in the Scottish Heart Health Study," *Scottish Medical Journal*, vol. 34, pp. 550–555, 1989.

[78] S. M. Kay and S. L. Marple, "Spectrum Analysis - A Modern Perspective," *Proceedings of the IEEE*, vol. 69, no. 11, pp. 1380–1419, November 1981; correction in *Proceedings of the IEEE*, vol. 70, p. 1238, October 1982.

[79] R. E. Challis and R. I. Kitney, "The Design of Digital Filters for Biomedical Signal Processing. Part 1: Basic Concepts," *Journal of Biomedical Engineering*, vol. 4, pp. 267–278, 1982.

[80] R. E. Challis and R. I. Kitney, "The Design of Digital Filters for Biomedical Signal Processing. Part 2: Design Techniques using the Z-plane," *Journal of Biomedical Engineering*, vol. 5, pp. 19–30, 1983.

[81] R. E. Challis and R. I. Kitney, "The Design of Digital Filters for Biomedical Signal Processing. Part 3: The Design of Butterworth and Chebychev Filters," *Journal of Biomedical Engineering*, vol. 5, pp. 91–102, 1983.

[82] P. A. Lynn, *Digital Signals, Processors and Noise*. ISBN 0333545877, The Macmillan Press Ltd., 1992.

[83] J. G. Proakis and D. I. Manolakis, *Introduction to Digital Signal Processing*. ISBN 0029462533, Macmillan Publishing Company, 1989.

[84] J. C. Principe and J. R. Smith, "Design and Implementation of Linear Phase FIR Filters for Biological Signal Processing," *IEEE Transactions on Biomedical Engineering*, vol. BME-33, no. 6, pp. 550–559, June 1986.

[85] Comdisco Systems, Inc., *SPW™ - The DSP Framework, Signal Calculator User's Guide*, September 1992.

[86] P. A. Lynn, *An Introduction To The Analysis And Processing Of Signals*. ISBN 0333340302, Macmillan Publishers Ltd., 1984.

[87] N. B. Jones, *Digital Signal Processing*. ISBN 0906048915, Peter Peregrinus Ltd., 1982.

[88] R. E. Challis and R. I. Kitney, "Biomedical signal processing. Part 1: Time-domain methods," *Medical and Biological Engineering and Computing*, vol. 28, pp. 509–524, November 1990.

[89] O. Rompelmann and H. H. Ros, "Coherent averaging techniques: A tutorial review," *Journal of Biomedical Engineering*, vol. 8, pp. 24–35, 1986.

[90] A. Cohen, *Biomedical Signal Processing - Volume 1, Time and frequency domains analysis*. ISBN 0849359333 (v. 1), CRC Press, Inc., 1986.

[91] J. E. Deardorff and C. R. Trimble, "Calibrated Real-Time Signal Averaging," *Hewlett Packard Journal*, vol. 19, no. 8, pp. 8–13, 1968.

[92] W. Craelius, M. Restivo, M. A. Assadi and N. El-Sherif, "Criteria for Optimal Averaging of Cardiac Signals," *IEEE Transactions on Biomedical Engineering*, vol. BME-33, no. 10, pp. 957–966, October 1986.

[93] R. Mehra and N. El-Sherif, "Signal averaging of electrocardiographic potentials: A review," *International Journal of Acupuncture and Electrotherapy Research*, vol. 7, pp. 133–155, 1982.

[94] C. Marven and G. Ewers, *A Simple Approach to Digital Signal Processing*. ISBN 0904047008, Texas Instruments, 1993.

[95] S. L. Marple, "A Tutorial Overview of Modern Spectral Estimation," *Proceedings IEEE International Conference on Acoustics, Speech and Signal Processing*, vol. 4, pp. 2152–2157, 1989.

[96] D. Brook and R. J. Wynne, *Signal Processing - Principles and Applications*. ISBN 0713135646, Edward Arnold, 1988.

[97] R. T. Lacoss, "Data adaptive spectral analysis methods," *Geophysics*, vol. 36, pp. 661–675, August 1971.

[98] T. S. Durrani and J. M. Nightingale, "Data Windows for Spectral Analysis," *Proceedings of the IEE*, vol. 119, no. 3, pp. 343–352, 1972.

[99] F. J. Harris, "On the Use of Windows for Harmonic Analysis with the Discrete Fourier Transform," *Proceedings of the IEEE*, vol. 66, no. 1, pp. 51–83, January 1978.

[100] A. H. Nuttall, "Some windows with very good sidelobe behaviour," *IEEE Transactions on Acoustics, Speech and Signal Processing*, vol. ASSP-29, no. 1, pp. 84–89, February 1981.

[101] B. W. Jervis, M. Coelho and G. W. Morgan, "Spectral analysis of EEG responses," *Medical and Biological Engineering and Computing*, vol. 27, pp. 230–238, May 1989.

[102] A. Sewards, "Introduction to DSP," *Electronics and Wireless World*, vol. 94, no. 1630, pp. 741–746, August 1988.

[103] C. W. Therrien, *Discrete Random Signals and Statistical Signal Processing*. ISBN 0132179857, Prentice-Hall, Inc., 1992.

[104] A. V. Oppenheim and R. W. Schafer, *Digital Signal Processing*. ISBN 0132146355, Prentice-Hall, Inc., 1975.

[105] D. A. Linkens, "Estimation of Circadian Rhythm Components Using Auto-regressive Model," *Journal of Interdisciplinary Cycle Research*, vol. 10, no. 1, pp. 1–40, 1979.

[106] S. L. Marple, *Digital Spectral Analysis With Applications*. ISBN 0132141493, Prentice-Hall, Inc., 1987.

[107] D. A. Linkens, "Short-time-series spectral analysis of biomedical data," *Proceedings of the IEE*, vol. 129, Part A, pp. 663–672, December 1982.

[108] J. A. Cadzow, "Spectral Estimation: An Overdetermined Rational Model Equation Approach," *Proceedings of the IEEE*, vol. 70, no. 9, pp. 907–939, September 1982.

[109] J. A. Cadzow, "High Performance Spectral Estimation - A New ARMA Method," *IEEE Transactions on Acoustics, Speech and Signal Processing*, vol. ASSP-28, no. 5, pp. 524–528, October 1980.

[110] J. A. Cadzow, "Signal Processing via Least Squares Error Modelling," *IEEE Signal Processing Magazine*, vol. 7, no. 4, pp. 12–31, October 1990.

[111] B. Friedlander and B. Porat, "The Modified Yule-Walker Method of ARMA Spectral Estimation," *IEEE Transactions on Aerospace and Electronic Systems*, vol. AES-20, no. 2, pp. 158–173, March 1984.

[112] S. M. Kay, *Modern Spectral Estimation : Theory and Application.* ISBN 013598582, Prentice-Hall, 1988.

[113] J. Makhoul, "Linear Prediction: A Tutorial Review," *Proceedings of the IEEE*, vol. 63, no. 4, pp. 561–580, April 1975; correction in *Proceedings of the IEEE*, vol. 64, p. 285, February 1976.

[114] S. Haykin, *Modern Filters.* ISBN 0029461537, Maxwell Macmillan Publishing Company, 1990.

[115] A. H. Gray and J. D. Markel, "A spectral-flatness measure for studying the autocorrelation method of linear prediction of speech analysis," *IEEE Transactions on Acoustics, Speech and Signal Processing*, vol. ASSP-22, pp. 207–216, June 1974.

[116] L. R. Rabiner and R. W. Schafer, *Digital Processing of Speech Signals.* ISBN 0132136031, Prentice-Hall, 1978.

[117] N. Andersen, "Comments on the Performance of Maximum Entropy Algorithms," *Proceedings of the IEEE*, vol. 66, no. 11, pp. 1581–1582, November 1978.

[118] N. Andersen, "On the Calculation of Filter Coefficients for Maximum Entropy Analysis," *Geophysics*, vol. 39, no. 1, pp. 69–71, February 1974.

[119] R. W. Herring, "The Cause of Line Splitting in Burg Maximum Entropy Spectral Analysis," *IEEE Transactions on Acoustics, Speech and Signal Processing*, vol. ASSP-28, no. 6, pp. 692–701, December 1980.

[120] P. F. Fougere, E. J. Zawalick and H. R. Radoski, "Spontaneous Line Splitting in Maximum Entropy Power Spectrum Analysis," *Physics Earth Planetary Interiors*, vol. 12, pp. 201–207, August 1976.

[121] D. N. Swingler, "A Modified Burg Algorithm for Maximum Entropy Spectral Analysis," *Proceedings of the IEEE*, vol. 67, no. 9, pp. 1368–1369, September 1979.

[122] M. Kaveh and G. A. Lippert, "An Optimum Tapered Burg Algorithm for Linear Prediction and Spectral Analysis," *IEEE Transactions on Acoustics, Speech and Signal Processing*, vol. ASSP-31, no. 2, pp. 438–444, April 1983.

[123] S. L. Marple, "A New Autoregressive Spectrum Analysis Algorithm," *IEEE Transactions on Acoustics, Speech and Signal Processing*, vol. ASSP-28, no. 4, pp. 441–454, August 1980.

[124] M. Morf, B. Dickinson, T. Kailath and A. Vieira, "Efficient Solution of Covariance Equations for Linear Prediction," *IEEE Transactions on Acoustics, Speech and Signal Processing*, vol. ASSP-25, no. 5, pp. 429–433, October 1977.

[125] M. Akay, *Biomedical Signal Processing*. ISBN 0120471450, Academic Press, Inc., 1994.

[126] J. Laroche, "A New Analysis/Synthesis System of Musical Signals using Prony's Method. Application to Heavily Damped Percussive Sounds.," *Proceedings IEEE International Conference on Acoustics, Speech and Signal Processing*, vol. 3, pp. 2053–2056, 1989.

[127] D. G. Childers, "Modern Spectral Analysis," *Proceedings IEEE Frontiers of Engineering in Health Care*, pp. 104–109, Denver 1979.

[128] H. Koymen, B. K. Altay and Y. Z. Ider, "A Study of Prosthetic Heart Valve Sounds," *IEEE Transactions on Biomedical Engineering*, vol. BME-34, no. 11, pp. 853–863, June 1987.

[129] H. Akaike, "A new look at statistical model identification," *IEEE Transactions on Automatic Control*, vol. AC-19, no. 6, pp. 716–723, December 1974.

[130] M. Wax and T. Kailath, "Detection of Signals by Information Theoretic Criteria," *IEEE Transactions on Acoustics, Speech and Signal Processing*, vol. ASSP-33, no. 2, pp. 387–392, April 1985.

[131] H. Akaike, "Power Spectrum Estimation through Autoregression Model Fitting," *Annals of the Institute of Statistics and Mathematics*, vol. 21, pp. 407–419, 1969.

[132] H. Akaike, "Automatic Data Structure Search by the Maximum Likelihood," *Proceedings 5th Annual International Conference System Sciences: Computers in Biomedicine supplement*, pp. 99–101, Hawaii 1972.

[133] A. Isaksson, A. Wennberg and L. H. Zetterberg, "Computer Analysis of EEG Signals with Parametric Models," *Proceedings of the IEEE*, vol. 69, no. 4, pp. 451–461, April 1981.

[134] R. L. Kashyap, "Inconsistency of the AIC Rule for Estimating the Order of Autoregressive Models," *IEEE Transactions on Automatic Control*, vol. AC-25, no. 5, pp. 996–998, October 1980.

[135] J. Rissanen, "A Universal Prior for the Integers and Estimation by Minimum Description Length," *Annals of Statistics*, vol. 11, pp. 417–431, 1983.

[136] E. Parzen, "Some Recent Advances in Time Series Modelling," *IEEE Transactions on Automatic Control*, vol. AC-19, no. 6, pp. 723–730, 1974.

[137] J. A. Cadzow, Y. Sun and G. Xu, "Detection of Multiple Sinusoids in White Noise: A Signal Enhancement Approach," *SVD and Signal Processing*, pp. 171–186, 1988.

[138] J. A. Cadzow, B. Baseghi and T. Hsu, "Singular-value decomposition approach to time series modelling," *Proceedings of the IEE*, vol. 130, no. Part F, pp. 202–210, April 1983.

[139] D. W. Tufts and R. Kumaresan, "Singular Value Decomposition and Improved Frequency Estimation Using Linear Prediction," *IEEE Transactions on Acoustics, Speech and Signal Processing*, vol. ASSP-30, no. 4, pp. 671–675, August 1982.

[140] M. L. van Blaricum and R. Mittra, "Problems and Solutions Associated with Prony's Method for Processing Transient Data," *IEEE Transactions on Antennas and Propagation*, vol. AP-26, no. 1, pp. 174–182, January 1978; correction in vol. AP-28, no.6, p. 949, November 1980.

[141] M. L. van Blaricum and R. Mittra, "A Technique for Extracting the Poles and Residues of a System Directly from Its Transient Response," *IEEE Transactions on Antennas and Propagation*, vol. AP-23, no. 6, pp. 777–781, November 1975.

[142] R. Kumaresan and D. W. Tufts, "Estimating the parameters of Exponentially Damped Sinusoids and Pole-Zero Modelling in Noise," *IEEE Transactions on Acoustics, Speech and Signal Processing*, vol. ASSP-30, no. 6, pp. 833–840, December 1982.

[143] J. N. Holt and R. J. Antill, "Determining the Number of Terms in a Prony Algorithm Exponential Fit," *Mathematical Biosciences*, vol. 36, pp. 319–332, 1977.

[144] D. N. Swingler, "A Modified Burg algorithm for maximum entropy spectral analysis," *Proceedings of the IEEE*, vol. 67, pp. 1368–1369, September 1979.

[145] D. N. Swingler, "A Comparison between Burg's maximum entropy method and a non-recursive technique for the spectral analysis of deterministic signals," *Journal of Geophysical Research*, vol. 84, pp. 679–685, February 1979.

[146] T. J. Ulrych and R. W. Clayton, "Time series modelling and maximum entropy," *Physics Earth Planetary Interiors*, vol. 12, pp. 188–200, August 1976.

[147] S. M. Kay and S. L. Marple, "Sources and Remedies for Spectral Line Splitting in Autoregressive Spectrum Analysis," *Proceedings IEEE International Conference on Acoustics, Speech and Signal Processing*, vol. 1, pp. 151–154, 1979.

[148] W. Gersch, "Spectral Analysis of EEG's by Autoregressive Decomposition of Time Series," *Mathematical Biosciences*, vol. 7, pp. 191–204, 1970.

[149] T. J. Ulrych and T. N. Bishop, "Maximum entropy spectral analysis and autoregressive decomposition," *Reviews of Geophysics and Space Physics*, vol. 13, pp. 183–200, February 1975.

[150] H. Sakai, "Statistical Properties of AR spectral analysis," *IEEE Transactions on Acoustics, Speech and Signal Processing*, vol. ASSP-27, no. 4, pp. 402–409, August 1979.

[151] Y. H. Pao and D. T. Lee, "Performance Characteristics of the Cadzow Modified Direct ARMA Method for Spectrum Estimation," *Proceedings IEEE Acoustics, Speech and Signal Processing Workshop on Spectral Estimation*, pp. 2.5.1–2.5.10, August 1981.

[152] M. Pagano, "Estimation of models of autoregressive signal plus white noise," *Annals of Statistics*, vol. 2, pp. 99–108, 1974.

[153] S. M. Kay, "The effects of noise on the autoregressive spectral estimator," *IEEE Transactions on Acoustics, Speech and Signal Processing*, vol. ASSP-27, no. 5, pp. 478–485, October 1979.

[154] W. Gersch and D. R. Sharpe, "Estimation of Power Spectra with Finite-Order Autoregressive Models," *IEEE Transactions on Automatic Control*, vol. AC-18, pp. 367–369, August 1973.

[155] B. H. Jansen, J. R. Bourne and J. W. Ward, "Autoregressive Estimation of Short Segment Spectra for Computerized EEG Analysis," *IEEE Transactions on Biomedical Engineering*, vol. BME-28, no. 9, pp. 630–638, September 1981.

[156] E. F. Blick, H. N. Sabbah and P. D. Stein, "One-Dimensional Model of Diastolic Semilunar Valve Vibrations Productive of Heart Sounds," *Journal of Biomechanics*, vol. 12, pp. 223–227, 1979.

[157] J. Mazumdar and D. Woodard-Knight, "A Mathematical Study of Semilunar Valve Vibration," *Journal of Biomechanics*, vol. 17, pp. 639–641, 1984.

[158] M. S. Hamid, H. N. Sabbah and P. D. Stein, "Vibrational Analysis of Bioprosthetic Heart Valve Leaflets Using Numerical Models: Effects of Leaflet Stiffening, Calcification and Perforation," *Circulation Research*, vol. 61, pp. 687–694, November 1987.

[159] D. L. Sikarskie, P. D. Stein and M. Vable, "A Mathematical Model of Aortic Valve Vibration," *Journal of Biomechanics*, vol. 17, pp. 831–837, 1984.

[160] R. W. D. Turner and R. G. Gold, *Auscultation of the Heart*. ISBN 0443028869, Churchill Livingstone, 1984.

[161] L. Cohen, "Time-frequency distributions - A review," *Proceedings of the IEEE*, vol. 77, no. 7, pp. 941–981, July 1989.

[162] P. M. Bentley and J. T. E. McDonnell, "Wavelet transforms: an introduction," *IEE Electronics and Communication Engineering Journal*, vol. 6, no. 4, pp. 78–81, August 1994.

[163] O. Rioul and M. Vetterli, "Wavelets and Signal Processing," *IEEE Signal Processing Magazine*, vol. 8, no. 4, pp. 14–38, October 1991.

[164] W. Martin and P. Flandrin, "Wigner-Ville spectral analysis of nonstationary processes," *IEEE Transactions on Acoustics, Speech and Signal Processing*, vol. ASSP-33, no. 6, pp. 1461–1470, December 1985.

[165] H. I. Choi and W. J. Williams, "Improved time-frequency representation of multicomponent signals using exponential kernels," *IEEE Transactions on Acoustics, Speech and Signal Processing*, vol. 40, no. 2, pp. 402–412, 1992.

[166] W. J. Williams, "Time-Frequency Analysis of Biological Signals," *Proceedings IEEE International Conference on Acoustics, Speech and Signal Processing*, vol. 1, pp. I–83–I–86, 1993.

[167] D. T. Barry and N. M. Cole, "Muscle vibrates at its resonant frequency," *IEEE Transactions on Biomedical Engineering*, vol. BME-37, no. 5, pp. 525–513, May 1990.

[168] P. M. Bentley and J. T. E. McDonnell, "Wavelet Analysis of Cardiovascular Signals," *Proceedings Seventh European Signal Processing Conference*, pp. 78–81, Edinburgh 1994.

[169] R. Beale and T. Jackson, *Neural Computing: An Introduction*. ISBN 0852742622, IOP Publishing Ltd, 1990.

[170] R. P. Lippmann, "An Introduction to Computing with Neural Nets," *IEEE Signal Processing Magazine*, pp. 4–22, April 1987.

[171] S. Haykin, *Neural Networks - A Comprehensive Foundation*. ISBN 0023527617, Macmillan College Publishing Company, 1994.

[172] S. Roberts and L. Tarassenko, "The Analysis of the Sleep EEG using a Multi-layer Network with Spatial Organisation," *IEE Proceedings: Part F*, vol. 139, no. 6, pp. 420–425, 1992.

[173] K. J. Cios, K. Chen and R. A. Langenderfer, "Use of neural networks in detecting cardiac diseases from echocardiographic images," *IEEE Engineering in Medicine and Biology Magazine*, vol. 9, no. 3, pp. 58–60, 1990.

[174] C. Yi, E. Micheli-Tzanakou, D. M. Shindler and J. B. Kostis, "Study of Echocardiogram for Myocardial Infarction using Neural Networks," *Proceedings 15th Annual International Conference IEEE Engineering in Medicine and Biology Society*, pp. 255–256, San Diego 1993.

[175] K. H. El-Maleh, H. C. Lee and L. G. Durand, "A Coherence-Based Criterion for Iterative Blind Deconvolution of Surface PCG," *Proceedings 15th Annual International Conference IEEE Engineering in Medicine and Biology Society*, pp. 377–378, San Diego 1993.

[176] S. Yong, H. C. Lee and J. G. Durand, "A homomorphic method to recover the intracardiac left-ventricular second heart sound," *Proceedings 12th Annual International Conference IEEE Engineering in Medicine and Biology Society*, pp. 254–255, Philadelphia 1990.

Appendix A

Original Publications

The research described in this thesis has been reported in the following publications:

1. R. Bedi and J. T. E. McDonnell, "Evaluation of Parametric methods for the Spectral Analysis of Carpentier Edwards Heart Valve Sounds," *Proceedings 20th Annual International Conference IEEE Computers in Cardiology*, pp. 675–678, London 1993.

2. †R. Bedi, J. T. E. McDonnell and K. A. A. Fox, "Forward-Backward Linear Predictive Spectral Analysis of Bioprosthetic Heart Valve Sounds," *Proceedings 15th Annual International Conference IEEE Engineering in Medicine and Biology Society*, pp. 890–891, San Diego 1993.

3. R. Bedi and H. P. Sava and J. T. E. McDonnell, "Spectral Analysis of Prosthetic Heart Valve Sounds," *Proceedings IEE Colloquium Signal Processing and Modelling in Cardiography*, Newcastle 1994, accepted for publication

4. R. Bedi and J. T. E. McDonnell, "Frequency Analysis of Bioprosthetic Heart Valves," *Digest of Abstracts Institute of Physical Sciences in Medicine and Biological Engineering Society Meeting on Signal Processing in Medicine*, London 1994, accepted for publication.

5. †R. Bedi and J. T. E. McDonnell and K. A. A. Fox, "Acoustic Analysis of Carpentier-Edwards Bioprosthetic Heart Valves," *Proceedings 16th Annual International Conference IEEE Engineering in Medicine and Biology Society*, Baltimore 1994, accepted for publication.

6. R. Bedi and J. T. E. McDonnell, "Evaluation of Parametric Methods for the Spectral Analysis of Carpentier-Edwards Bioprosthetic Heart Valve Closing Sounds," *IEEE Transactions on Biomedical Engineering*, 1993, accepted for second-stage review.

7. R. Bedi and J. T. E. McDonnell, "Model Order Considerations when Analysing the Spectra of Bioprosthetic Heart Valve Closing Sounds Part 1 : Hypothesis and Multiple Decision-Based Selection Criteria," *IEEE Transactions on Biomedical Engineering*, 1994, accepted for second-stage review.

8. R. Bedi and J. T. E. McDonnell, "Model Order Considerations when Analysing the Spectra of Bioprosthetic Heart Valve Closing Sounds Part 2 : Linear-Algebra-Based Selection Criteria," *IEEE Transactions on Biomedical Engineering*, 1994, accepted for second-stage review.

9. R. Bedi and J. T. E. McDonnell, "Acoustic Analysis of Aortic Bioprosthetic Heart Valves," *IEEE Transactions on Biomedical Engineering*, 1994, submitted for review.

10. R. Bedi and J. T. E. McDonnell, "Acoustic Analysis of Mitral Bioprosthetic Heart Valves," *IEEE Transactions on Biomedical Engineering*, 1994, submitted for review.

Paper 1 was also presented at the "*Meeting of the Biomaterials Group, Biological Engineering Society, on Cardiovascular Biomaterials, Devices and Evaluation*, University of Strathclyde, Glasgow, September 1993.

†Reprinted in this appendix.

FORWARD-BACKWARD LINEAR PREDICTIVE SPECTRAL ANALYSIS OF BIOPROSTHETIC HEART VALVE SOUNDS

R. Bedi†, J.T.E. McDonnell† and K.A.A. Fox *

†Department of Electrical Engineering, *Cardiovascular Research Unit,
The University of Edinburgh, King's Buildings, Mayfield Road, Edinburgh EH9 3JL, U. K.

ABSTRACT

This paper examines the performance of least squares methods which use a combination of both forward and backward linear prediction in estimating the spectral distribution of bioprosthetic valve sounds. The Burg algorithm and two weighted variations of this method were applied to bioprosthetic valve sounds. A new method of analysing the frequency spectrum produced by these valve sounds is also proposed, whereby the Levinson recursion constraint imposed by Burg is removed. This unconstrained forward-backward method is known as the Modified Covariance method (MCV). Autoregressive (AR) spectra of *sinusoids* generated using this MCV method show improved performance over other least squares methods, including less bias in the frequency estimates of spectral components, reduced variance in frequency estimates over an ensemble of spectra and absence of observed spectral line splitting. When applied to bioprosthetic valve sounds, preliminary results generated using this MCV method show at least comparable performance with other least squares methods. Like the Burg algorithm, this MCV method has computational complexity proportional to the process order squared.

INTRODUCTION

Spectral analysis of the closing sounds produced by bioprosthetic heart valves has been used for over a decade to monitor the degenerative changes which can lead to valvular dysfunction. Previous work [1] has shown that the dominant frequency peaks of the closing sounds shift towards the higher frequencies as a result of valve tissue calcification, fibrosis and stiffening.

A number of digital spectral analysis techniques have previously been used to obtain the spectral characteristics of bioprosthetic valve sounds [2]. Some of these were based on the Fast Fourier Transform (FFT) while others concentrated on more recent parametric modelling techniques. However, due to the short duration of heart sounds, FFT-based methods do not provide the frequency resolution required in order to completely characterise the spectrum of bioprosthetic valve sounds.

Previous work on AR spectral analysis of bioprosthetic valve sounds [2] has concentrated on least squares estimates using forward linear prediction solely, namely: the autocorrelation and covariance methods as defined by Makhoul [3]. The autocorrelation method, however, has the worst frequency resolution relative to other linear-prediction based estimation methods. Moreover, the covariance method can produce AR parameters whose resulting spectra have more false peaks and greater perturbations of spectral peaks from their correct frequency locations than other AR estimation approaches. The covariance normal equations also lead to AR parameter estimates with greater sensitivity to noise. Spectral line splitting has also been observed with these two methods. The use of the MCV method alleviates these problems.

METHOD

A. Data Acquisition

The phonocardiogram (PCG) was recorded from male and female patients with implanted Hancock or Carpentier-Edwards bioprosthetic valves in the mitral or aortic positions. The PCG was recorded in the supine position using a contact microphone (Hewlett Packard 21050A).

B. Spectral Estimation

The forward and backward linear prediction estimates have similar statistical information. By combining the linear prediction error statistics of both the forward and backward errors more error points are generated, with the net result being an improved estimate of the AR parameters. Burg minimised the sum of the forward and backward prediction errors subject to the constraint imposed by the Levinson recursion. At each order p the arithmetic mean of the forward and backward linear prediction error is minimised:

$$\rho_p^{fb} = \sum_{n=p+1}^{N} [\, |e_p^f[n]|^2 + |e_p^b[n]|^2 \,] \qquad (1)$$

The Burg method, however, has the same problems as previously outlined. This led some researchers to pro-

pose variations to the Burg method in order to reduce the biases in the estimation of sinusoidal frequencies. The basic variation is a weighting applied to the squared prediction error. The weightings used in our analysis of bioprosthetic valve sounds were a Hamming window [4] and a parabolic quadratic taper [5].

Performing a least squares unconstrained minimisation yields significant improvements in the spectral estimate of sinusoidal signals. The improvements of this MCV method [6] include less bias in the frequency estimate of spectral components, reduced variance in the frequency estimation and absence of spectral line splitting. Previous work [6] has also shown that the Burg and MCV methods have the least spectral variance and the least frequency variance when tested with nonsinusoidal signals.

RESULTS AND DISCUSSION

The spectral estimation of first sounds using the various constrained Burg methods results in very similar instantaneous and ensemble power spectral density (PSD) estimates. The ensemble PSD estimates of figures 1 and 2 were based on fifteen consecutive first sounds produced by a Hancock valve implanted in the mitral position. Spectra produced by other patients with the same bioprostheses showed similar results. The bias of these estimates appears to be negligible as shown in Fig.1.

PSD estimates of the first sound obtained using the constrained Burg method, unconstrained single prediction covariance method and the unconstrained forward-backward MCV method are shown in Fig.2. All three estimates produce similar spectra.

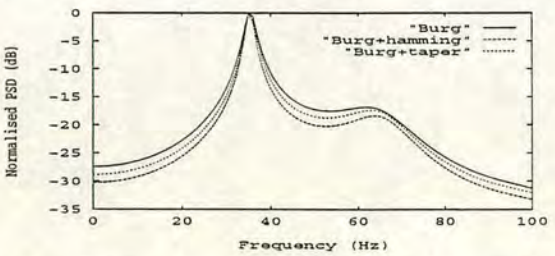

Figure 1: *PSD ensemble estimates of the first heart sound obtained using constrained Burg methods.*

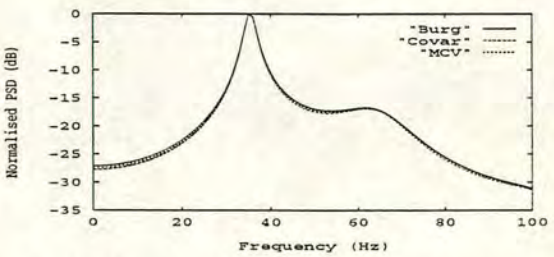

Figure 2: *PSD ensemble estimates of the first sound obtained using the Burg, Covariance and MCV methods.*

CONCLUSIONS

Extensive use of the MCV method has been made in analysing spectra of *sinusoidal processes* as a result of its superior performance over all other least squares linear predictive methods.

Using this MCV method to analyse bioprosthetic valve sounds produces at least comparable spectra with other methods. These spectra represent preliminary results and work is currently continuing with data from many more patients to investigate the advantages of the MCV method over the other least squares methods. Current work also suggests that the MCV method is insensitive to the initial phase of *simulated* heart sounds. We thus conclude that the MCV method can be used to determine accurately the PSD estimate of actual and simulated bioprosthetic valve sounds.

ACKNOWLEDGMENTS

The authors would like to thank Dr. P. Bloomfield, A. Colthart, P. Bentley, H. Sava and the staff at The Royal Infirmary of Edinburgh for their assistance in obtaining recordings of bioprosthetic valve sounds.

REFERENCES

[1] P. Stein *et al.*, "Frequency Spectra of the First Heart Sound and of the Aortic Component of the Second Heart Sound in patients with Degenerated Porcine Bioprosthetic Valves," *The American Journal of Cardiology*, vol. 53, pp. 557–561, February 1984.

[2] L. Durand *et al.*, "Spectral analysis of closing sounds produced by Ionescu-Shiley bioprosthetic aortic heart valves: Part 3," *Medical and Biological Engineering and Computing*, vol. 25, pp. 497–503, September 1987.

[3] J. Makhoul, "Linear Prediction: A Tutorial Review," *Proceedings of the IEEE*, vol. 63, no. 4, pp. 561–580, April 1975.

[4] D. Swingler, "A Modified Burg Algorithm for Maximum Entropy Spectral Analysis," *Proceedings of the IEEE*, vol. 67, no. 9, pp. 1368–1369, September 1979.

[5] M. Kaveh and G. Lippert, "An Optimum Tapered Burg Algorithm for Linear Prediction and Spectral Analysis," *IEEE Transactions on Acoustics, Speech and Signal Processing*, vol. 31, no. 2, pp. 438–444, April 1983.

[6] S. Marple, *Digital Spectral Analysis With Applications.* ISBN 0132141493, Prentice-Hall, INC., 1987.

ACOUSTIC ANALYSIS OF CARPENTIER-EDWARDS BIOPROSTHETIC HEART VALVES

R. Bedi†, J.T.E. McDonnell† and K.A.A. Fox *

†Department of Electrical Engineering, *Cardiovascular Research Unit,
The University of Edinburgh, King's Buildings, Mayfield Road, Edinburgh EH9 3JL, U. K.

ABSTRACT

This paper characterises the spectra of closing sounds produced by the Carpentier-Edwards bioprosthetic heart valve by extracting from the sound spectrum heuristic features of diagnostic significance. Algorithms were tested on sounds recorded from forty patients with the Carpentier-Edwards bioprosthesis (twenty-four aortic and sixteen mitral). Results show that normally functioning aortic valves are characterised by four to five dominant peaks, with the major concentration of spectral energy occurring between 25Hz and 125Hz, whereas, normally functioning mitral valves are characterised by two to three dominant peaks with the major concentration of spectral energy occurring between d.c. and 100Hz. For leaky, regurgitant valves and valves diagnosed as having stiffening, calcified cusps, a shift in spectral energy was observed, to the regions between d.c.and 75Hz and 50Hz and 200Hz respectively. It was found that the frequency occurring at the -10dB level can be used to discriminate between normally functioning, leaky and stiffening aortic prostheses, where mean frequencies were observed of 113.6Hz, 53.7 Hz and 238.1Hz respectively. This paper presents the first publication of these findings for the Carpentier-Edwards bioprosthesis.

INTRODUCTION

Previous related work by the authors [1–3] describes in detail the procedures involved regarding the acquisition of phonocardiographic signals from patients with implanted bioprosthetic heart valves, as well as the theory, suitability and performance of spectral estimation techniques when applied to valvular closing sounds. In this paper, heuristic features of diagnostic significance are extracted from the sound spectrum produced by normally functioning, leaky and stiffening Carpentier-Edwards bioprostheses, in an attempt to uniquely characterise the sound spectrum of each of these states of physiological and pathological functionality. Quantitative analysis of the spectrum of normally functioning valves should assist in the detection of leaky and stiffening valves through changes in the sound spectrum.

DIAGNOSTIC FEATURE SELECTION

The selection of diagnostic features was based on the empirical identification of a number of dominant frequency peaks to quantify the natural resonance modes of bioprosthetic heart valves, and to characterise the distribution of energy in the sound spectrum by evaluating bandwidth, energy and root mean square (RMS) measurements over the entire spectral profile.

RESULTS AND DISCUSSION

For normally functioning aortic prostheses, Prony's method of spectral analysis identified four to five dominant frequency peaks and one to two weaker secondary peaks. Mean frequencies and amplitudes of these peaks were: $F1$ = 37.4Hz @ 0dB, $F2$ = 77.8Hz @ -7.66dB, $F3$ = 116.5Hz @ -10.04dB, $F4$ = 171.1Hz @ -14.17dB, $F5$ = 245.8Hz @ -16.59dB, $F6$ = 292.4Hz @ -17.0dB. The major distribution of spectral energy occurred in the region between 25Hz and 125Hz, with mean relative energies and RMS energies of 35.73% and 33.49% respectively.

For leaky aortic prostheses, Prony's method identified four dominant peaks and one weaker secondary peak, with mean frequencies and amplitudes of: $F1$ = 30.6Hz @ 0dB, $F2$ = 55.3Hz @ -7.54dB, $F3$ = 114.0Hz @ -17.69dB, $F4$ = 149.2Hz @ -19.21dB, $F5$ = 210.7Hz @ -22.05dB. These results are slightly lower than those produced by normally functioning prostheses, particularly the amplitudes of peaks $F3$ to $F6$. The major distribution of spectral energy occurred in the region between d.c. and 75Hz, with mean relative energies and RMS energies of 28.67% and 26.3% respectively. The higher frequency peaks, $F3$ to $F6$, which characterised normally functioning prostheses have less energy, with the remainder of the energy being evenly distributed throughout the other frequency bands of the sound spectrum. This concentration of energy in the lowest frequency regions of the sound spectrum is due primarily to the presence of diastolic murmurs produced by incompetent, regurgitant aortic prostheses.

For aortic prostheses diagnosed as having stiffening, calcified cusps, a shift in spectral energy was observed, with the higher frequency peaks assuming more energy. Mean frequencies and amplitudes of these peaks were: $F1$ = 181.2Hz @ 0dB, $F2$ = 147.1Hz @ -0.77dB, $F3$ = 101.0Hz @ -0.82dB, $F4$ = 67.1Hz @ -1.49dB, $F5$ = 44.2Hz @ -2.97dB, $F6$ = 216.3Hz @ -6.68dB. The major distribution of spectral energy occurred in the region between 50Hz and 200Hz, with mean relative energies and RMS energies of 62% and 61% respectively.

For normally functioning mitral prostheses, Prony's method identified two to three dominant frequency peaks and one to two weaker secondary peaks. The major distribution of spectral energy occurred in the region between d.c. and 100Hz with mean relative energies and RMS energies of 39.22% and 36.62% respectively. A similar shift in spectral energy to the region between d.c. and 75Hz was observed for leaky mitral prostheses. Figure 1 shows examples of spectra and distributions of spectral energy produced by Carpentier-Edwards bioprostheses.

In general, it was observed that for normally functioning prostheses, there was a correlation between spectral energy and the period of implantation. As the duration of implantation increased, the amount of energy decreased slightly, having been redistributed in the higher-frequency regions of the sound spectrum. This is a result of the inevitable gradual stiffening associated with the cusps of porcine bioprosthetic heart valves.

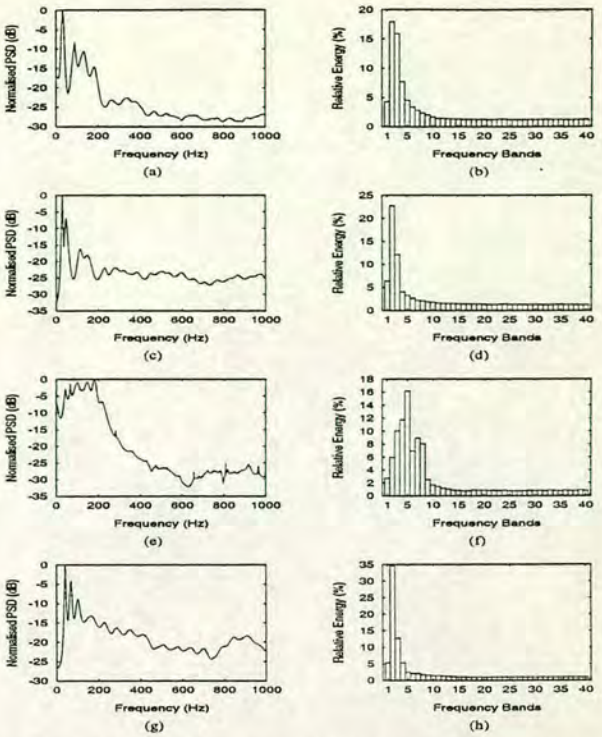

Figure 1: *Characteristics of Carpentier-Edwards bioprostheses. (a and b) Spectral estimate and energy distribution of normally functioning aortic prostheses, (c and d) Spectral estimate and energy distribution of leaky aortic prostheses, (e and f) Spectral estimate and energy distribution of stiffening aortic prostheses, (g and h) Spectral estimate and energy distribution of normally functioning mitral prostheses.*

CONCLUSIONS

This paper has characterised the spectra of the closing sounds produced by the Carpentier-Edwards bioprosthetic heart valve. Results have shown that normally functioning, leaky and stiffening prostheses each exhibit unique spectral characteristics. For leaky prostheses, a shift in spectral energy was observed, from the higher frequency peaks to the lower frequency peaks. For stiffening prostheses, a shift in spectral energy was also observed, with the higher frequency peaks assuming more energy. It was found that the frequency occurring at the -10dB can be used to discriminate between normally functioning, leaky and stiffening aortic prostheses.

This study has indicated that features extracted from the sound spectrum offer the potential of diagnosing prostheses as normally functioning, leaky or stiffening. The suitability of these features in the development of classification and neural network algorithms is currently being investigated.

This work has shown that valuable information regarding the physiological and pathological state of bioprosthetic heart valves is contained within the sound spectrum. The results obtained are very encouraging and suggest that it is now possible to develop a low-cost prototype system to provide periodic evaluation of aortic and mitral bioprosthetic heart valves. Such a system would be non-invasive, passive, atraumatic and accurate, detecting impending valvular malfunctions, dysfunctions and degenerations.

REFERENCES

[1] R. Bedi and J. T. E. McDonnell, "Evaluation of Parametric Methods for the Spectral Analysis of Carpentier-Edwards Heart Valve Sounds," *Proceedings 20th Annual International Conference IEEE Computers in Cardiology*, pp. 675–678, London 1993.

[2] R. Bedi, J. T. E. McDonnell and K. A. A. Fox, "Forward-Backward Linear Predictive Spectral Analysis of Bioprosthetic Heart Valve Sounds," *Proceedings 15th Annual International Conference IEEE Engineering in Medicine and Biology Society*, pp. 890–891, San Diego 1993.

[3] R. Bedi, H. P. Sava and J. T. E. McDonnell, "Spectral Analysis of Prosthetic Heart Valve Sounds," *Proceedings IEE Colloquium Signal Processing and Modelling in Cardiography*, Newcastle 1994, accepted for publication.

Appendix B

Personal Communication

The following is an email message received from Professor T. E. Posch of the Hughes Aircraft Company in the United States.

```
   From: 0001913@MRAM_EDEN@EDEN
 Author: Posch, Theodore E
     To: SMTPGATE
Created: //
   Time: ::
Subject: RE: Heart Sound Information


To  : EDEN::SSW::SMTPGATE::RB2
Date:  8-DEC-1993 11:25:17.00

Dear Rajan,

I received your wonderful letter regarding what you and your group are doing
in the area of phonocardiograms, and your e-mail of 11/15.

We will be doing a 100 patient case load at Brooke Army Medical Center for t
valve study next year.  We will be using many t-F distributions for the stud
including the spectrogram, the Zamogram, the binomial, and some positive
time-frequency distributions.

Thank-you for your paper on the STFT and wavelet analysis approach.  The pap
looks encouraging to us since in the time-frequency plane we have obtained
similar results. What is the time resolution and frequency resolution that y
are using in your analysis.  We have been analyzing our data using 4 msec.
time resolution, and 1 Hz. frequency resloution.  In the future I will be
sending you some of our results and color print outs.

Thank-you for your kind reply to our conversations and I look forward to
hearing from you in the future.

Best regards,

Ted Posch
```